CARBON-FIBER COMPOSITE MOLECULAR SIEVES FOR GAS SEPARATION

M. Jagtoyen and F. Derbyshire

University of Kentucky, Center for Applied Energy Research,
3572 Iron Works Pike, Lexington KY 40511-8433, USA

ABSTRACT

This report describes continuing work on the activation and characterization of formed carbon fiber composites. The composites are produced at the Oak Ridge National Laboratory (ORNL) and activated at the Center for Applied Energy Research (CAER) using steam, CO_2, or O_2 at different conditions of temperature and time, and with different furnace configurations. The general aims of the project are to produce uniformly activated samples with controlled pore structures for specialist applications such as gas separation and water treatment.

In previous work we reported that composites produced from isotropic pitch fibers weighing up to 25g can be uniformly activated through the appropriate choice of reaction conditions and furnace configurations. We have now succeded in uniformly activating composites of dimensions up to 12x7x6 cm, or up to about 166 gram- a scale-up factor of about six. Part of the work has involved the installation of a new furnace that can accommodate larger composites. Efforts were made to achieve uniform activation in both steam and CO_2. We have also succeded in producing materials with very uniform and narrow pore size distributions by using a novel method involving low temperature oxygen chemisorption in combination with heat treatment in N_2 at high temperatures. Work has also started on the activation of PAN based carbon fibers and fiber composites with the aim of producing composites with wide pore structures for use as catalyst supports. So far activation of the PAN fiber composites supplied by ORNL has been difficult which is attributed to the low reactivity of the PAN fibers. As a result, studies are now bing made of the activation of the PAN fibers to investigate the optimum carbonization and activation conditions for PAN based fibers.

Activated samples of pitch fiber composites have been characterized for the adsorption and desorption of CO_2, and to determine the butane (working capacities). CO_2 working capacities were also determined to further elucidate the function of the composites in the separation of CO_2 / CH_4 mixtures. The maximum CO_2 working capacity occurs at low burn-off (around 10 wt%) which is in the same region where maximum CO_2 / CH_4 separation is attained.

The activated carbon fiber composites have also been tested for possible water treatment applications by studying the adsorption of sodium pentachlorophenolate, PCP (a common herbicide/wood preservative). In preliminary tests, a composite specimen has shown superior performance to a commercial water treatment carbon.

INTRODUCTION

This project involves collaborative research between the ORNL and the CAER, for the development of novel, rigid, monolithic adsorbent carbon fiber composites that can be produced in single pieces to a given size and shape. The carbon fiber composites are produced at the ORNL and activated at the CAER using steam or CO_2 under different conditions, with the aims of producing a uniform degree of activation, and of closely controlling pore structure and adsorptive properties. The principal aims of the work to date have been to produce uniformly activated samples with narrow porosity for use in gas separations, although numerous other areas of application are envisaged. So far, it has been shown that the composites have excellent capacities for gas separation e.g methane and CO_2 separation and for adsorption of CO_2[5-12].

The project originated in research conducted at the ORNL in the 1980s[1], when carbon fiber composite material was developed as a low-density, mechanically strong thermal insulator for a radioisotopic heat source on spacecraft for the Galileo and Ulysses Missions. The basis for the present project was to adapt the process to produce high surface area materials through the activation of similar composites, in which porosity is developed in the carbon fibers to produce high surface areas for adsorption. One of the principal changes, compared to the original work, is to utilize lower cost carbon fibers that are produced from isotropic pitches (other types of fiber will also be included in the studies). In recent years, a great interest has developed in the activated forms of such isotropic carbon fibers, where high surface areas can be produced by partial gasification in steam or other oxidizing gas[2,3]. Moreover, while porosity can be generated in most types of carbon fiber, low-modulus fibers produced from isotropic pitch are particularly suited for activation due to their unique structure in which the random packing of small crystallites allows the development of an extensive pore structure.

Activated carbon fibers are of interest in several areas of adsorption and environmental protection due to their novel properties that make them more attractive than conventional forms (powder or large-size carbons) for certain applications[1,2]. Among the possible applications, activated carbon fiber composites are of interest for the adsorption and recovery of organic vapors; the removal of SO_x and NO_x from flue gases; the improvement of air quality; and water treatment[2-5]. The incorporation of the fibers into composites surmounts the difficulties in handling and utilizing activated fibers.

The specific objectives of the research described in this report have been to examine the activation of large composites, and to ascertain the uniformity of activation through the body of the materials. Previously, specimens have been activated as plates of dimensions of 12 x 1.5 x 4 cm, and sample weights of about 25 grams. In the present report we have activated composites of dimensions up to 12 x 7 x 6 cm, which corresponds to about 166 gram per sample- a scale-up factor of about six. Part of the work has involved the installation of a new furnace that can accommodate the larger composites. The report provides an account of studies of composite activation, the uniformity of porosity development, and the measurement of physical properties (dimensional changes during activation, gas permeability). The composites have been further characterized for their efficiency in gas separation (CH_4/CO_2 mixtures) as well as determinations of their butane and CO_2 working capacities, and their performance in water treatment applications, specifically adsorption of herbicides.

DISCUSSION OF CURRENT ACTIVITIES

Experimental

Composite Preparation

Carbon fiber composites are prepared at ORNL[9,10] by vacuum molding from water slurries containing powdered phenolic resin and chopped isotropic petroleum pitch fibers, (P-200, ~ 17.5 μm diameter, average length 380μm, supplied by courtesy of Ashland Carbon Fibers Division, Ashland Inc.). The slurry is vacuum molded into tubular, plate or rod configuration, followed by drying, curing, and carbonization to about 650°C.The carbon fiber composites are supplied to the CAER usually in the form of plates (28x12x1.5cm).

Activation

The formed carbon fiber composites were activated at the CAER[11,12]. The specimens have been activated as plates of dimensions ranging from 12 x 1.5 x 4 cm (about 25 grams) to 12 x 7 x 6 cm (about 166 grams). The reactor furnace used for the activation of composite samples has been described in an earlier report[11]. A new furnace has now been installed that can activate larger pieces. The furnace is a Lindberg Blue M laboratory box furnace with chamber size 12x12x18 inches and maximum operating temperature 1100°C. The specimen is contained in a sealed stainless steel cylindrical chamber of diameter 6", and height 6". The activating agent, steam, CO_2 or O_2, is distributed into the stainless steel chamber through a perforated plate positioned 1 cm above the bottom of the container. The materials have been activated using three different techniques, steam activation, CO_2 activation, and oxygen activation. For steam activation, the composite samples are activated in an atmosphere of steam mixed with nitrogen. Water is pumped into the reaction chamber at a flow rate ranging from 60-150cc/hr and is vaporized in the bottom of the chamber. The flow rate of N_2 is varied between 2-3 l/min. The reaction temperature is varied from 800-900°C, and reaction times from 0.5-3 hrs. As CO_2 activation is significantly slower than steam, the CO_2 activation is carried out at temperatures from 850-950°C, for reaction times of 1-3 hours. The flow rate of CO_2 is varied from 2-3 l/min. A third method of activation involves the chemisorption of oxygen onto the carbon at low temperatures, from 225-250°C, and subsequent heat treatment in nitrogen to 850-925°C when the oxygen is removed as COx. It is believed that this method can create a uniform pore structure.

Characterization

Porosity. Surface area and pore size distributions were measured on a 10 port automated surface area analyzer, OMNISORB 610. The high efficiency of the instrument allows the measurement of surface areas, as well as the characterization of pore sizes down to 4 A, using nitrogen at 77K as the adsorbate. Surface areas were determined from the isotherms by the BET method, and pore volumes by the D-R method and BJH method.

Butane and CO_2 Working Capacity Test. The butane working capacity (BWC) was developed as a measure of the effectiveness of activated carbons that are used to trap hydrocarbons released by evaporative losses from vehicle fuel systems (used in evaporative loss control devices, or ELCDs). However, it is also

a useful indication of the properties of activated carbons with respect to other applications. Essentially, the BWC is the difference between the saturation adsorptive capacity of butane, and the amount retained upon the carbon after purging under specified conditions. The retained butane is too strongly adsorbed to allow facile desorption.

The tests were performed according to ASTM method D5228-92 for the determination of the Butane Working Capacity of Activated Carbon. The activated carbon sample is outgassed under vacuum at 150°C for 4 hours, and packed in a constant volume bed according to a standard procedure (ASTM D 2854) immersed in a constant temperature water bath at 25°C. Butane is then passed through the activated carbon sample at a flow rate of 250cc/min for 900 seconds. The sample is then weighed, and gas is adsorbed for another 600 seconds. When the sample has reached constant weight, the bed is desorbed with dry air that is passed through the sample at a flow rate of 300mL/min for 2400 seconds. The difference in mass is the BWC and is expressed as mass of butane per unit volume of carbon. In this report we also report CO_2 working capacities that were determined using the same procedure for the butane working capacity.

Permeability of Composites to Liquid Flow. Previously we have reported on the high permeability of the composites to the flow of gases. We have now extended these measurements to include the flow of liquids. Specimens for permeability testing were cut from a composite sample using a hole cutter with 1/2 inch diameter. The samples were about 5.7 cm long, giving a total specimen volume of about 12.5cc. A simple apparatus was used for the permeability test, where water flowed through the cylindrical specimen that was sealed on the outside using heat shrink tubing. The water flow was varied between 8-170 ml/min or 4-90 gpm/ft^2. The differential pressure was measured using a digital pressure gauge upstream of the sample. The pressure drop was determined as the difference between this pressure and atmospheric pressure.

Adsorption of Herbicides from Water. The adsorptive capacity of an activated carbon composite sample for sodium pentachlorophenolate (PCP) was measured by sealing a 2.0 g sample of carbon into polyolefin tubing to create a column of volume 8 cm^3 and length 6 cm. Plugs of quartz wool were fitted at the column ends to contain the bed. A peristaltic pump, Pulsafeeder - Mec-o-matic VSP-20, located downstream of the column continuously drew a 40 ppm solution of sodium pentachlorophenolate (NaC_6Cl_5O) from a reservoir and through the column. The concentration of PCP in the column effluent stream was monitored via a UV-Vis spectrophotometer (Varian, Series 634) fitted with a 10 mm path length flow-through quartz cell, at a wavelength of 317.5 nm. Column breakthrough was determined as the point where the ratio of effluent to inlet PCP (C/Co) was equal to 0.3. The flow rate of PCP solution through the column was held constant at 1 ml.min^{-1}. An equivalent experiment was conducted using a granular Norit commercial water treatment carbon to provide a basis for comparison.

Results and Discussion

Uniformity of Steam and CO_2 Activation

The focus of this part of the work has been to scale up the activation of carbon fiber composites supplied by ORNL. In previous work we reported that composites weighing up to 25 g can be uniformly activated through the appropriate choice of reaction conditions and furnace configurations. We have now examined the activation of composites with dimensions up to 12 cm x 7 cm x 6 cm and weighing 166 g. The uniformity of activation was determined by measuring BET surface areas and micropore volumes on samples taken from 3 or 6 different positions in the composite, as indicated in Figure 1. The results are shown in Table 1. Three different activating methods were used; steam, CO_2, and a procedure involving activation in steam for 1 hour and then in CO_2 for one hour. The uniformity of activation appears to be similar for all three methods. The standard deviation of BET surface area for steam activated samples ranged from 0.5-18%, and

for CO_2 activation from 5-8%. The combination of activating agents gave a standard deviation of 9%. The spread in surface area through the samples produced at different burnoffs under the conditions summarized in Table 2 are shown in Figure 2.

Dimensional Changes. There is an overall shrinkage of the composites during activation. The effects of burnoff on dimensional change have been discussed earlier[7]. However, we have now generated additional data that confirm the earlier findings. Generally, the volume decreases with burn-off. A linear relationship exists to about 35% burnoff, but at higher burnoff there is a steeper increase in shrinkage. Moreover, above a certain temperature (~ 850°C) and only in steam, the extent of contraction induces sufficient stress to split the composite and destroy its physical integrity. Another interesting phenomenon is that while CO_2 activation gives the same relationship between burnoff and dimensional change as steam activation, it does not lead to sample cracking, even at high burn-offs.

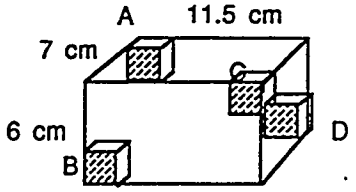

	BET surface area(m2/g)
A	839
B	734
C	825
D	1101
	St.dev 17%

OR 190, sample wt. 160 g, burnoff=19%

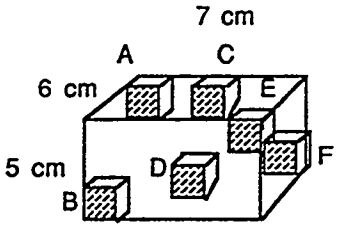

	BET surface area(m2/g)
A	1099
B	1000
C	1164
D	988
E	965
F	1085
	St.dev 7.4%

OR 200, sample wt. 78 g, burnoff=35%

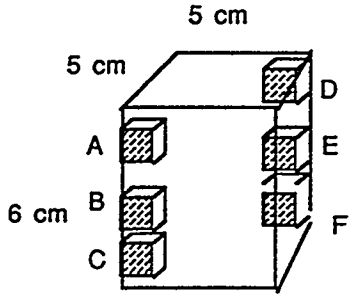

	BET surface area(m2/g)
A	914
C	803
D	825
F	805
	St.dev 6 %

OR 186, sample wt. 57 g, burnoff=25%

Figure 1: Uniformity of Activation of Carbon Fiber Composites

Table 1: Uniformity of activation of carbon fiber composites

ID (SA-)	B. off (%)	HTT (°C)	Time (hr)	BET surf. area (m^2/g)	pore width,L (A)	W_0,micro pore vol. (cc/g)	st.dev in BET (%)
	Activating Agent						
Sample ID							
	Steam						
181	9	850	1	484-487	6.4-6.5	0.23-0.24	0.5
185	19	877	1	465-568			10.0
190	19	877	2	734-1101			18.0
182	25	900	2	812-867	7.3-7.6	0.41	4.6
186	25	877	2	803-914			6.3
106	27	800	4	762-865			9.0
109	41	877	2	1089-1109			1.3
	CO_2						
179	5	850	3	390-431	6.7-8	0.19-0.21	5.7
180	11	900	3	426-469	6.2-6.9	0.21-0.23	4.9
126	20	900	3	632-578	6.6-6.3		6.3
	Steam/CO_2						
183	19	850	1/1	442-559	5.8-6.4	0.26-0.27	8.9

SA<178 sample weight 20 gram, SA>178 sample weight 50-60 gram, SA=190 sample weight 166 gram
* sample was physically disrupted, and split along plane perpendicular to settling direction during formation of composite

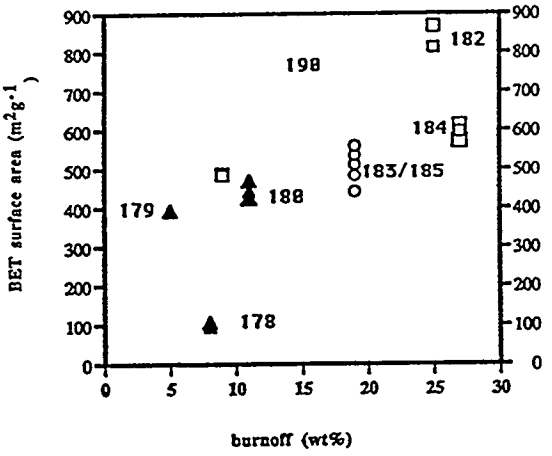

Figure 2: BET surface area of sample from specimens produced at different burnoffs. (Sample numbers shown on graph).

Uniformity of Oxygen Activation

Oxygen chemisorption at low temperature combined with heat treatment at high temperatures was tried as an alternative to steam or CO_2 activation in order to produce uniform activation and a narrow pore size distribution in the carbon fiber composites. Oxygen is chemisorbed onto the composites at 225-250°C, and the samples are subsequently heat treated in nitrogen to 850-925°C. It is believed that the slow chemisorption of O_2 can create a uniform distribution of surface oxygen groups that are later released as CO and CO_2. It is known that CO_2 is released at temperatures from 300-800°C with a maximum at about 350°C while CO is released at temperatures from 500-900°C with a maximum at

700°C. The surface area development in the composites was very uniform, with a variation in surface area within the samples of only 3-6%, Table 2. Increasing the chemisorption temperature from 225 to 250°C gave sufficient uptake of oxygen to triple the BET surface area upon heat treatment to 900°C. Heat treatment to 850°C is not sufficient to achieve significant microporosity, and heat treatment to 925°C also give low surface area. The optimum upper temperature for maximizing the production of narrow micropores appears to be around 900°C. The influence of repeated chemisorption/heat treatment cycles will be examined in continuing studies.

Table 2: BET surface area in petroleum based carbon fiber composites activated by oxygen chemisorption/heat treatment at high temperature (single heat treatment cycle).

Sample#	Oxidation		Heat treatm.		Burnoff	Surface area (m^2/g)		Pore vol	
	T(°C)	t(hr)	T(°C)	t(hr)	(wt%)	BET	mesopore	micro	meso
221	225	3	900	2	4	183	24	0.11	0.03
						107	22	0.04	0.04
						111	24	0.05	0.03
216	250	3	850	2	5	298	50	0.11	0.07
						263	30	0.16	0.03
						384	19	0.18	0.02
218	250	3	900	2	6	408	7	0.21	0.0
						391	5	0.20	0.0
						362	8	0.18	0.0
219	250	3	925	2	6	225	20	0.13	0.03
						227	14	0.12	0.02
						238	23	0.14	0.03

Activation of PAN-Based Carbon Fibers and Composites.

A further objective of the work during this period has been to activate PAN-based carbon fibers and PAN based carbon fiber composites in order to produce composites with wider pore size distributions than the petroleum pitch based fibers that have been used so far. PAN-based Fortafil P-200 composites were supplied by ORNL. The composites were first activated in steam at 850°C at the CAER. However, the surface areas developed in the PAN composites were very low, Table 4. The mechanical strength of the composites was also low, and they were extremely weak after burnoff to 29%. It is believed that the PAN fibers had been heat treated to a temperature in excess of 1000°C prior to incorporation into the composites, which would explain the low response to activation. If the fibers are relatively inert, the binder will be preferentially activated which could account for the poor strength.

New PAN fibers were obtained from Dr. Novis Smith with RK Carbon. These fibers had not been heat treated above 600°C. The fibers were carbonized in nitrogen at 800-850°C and subsequently steam activated at temperatures from 800-877°C. Carbonization resulted in yield loss of 15%. Steam activation to burnoffs from 15-95% at temperatures of 800 and 877 respectively produced very low surface areas. The surface area was only 149 m^2/g at a 40% burnoff, Table 3. The high weight loss is attributed to external burning of the carbon fibers, and not micropore development. In future runs, carbonization and activation will be performed at temperatures from 600- 700°C.

Table 3: Activation of PAN fibers by steam activation

Sample#	Carboniz.		Activation		Burnoff	Surface area (m^2/g)		Pore vol	
	T(°C)	t(hr)	T(°C)	t(hr)	(wt%)	BET	mesopore	micro	meso
222	800	1	850	1	40	149	10	0.21	0.05
229	700	2	750	4	46				

CO_2 Working capacity

It has already been reported that the activated composites have the ability to separate mixtures of CO_2 and CH_4. The optimum separation was found for samples with a burnoff of 8-10%, Figure 3.

To further investigate this separation, we have measured CO_2 working capacities of the composites, using a test similar to the standard test for butane working capacity. Interestingly, the specimen with the highest CO_2 working capacity has a burnoff of only 9% and a BET surface area of 484 m^2g^{-1}, while a sample with 25% burnoff and a surface area of 850m^2g^{-1} has a significantly lower CO_2 working capacity. The relationship between pore size distribution and CO_2 working capacity is not so straightforward, but again the samples with narrow pore size distribution show the highest CO_2 working capacity. These results are in excellent agreement with our earlier reported results for the separation of CO_2 from CH_4. The maximum CO_2 working capacity occurs with samples at a burnoff of around 10% which is also the optimum burn-off for the separation of CO_2 and CH_4.

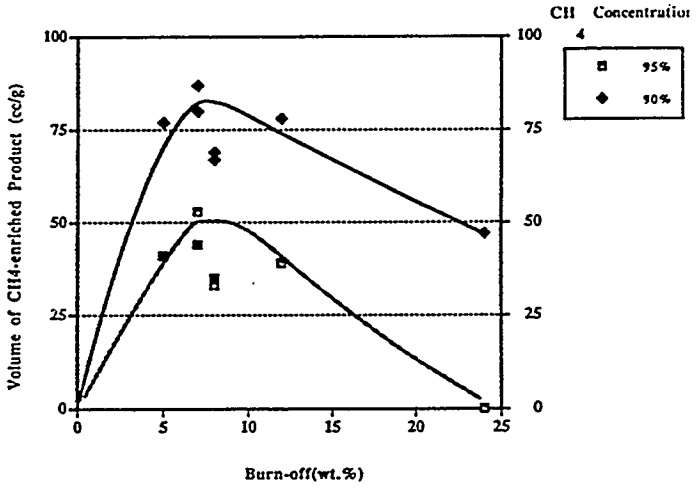

Figure 3: Volume of CH_4 produced at 95 and 90% concentration from a mixture of 75% CH_4/25% CO_2.

Butane working capacity, BWC

The purpose of the BWC test is to investigate how the adsorptive properties of the activated composites compare to those of commercial granular carbons that are currently used in ELCD devices. These commercial carbons have a BWC of around 15 g/100 mL. Two samples were tested, SA182 with a surface area of 850m^2g^{-1} and SA 177 with a surface area of 1411 m^2g^{-1}. The results are shown in Table 4. Sample SA 177 had about twice the BWC of 182, which corresponds to its higher surface area. The same sample had a high uptake of butane (40% by weight and 10% by volume: note the low volumetric capacity, due to the low composite density). However, the retentivity of butane was high, (4.5% by volume) giving a butane working capacity of only 5.5 g/100mL. This is significantly lower than that of the commercial carbons including the wood-based sample, Te-7, produced at CAER, shown in Table 4. One reason for the low performance of the pitch based carbon fiber composite is the narrow pore size distribution that gives high retentivity of butane.The average pore size for wood based carbons is usually around 20-50A, allowing much more effective desorption. The pitch based activated carbon fibers are therefore not suitable for butane or gasoline vapor storage. However, if the composites were made from a different fiber, like PAN or rayon, the butane working capacity should be much higher as these fibers would develop wider micropores.

Table 4: Butane working capacities of activated carbon.

Sample	SA177[1]	SA182[1]	TE-7[2]
Apparent density(g/cc)	0.249	0.29	0.27
Burn-off (%)	56.0	25.0	-
BET surface area(m^2g^{-1})	1411.0	850.0	1569.0
Average pore size(A)	9.6	7.4	15.0
Butane working capacity,W/W(%)	22.1	9.4	39.8
Butane working capacity,W/V (g/100mL)	5.5	2.8	10.7

1: activated composites, 2: wood based extrudate, prepared in-house

Adsorption of Herbicides from Water

The breakthrough plot for PCP in the carbon fiber composites and a commercial carbon specifically designed for water treatment (Norit Hydarco) is shown in Figure 4[13]. The breakthrough time for the composite was found to be almost 1400 column volumes, whereas it was closer to 150 column volumes for the granular carbon - a factor of about nine. At first sight, the difference in the performance of these carbons is surprising, since they are of comparable surface area. However, we believe that the superior performance of the carbon fiber composite is due to the narrow diameter of the fibers (15 - 20 μm) that essentially minimizes mass transfer limitations, and allows much faster rates of adsorption (and desorption) than is possible over large granules. A second factor is that the composites have a very open architecture (approximately 90% is free volume), which means that the contacting fluid enjoys free access to the adsorbent surfaces. Essentially, the composite can be viewed metaphorically as a situation in which the granules have been "peeled open" to allow the adsorbent to readily access all of the inner adsorbent surface, which can otherwise only be approached by diffusion through an extensive pore network.

Liquid Phase Pressure Drop of Activated Composites

One of the most important parameters when considering a carbon for water treatment applications is the pressure drop that is developed over the adsorbent. We have previously reported pressure drops for gas flow, and in this report we have determined the pressure drop developed due to the flow of a liquid. The pressure drop over a 12.5 cc bed of composite at different flow rates of water is shown in Figure 5 along with data from the literature on pressure drop for a granular bed of activated carbon. The composite samples shown have comparable pressure drops to that for the bed of granular carbon, over the range of flow for which it was tested. The differences in pressure drop for the two composite specimens are due to differences in the density of the precursor composite.

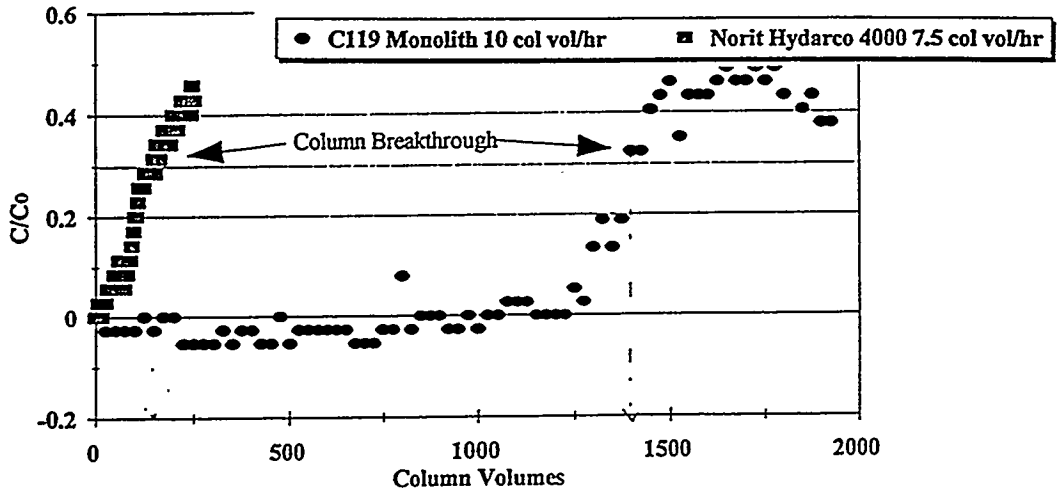

Figure 4: Adsorption of the herbicide sodium pentachlorophenolate, PCP from water for a composite sample and a commercial granular activated carbon.

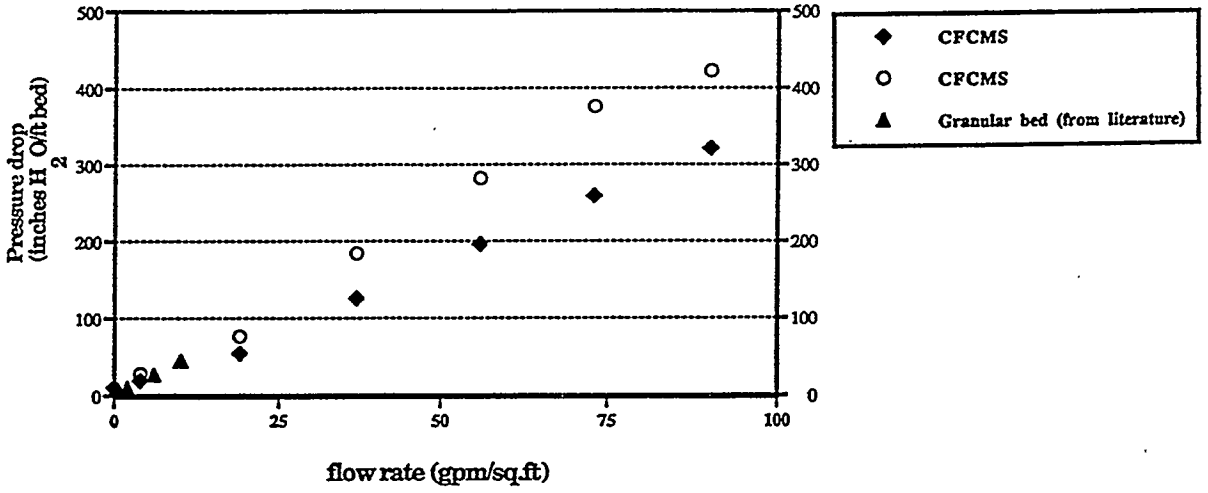

Figure 5: Pressure drop of water over composite samples

REFERENCES

1) K. OKUDA, Petrotech, 5(1) (1982) 37.
2) Y. MATSUMURA, Seikiyu Gakaishi, 30(5) (1987) 291.
3) M. W. THWAITES, M. L. STEWART, B. E. McNEESE, and M. SUMNER, Fuel Proc.Tech.34 (1993)137.
4) M.SUZUKI, Proc. Biennial Carbon Conference, Buffalo (1993)
5) F. DERBYSHIRE, M. JAGTOYEN, Y. Q. FEI and G. KIMBER, Am. Chem. Soc., Div. Fuel Chem. Preprint, 39(1) (1994) 113-120.
6) T. D. BURCHELL, J. W. KLETT AND C. E. WEAVER, Proceedings of the Ninth Annual Conference on Fossil Energy Materials, Fossil Energy AR&TD Materials Program, for USDOE,Oak Ridge National Laboratory, May 16-18, (1995) 447-457.
7) M. JAGTOYEN, F. DERBYSHIRE, G. KIMBER, Y. Q. FEI, Proceedings of the Ninth Annual Conference on Fossil Energy Materials, Fossil Energy AR&TD Materials Program, for USDOE, Contract DE-ACo5-84OR21400,Oak Ridge National Laboratory, May 16-18(1995) 457-467.
8) M. JAGTOYEN, F. DERBYSHIRE, N, CUSTER, T. BURCHELL, 1994 Spring Meeting, Materials Research Society, San Francisco, April 4-8, 1994,Symposium Proceedings, 344, (1994) 77.
9) T. D. BURCHELL, F. DERBYSHIRE, Y.Q. FEI AND M. JAGTOYEN, C. E. WEAVER, Proceedings of Eighth Cimtec World Ceramics Conference, 6/28, Florence, Italy (1994) 120.
10) G. C. WEI, and J. M. ROBBINS, Ceramic Bull., 64(5) (1985)691.
11) F. DERBYSHIRE, Y.Q. FEI AND M. JAGTOYEN, G. KIMBER, T. D. BURCHELL, C. E. WEAVER,Proceedings of CARBON'94, 3-8 July, Granada, Spain, (1994) 654-5.
12) F. DERBYSHIRE, T. BURCHELL, Y. Q. FEI, M. JAGTOYEN, C. WEAVER, Conference on Applications of Microporous Carbons, The British Carbon Group, 28-29 Sep, Leeds, UK (1994).
13) M. JAGTOYEN, C. LAFFERTY, F. DERBYSHIRE AND G. KIMBER, Proceedings for the Kentucky Water Resources Annual Symposium, Holiday Inn, Lexington, KY, Feb13(1996)41-42.

ACKNOWLEDGEMENTS

The authors wish to acknowledge G. Kimber D. Turner and C. Lafferty of the CAER, the Commonwealth of KY and Rod Judkins of the ORNL for financial support of this work. This work is sponsored by the Fossil Energy AR&TD Materials Program, US Department of Energy, under contract no.SC19X-SN719C.

STABILITY OF SOLID OXIDE FUEL CELL MATERIALS[1]

T. R. Armstrong, J. L. Bates, G. W. Coffey, L. R. Pederson,
P. J. Raney, J. W. Stevenson , W. J. Weber, and F. Zheng

Pacific Northwest National Laboratory
P.O. Box 999
Richland, WA 99352

Chromite interconnection materials in an SOFC are exposed to both highly oxidizing conditions at the cathode and to highly reducing conditions at the anode. Because such conditions could lead to component failure, we have evaluated thermal, electrical, chemical, and structural stabilities of these materials as a function of temperature and oxygen partial pressure. The crystal lattice of the chromites was shown to expand for oxygen partial pressures smaller than 10^{-10} atm, which could lead to cracking and debonding in an SOFC. Highly substituted lanthanum chromite compositions were the most susceptible to lattice expansion; yttrium chromites showed better dimensional stability by more than a factor of two. New chromite compositions were developed that showed little tendency for lattice expansion under strongly reducing conditions, yet provided a good thermal expansion match to other fuel cell components. Use of these new chromite interconnect compositions should improve long-term SOFC performance, particularly for planar cell configurations.

Thermodynamic properties of substituted lanthanum manganite cathode compositions have been determined through measurement of electromotive force as a function of temperature. Critical oxygen decomposition pressures for Sr and Ca-substituted lanthanum manganites were established using cells based on a zirconia electrolyte. Strontium oxide and calcium oxide activities in a lanthanum manganite matrix were determined using cells based on strontium fluoride and calcium fluoride electrolytes, respectively. The compositional range of single-phase behavior of these ABO_3-type perovskites was established as a function of A/B cation ratios and the extent of acceptor doping. Before this work, very little thermodynamic information was in existence for substituted manganite compositions. Such information is needed to predict the long-term stability of solid oxide fuel cell assemblies.

INTRODUCTION

Acceptor-doped lanthanum chromites are used as the electrical interconnect in solid oxide fuel cells (SOFC) operating at high temperatures because of their high electrical conductivity, chemical stability in oxidizing and reducing environments, high thermal conductivity, and good thermal expansion match to other fuel cell materials.[1] Calcia-substituted yttrium chromite also show promise for this purpose.

The electrical interconnect in an SOFC is exposed to both oxidizing conditions at the air electrode and reducing conditions at the fuel electrode. In a reducing environment, many

[1] Research sponsored by the U. S. Department of Energy, Fossil Energy AR&TD Materials Program. Pacific Northwest National Laboratory is operated by Battelle for the U. S. Department of Energy under Contract DE-AC06-76RLO 1830.

chromite compositions undergo a lattice expansion.[2-6] The extent of this lattice expansion depends on several factors, including oxygen partial pressure, temperature, and dopant concentration. The observed expansion is well-correlated with the defect structure of the chromites, particularly the reduction of Cr^{4+} to Cr^{3+} and the concomitant formation of oxygen vacancies. In the present work, we show that small additions of both acceptor and donor substitutions can be used to control the magnitude of this dimensional instability of interconnect materials when exposed to reducing conditions.

Acceptor-doped lanthanum manganite perovskites are used as the cathode in SOFCs due to high electrical conductivity in oxidizing atmospheres, high electrocatalytic activity for the reduction of molecular oxygen to oxygen anions, and good thermal expansion match to other fuel cell components.[1] Interactions between the cathode and the electrolyte are among the causes of long-term performance losses in SOFCs, the extent of which may be predicted from thermodynamic properties of fuel cell components.[7,8] While undoped lanthanum manganite has been well-studied, very little thermodynamic information on doped compositions is known. In this study, solid electrolyte galvanic cells were utilized to evaluate the chemical activity of strontium oxide in doped lanthanum manganite and to determine the free energy of formation of doped lanthanum manganite from the base oxides.

EXPERIMENTAL METHODS

Doped lanthanum and yttrium chromite powders were prepared using the glycine-metal nitrate combustion synthesis method, with a stoichiometric glycine to nitrate ratio.[9] The powders were calcined at 650°C to remove any residual carbon, coarsened at 1000°C, uniaxially pressed into bars (55 MPa), and isostatically pressed (140 Mpa). Similar procedures were followed to prepare doped lanthanum manganite samples.

Dilatometry measurements were used to evaluate dimensional changes in oxidizing and reducing environments at 800, 900, and 1000°C. The oxygen partial pressure was controlled in the 10^{-5} to 10^{-18} atm. range using a buffered carbon dioxide/hydrogen gas system equipped with mass flow controllers. The initial oxygen stoichiometry of each of the chromite compositions was determined by potentiometric titration, where the sample was first dissolved in a concentrated solution of sulfuric acid and vanadium sulfate, and then titrated with ferrous ammonium sulfate.[10] Changes in oxygen stoichiometry on heating were determined thermogravimetrically.

Galvanic cells were utilized to determine the activity of strontium and calcium oxide in doped lanthanum manganite cathode materials and to evaluate the critical oxygen

decomposition pressure for these materials. Strontium oxide activities were evaluated using the cell:

$$O_2, Pt \mid SrO, SrF_2 \parallel SrF_2 \parallel (La,Sr)MnO_3, SrF_2 \mid Pt, O_2$$

For calcium-doped lanthanum manganite compositions, calcium fluoride served as the electrolyte rather than strontium fluoride. Such cells have been found to yield accurate thermochemical data, although establishment of equilibrium is slow.[11]

Critical oxygen decomposition pressures were also measured as a function of temperature using the galvanic cell approach for strontium-doped lanthanum manganite compositions. Yttria-stabilized zirconia served as the electrolyte in the cell:

$$O_2, Pt \parallel ZrO_2 (+8Y_2O_3) \parallel (La,Sr)MnO_3 \mid Pt$$

Small zirconia tubes (5mm dia. x 50 mm length) were fabricated by slip casting. Two areas were platinized on the surface of the tubes, one of which served as an oxygen pump while the other served as an oxygen sensor. The zirconia tubes were sealed to an alumina support using an alumina-based cement. Oxygen was electrochemically pumped from the small zirconia tubes to a residual oxygen pressure of less than 10^{-22} atm at the beginning of each test. The oxygen pump was then turned off and the system allowed to achieve a steady state oxygen partial pressure.

RESULTS AND DISCUSSION

Dimensional Stability of Chromite Interconnects

In a reducing environment encountered at the fuel electrode (below $\approx 10^{-10}$ atm oxygen partial pressure), lattice oxygen vacancies may be formed in chromite interconnects.[2-6] Accompanying the formation of oxygen vacancies are changes in thermal expansion behavior, loss of mechanical strength, and a lowering in the electrical conductivity in these materials. In this work, we have characterized the extent of isothermal linear expansion as a function of oxygen partial pressure for a wide range of chromite compositions to better understand and control these effects. A series of acceptors, donors, and isovalent dopants have been added to base compositions and their stability evaluated. Multicomponent compositions were developed that show very good dimensional stability over a wide range of oxygen partial pressures and provide a good match to other fuel cell components.

The extent of isothermal linear expansion was found to increase significantly with increases in the extent of strontium substitution for lanthanum in the lanthanum strontium chromites, as shown in Figure 1. Calcium-substituted lanthanum chromites behaved in a manner very similar to the strontium-substituted compositions. Undoped lanthanum chromite showed no tendency to expand under very low oxygen partial pressures, expected since there is no tetravalent chromium present that could be reduced to the trivalent state. The onset of lattice expansion for doped compositions was approximately 10^{-10} atm oxygen. A good correlation was developed between the extent of isothermal linear expansion and oxygen stoichiometry, established through thermogravimetry and potentiometric titration measurements.

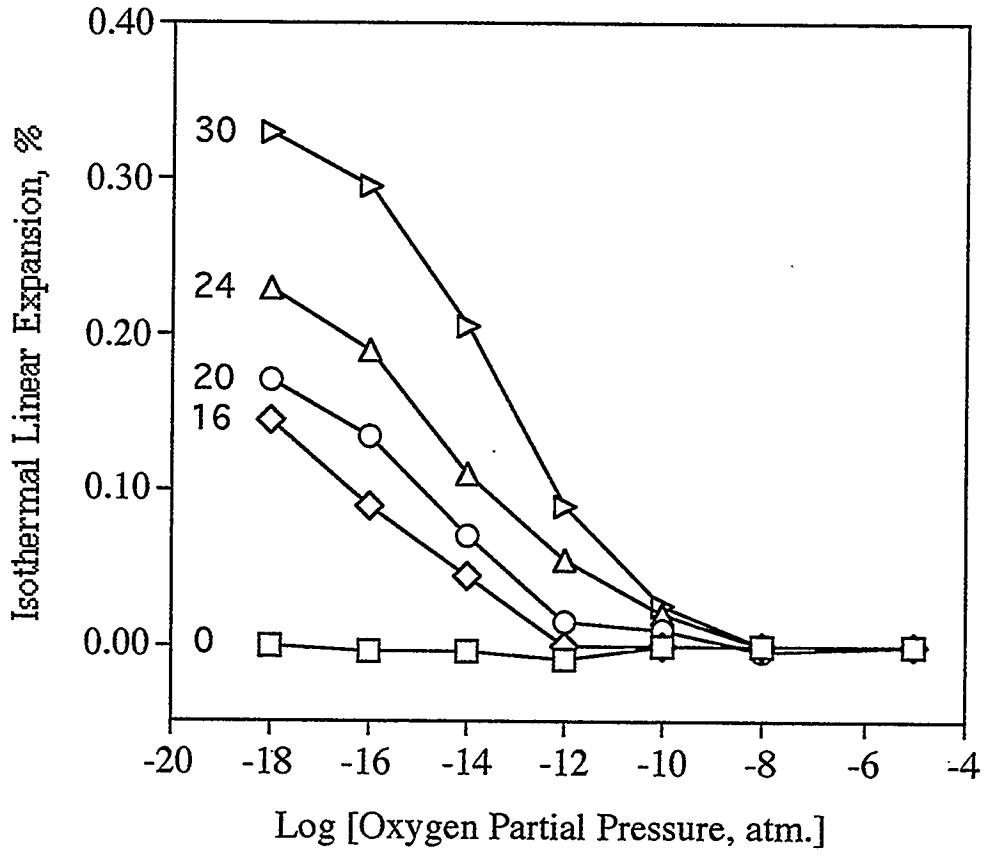

Figure 1. Isothermal linear expansion of lanthanum strontium chromite compositions at 1000°C as a function of the oxygen partial pressure. The indicated values refer to the percent of strontium that has been substituted for lanthanum in the structure.

Lattice dimensions of yttrium calcium chromites also expanded when exposed to reducing environments. The extent of expansion was approximately 40 percent less than the corresponding lanthanum chromites, however. Isothermal linear expansion for several yttrium calcium chromite compositions are given in Figure 2 as a function of oxygen partial pressure at 1000°C. The onset of isothermal linear expansion moved to higher oxygen partial pressures for more highly substituted yttrium chromite compositions. Sample expansion was dependent on not only the concentration of the acceptor dopant (Ca^{2+}) but also on the formation of a secondary phase, $CaCrO_4$, which formed in compositions containing more than 25 mole percent calcium oxide. The unit cell dimensions of yttrium chromite compositions are approximately 6 percent smaller than corresponding lanthanum chromites, due primarily to the smaller size of the yttrium ion.

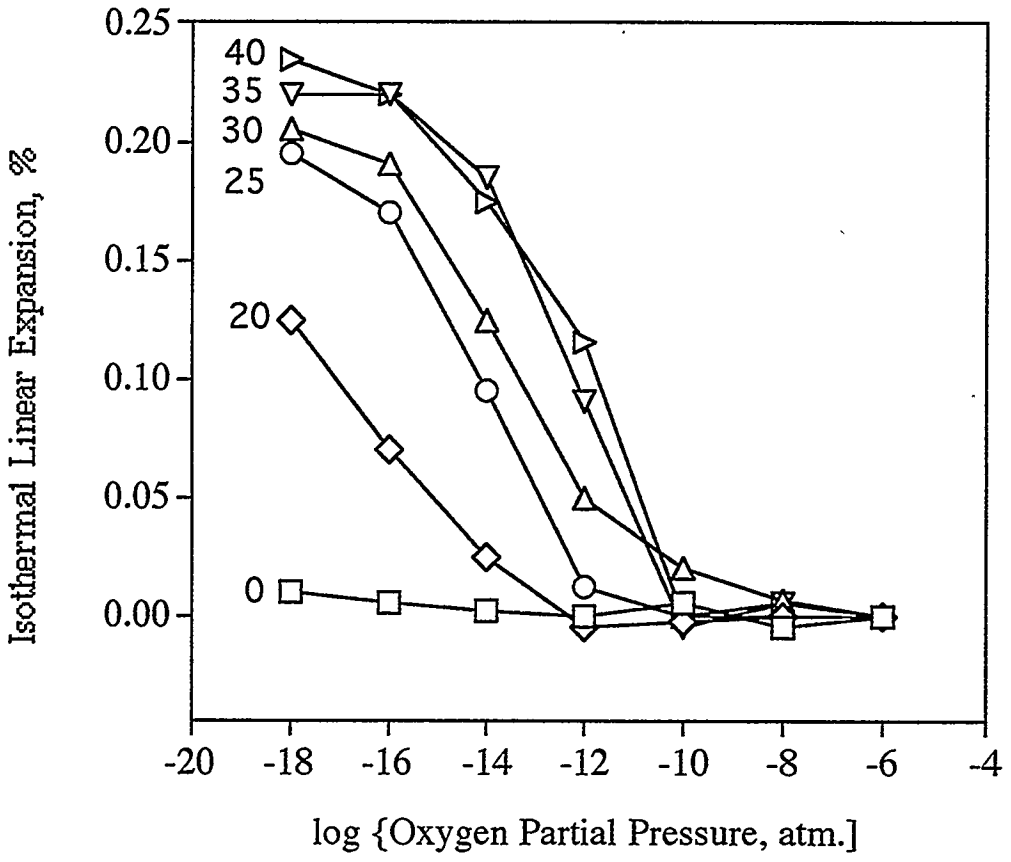

Figure 2. Isothermal linear expansion of yttrium calcium chromite compositions at 1000°C as a function of oxygen partial pressure.The indicated values refer to the percent of calcium that has been substituted for yttrium in the structure.

Interconnect compositions containing various donor, acceptor, and isovalent dopants were prepared as part of an effort to control the dimensional instability of these materials in reducing environments. Donor dopants were expected to be the most effective, by suppressing the initial concentration of Cr^{4+} in the chromite lattice that could be eventually reduced to Cr^{3+}. Acceptor dopants were also found to be quite effective. Through doping on both the A- and B-sites of these ABO_3 perovskites, compositions were developed that showed little tendency to expand under conditions expected at the fuel electrode. Isothermal linear expansion behavior for two of these compositions are given in Figure 3; included also in Figure 3 are results for undoped yttrium chromite and 30 mole percent calcia-substituted yttrium chromite. The tailored chromite compositions retained properties of high electrical conductivity as well as a good thermal expansion match to other fuel cell components.

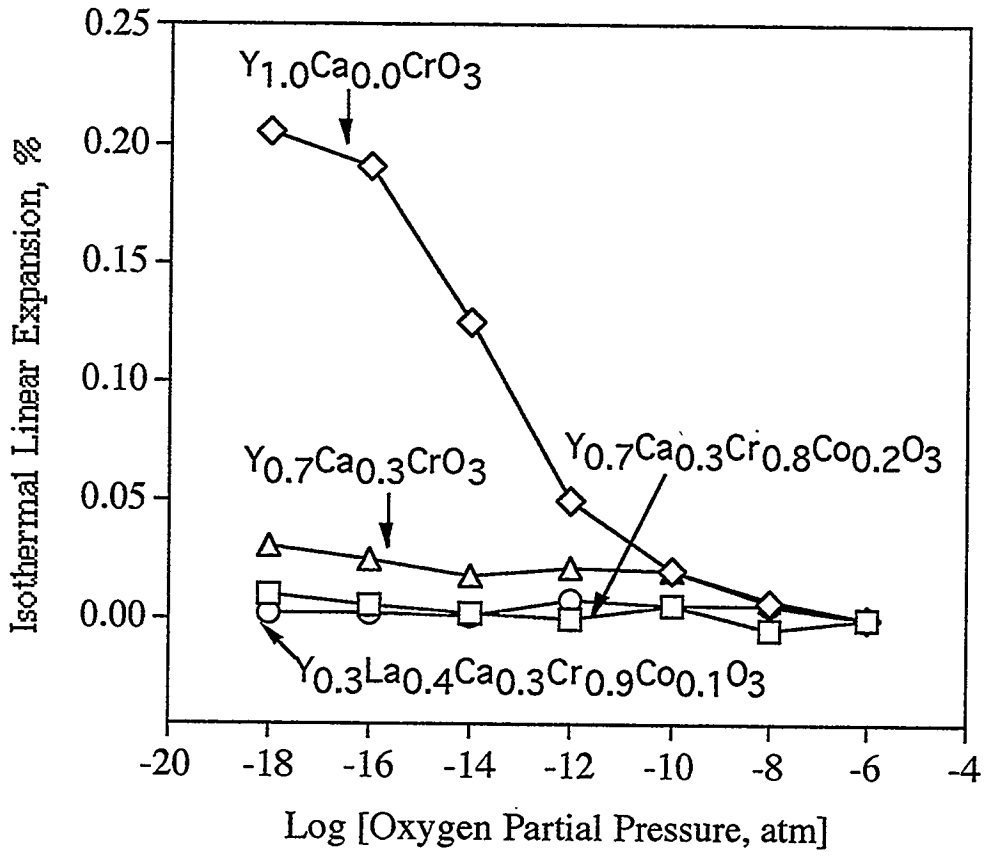

Figure 3. Isothermal linear expansion of chromite interconnection compositions that show little tendency to expand under reducing conditions typical of the fuel electrode side of a fuel cell. Results for undoped yttrium chromite and for 30 mole percent calcium-substituted yttrium chromite are shown for comparison.

Thermochemical Properties of Lanthanum Manganite Cathodes

Thermodynamic parameters for doped lanthanum manganite cathode compositions were established as a function of temperature using the galvanic cell approach. Such information is needed to predict the long-term stability of materials and interfaces in SOFCs. Strontium and calcium oxide activities and critical oxygen decomposition pressures were determined as a function of temperature using cells constructed with strontium fluoride and calcium fluoride electrolytes, respectively. The relation between strontium oxide activity in a doped lanthanum manganite matrix and cell voltage is given by

$$E\ (\text{volts}) = RT/2F \ln [a(\text{SrO in sample})/a(\text{SrO in reference})] \quad (1)$$

$$\Delta G^\circ = -RT \ln a(\text{SrO}) \quad (2),$$

where R is the gas constant, F is the Faraday constant, and T is temperature, K. The free energy of formation for strontium oxide in several substituted lanthanum manganite compositions is given in Figure 4 as a function of temperature. These materials become progressively less stable as the extent of strontium substitution is increased. These results predict that lanthanum oxide will be displaced by the addition of excess strontium oxide in the manganite structure, confirmed by extensive characterization of phase relations in this system by x-ray diffraction. The formation of a separate lanthanum oxide phase is to be avoided, due to its tendency to readily hydrate and swell.

Critical oxygen decomposition pressures determined by zirconia-based galvanic cell methods showed a lowering in stability of the lanthanum manganites with increased temperature and with increased levels of strontium substitution for lanthanum, as shown in Figure 5. These decomposition pressures correspond to the reaction:

$$La_{1-x}Sr_xMnO_3(s) = (1-x/2)La_2O_3(s) + x\ SrO + MnO(s) + 1/4\ O_2(g) \quad (3).$$

Substituted lanthanum manganites decomposed at oxygen partial pressures one to two orders of magnitude higher than the unsubstituted lanthanum manganite at temperatures typical of an operating SOFC. Unlike galvanic cells based on alkaline earth fluoride electrolytes, thermodynamic equilibrium was established very rapidly in zirconia-based galvanic cells - within an hour in most cases compared to days with fluoride electrolytes. The principal disadvantage is the requirement for a virtually perfect seal between the electrolyte and base.

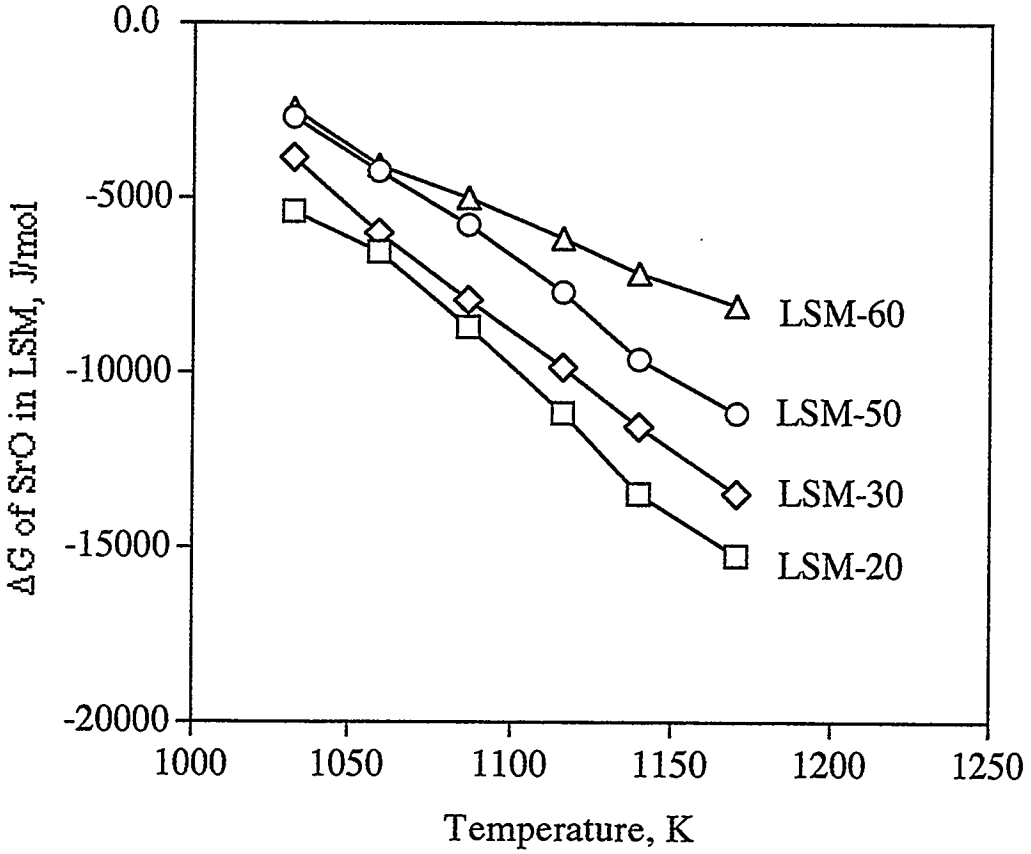

Figure 4. Free energy of formation for strontium oxide substitution in doped lanthanum manganite cathode compositions as a function of temperature, determined using the galvanic cell approach.

Phase relationships in the lanthanum manganite system has been investigated, with the purpose of establishing the compositional range of single-phase behavior. Series of samples where the A/B cation ratio was varied from 0.9 to 1.1 were prepared, heated to 1450°C, quenched into an oil or water bath, and examined by x-ray diffraction. Single phase perovskites were found for A/B cation ratios varying from 0.98 to 1.00 for all levels of strontium substitution for lanthanum. A-site enriched compositions typically contained lanthanum oxide as a second phase, which is easily hydrated to form the hydroxide. B-site enriched compositions contained lanthanum strontium manganite spinel phases plus Mn_3O_4 for compositions with an A/B cation ratio smaller than 0.98. The presence of either the spinel phase or manganese oxide is not particularly problematic. Impedance spectroscopy measurements showed that excess manganese oxide actually improved the electrocatalytic

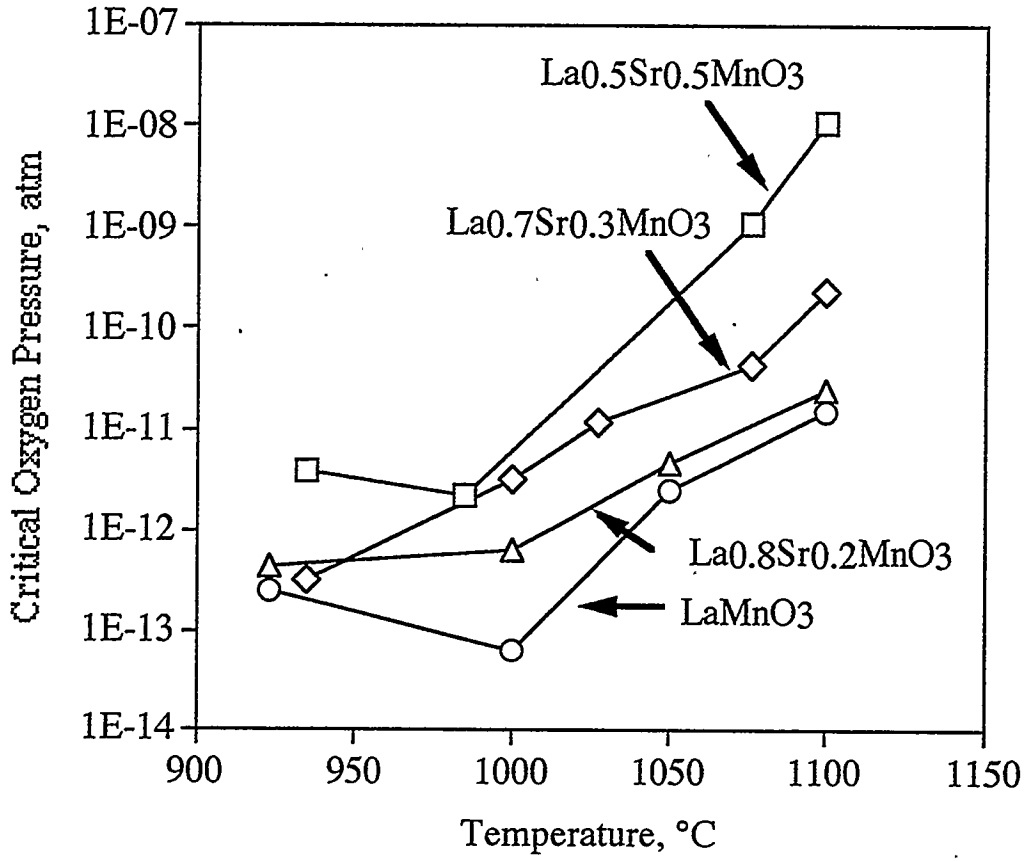

Figure 5. Critical oxygen decomposition pressure for lanthanum manganite compositions versus temperature determined by the galvanic cell method.

activity of the cathode composition. In consideration of ease of sintering and overall phase stability, an A/B cation ratio of 0.98 appears to be optimum for the lanthanum strontium manganite system.

SUMMARY

The dimensional instability of lanthanum and yttrium chromite interconnect materials has been evaluated as a function of oxygen partial pressure and temperature. Highly substituted lanthanum chromites were the most susceptible to lattice expansion under reducing conditions. Corresponding yttrium chromite compositions were dimensionally more stable by more than a factor of two. New chromite compositions were developed that showed little tendency for lattice expansion even under severely reducing conditions, while retaining high electrical conductivity and a good thermal expansion match to other fuel cell components.

Thermodynamic properties of substituted lanthanum manganite cathode materials have been evaluated using the galvanic cell approach. Activities of strontium and calcium oxide in lanthanum manganite were determined using corresponding fluoride electrolytes, while critical oxygen decomposition pressures were determined using zirconia electrolytes. The thermodynamic stability of these materials was shown to decrease with the degree of A-site substitution. Such thermodynamic information is needed to predict the long-term stability of fuel cell assemblies.

REFERENCES

1. N. Q. Minh and T. Takahashi, *Science and Technology of Ceramic Fuel Cells* (Elsevier, Amsterdam, 1995).

2. W. J. Weber, C. W. Griffin and J. L. Bates, *J. American Ceramic Society* 70, 265 (1987).

3. M. M. Nasrallah, J. D. Carter, H. U. Anderson, and R. Kroc, in *Proc. 2nd Int. Symp. Solid Oxide Fuel Cells,* Athens, Greece, eds. F. Grosz, P. Zegers, S. C. Singhal, and O. Yamamoto (Commision of the European Communities, Luxembourg, 1991) p. 637.

4. G. F. Carini, H. U. Anderson, D. M. Sparlin, and M. M. Nasrallah, *Solid State Ionics* 49, 233 (1991).

5. T. R. Armstrong, J. W. Stevenson, P. E. Raney, and L. R. Pederson, in *Fuel Cell Seminar Abstracts* San Diego, CA (Courtesy Associates, 1994) p. 105.

6. T. R. Armstrong, J. W. Stevenson, L. R. Pederson, and P. E. Raney, in *Proc. 4th Int. Symp. Solid Oxide Fuel Cells*, Yokohama, Japan, ed. S. G. Singhal (The Electrochemical Society, Pennington, NJ 1995) p. 944.

7. H. Yokokawa, N. Sakai, T. Kawada, and M. Dokiya, *Solid State Ionics* 52, 43 (1992).

8. H. Yokokawa, T. Horita, N. Sakai, T. Kawada, and M. Dokiya, *Solid State Ionics* 78, 203 (1995).

9. L.A. Chick, L.R. Pederson, G.D. Maupin, J.L. Bates, L.E. Thomas, and G.J. Exarhos, *Materials Letters* 10, 6 (1990).

10. R. Nadalin and W. Brozda, *Analytica Chimica Acta* 28, 282 (1963).

11. C. B. Alcock, *High Temperature Science* 28, 183 (1990)

12. R. Hildrum, M. Brustad, W. Changshen, and O. Johannesen, *Materials Research Bulletin* 29, 851 (1994).

PROTON-CONDUCTING CERATE CERAMICS[1]

L. R. Pederson , G. W. Coffey, J. L. Bates, and W. J. Weber

Pacific Northwest National Laboratory
P.O. Box 999
Richland, WA 99352

Single-cell solid oxide fuel cells were constructed using strontium cerate as the electrolyte and their performance tested. Like certain zirconates, hafnates, and tantalates, the cerate perovskites are among a class of solid electrolytes that conduct protons at elevated temperatures. Depending on the temperature and chemical environment, these ceramics also support electronic and oxygen ion currents. A maximum power output of ≈100 mW per cm^2 electrolyte surface area was obtained at 900°C using 4% hydrogen as the fuel and air as the oxidant.

A series of rare earth/ceria/zirconia were prepared and their electrical properties characterized. Rare earth dopants included ytterbia, yttria, terbia, and europia. Ionic conductivities were highest for rare earth/ceria and rare earth zirconia compositions; a minimum in ionic conductivity for all series were found for equimolar mixtures of ceria and zirconia.

Cerium oxysulfide is of interest in fossil energy applications because of its high chemical stability and refractory nature. An alternative synthesis route to preparing cerium oxysulfide powders have been developed using combustion techniques.

INTRODUCTION

Protonic conductivity has been observed in both cerate and zirconate ceramics including doped $SrCeO_3$, $BaCeO_3$, $CaZrO_3$, $SrZrO_3$, and $BaCeO_3$.[1-3] The presence of water is necessary for protonic conduction; water reacts with oxygen vacancies to produce sites for conduction.[1] Depending on temperature and on the partial pressures of oxygen and water, protons, oxygen ions, and electrons contribute to the overall current.[4,5] In this work, we have constructed single-cell SOFC assemblies using Yb-doped $SrCeO_3$ as the electrolyte, and evaluated cell performance. While ceria-based compositions generally give higher overall conductivities than the zirconates, the zirconates are chemically more stable. To take advantage of the good conductivity properties of the cerates and chemical durability of the zirconates, ternary rare earth/zirconia/ceria compositions were also prepared and electrical properties examined.

---

[1] Research sponsored by the U. S. Department of Energy, Fossil Energy AR&TD Materials Program. Pacific Northwest National Laboratory is operated by Battelle for the U. S. Department of Energy under Contract DE-AC06-76RLO 1830.

Certain rare earth oxysulfides are well known for their refractory nature and good stability towards metallic melts and slags.[6,7] Cerium oxysulfide, Ce_2O_2S, has been used to lower the concentration of sulfur in steel and to remove sulfur from gaseous fuels through an equilibrium involving cerium oxide, cerium oxysulfide, and sulfur.[7] The stability of this material under coal slagging conditions has not been tested to date, partially due to difficulty in preparing appropriate test coupons. We have applied combustion synthesis techniques to preparing cerium oxysulfides and are examining sintering characteristics.

STRONTIUM CERATE-BASED FUEL CELL

Because the strontium cerates conduct both protons and oxygen ions, there may be significant advantages in using such materials as the electrolyte in an SOFC.[1-3,5] There are two potential-determining ions rather than one. Water is produced at both the cathode and the anode in an SOFC constructed using a strontium cerate electrolyte. In contrast, water is produced only at the anode in an SOFC that utilizes an oxygen ion-conducting zirconia electrolyte.

The open cell potential of a single-cell SOFC with a strontium cerate electrolyte showed a distinctly non-Nernstian behavior at temperatures greater than ≈500°C, as shown in Figure 1. Porous platinum served as both the cathode and the anode in this test cell. Air was supplied to the cathode in this test, while 4% hydrogen/argon was supplied to the anode. The open cell potential was nearly constant in the temperature range 600 to 900°C. Non-Nernstian behavior is attributed to losses associated with an increased electronic conductivity in this temperature range.[4,5] Higher cell potentials would have resulted if pure hydrogen were used rather than 4% hydrogen; the latter was chosen because the hydrogen concentration is below the lower flammability limit.

Current/voltage curves were determined for cerate-based, single-cell SOFC assemblies. Typical results obtained at 910°C are shown in Figure 2 using a 4% hydrogen/argon fuel and an air oxidant. At low cell currents, the cell potential approached the open cell voltage of Figure 1. A maximum in the cell power of approximately 100 mW/cm^2 was obtained, corresponding to a cell potential of ≈0.5 V. A power level of 80 mW/cm^2 at a cell potential of 0.6 V was sustained for several days with no obvious loss in performance. While open cell potentials remained essentially constant in the temperature range 600 to 900°C, cell power output fell with decreased temperature due to lower ionic conductivities, as expected. However, the electronic contribution to the overall cell current also decreased,[4,5] partially off-setting the effects of lowered ionic conductivity.

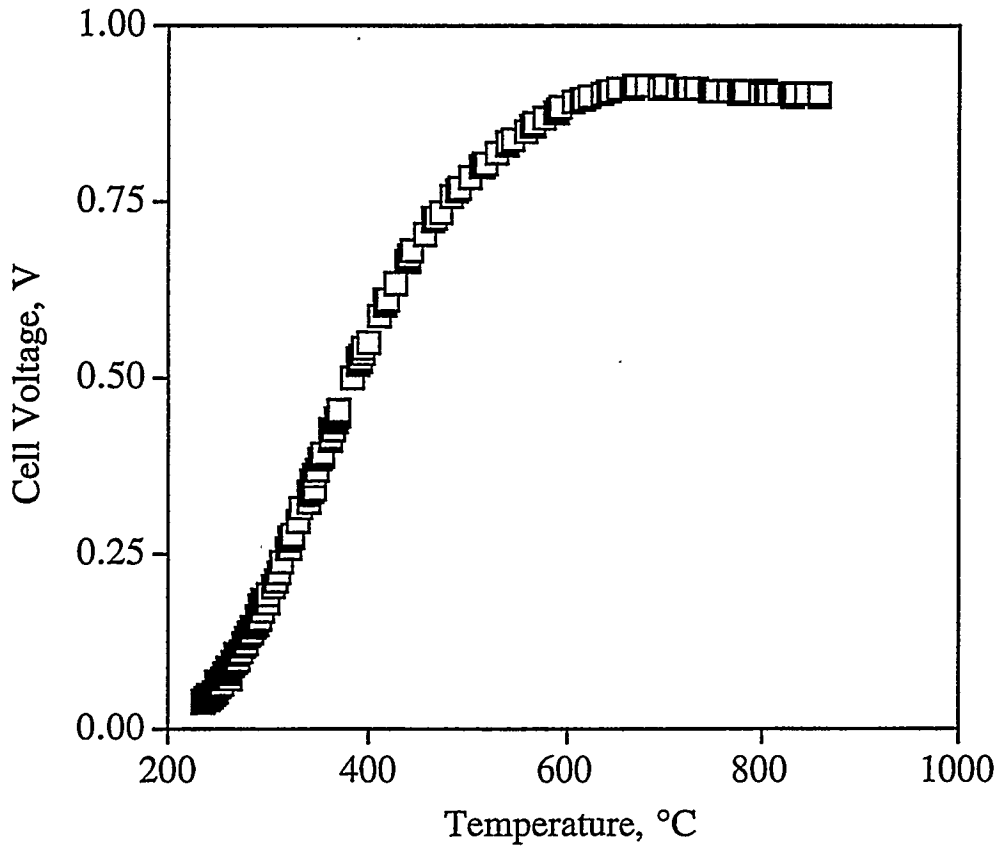

Figure 1. Open cell voltage versus temperature for a single-cell SOFC using a strontium cerate electrolyte. Air was supplied to the cathode and 4% hydrogen/argon was supplied to the anode.

RARE EARTH-ZIRCONIA-CERIA ELECTROLYTES

A series of rare earth/ceria/zirconia compositions were prepared and their electrical and structural properties characterized. The purpose was to attempt to combine the high conductivities associated with cerate compositions with high chemical durabilities associated with the zirconates. The glycine-nitrate combustion synthesis method was used to prepare the ternary rare earth/zirconia/ceria compositions $(MO_{1.5})O_2(ZrO_2)_{0.8-x}(CeO_2)_x$, with M = Yb, Y, Tb, and Eu.[6] For the zirconia/ceria compositions, the chosen dopants all exhibit ionic radii in the trivalent state on an octahedral site that are larger than either tetravalent zirconium or cerium ions, and stabilize the cubic structure. Electrical conductivities were measured using a four-probe, pulsed dc technique with platinum knife-edge contacts at about 25 K intervals. Measurements were made in air, during both heating and cooling cycles.

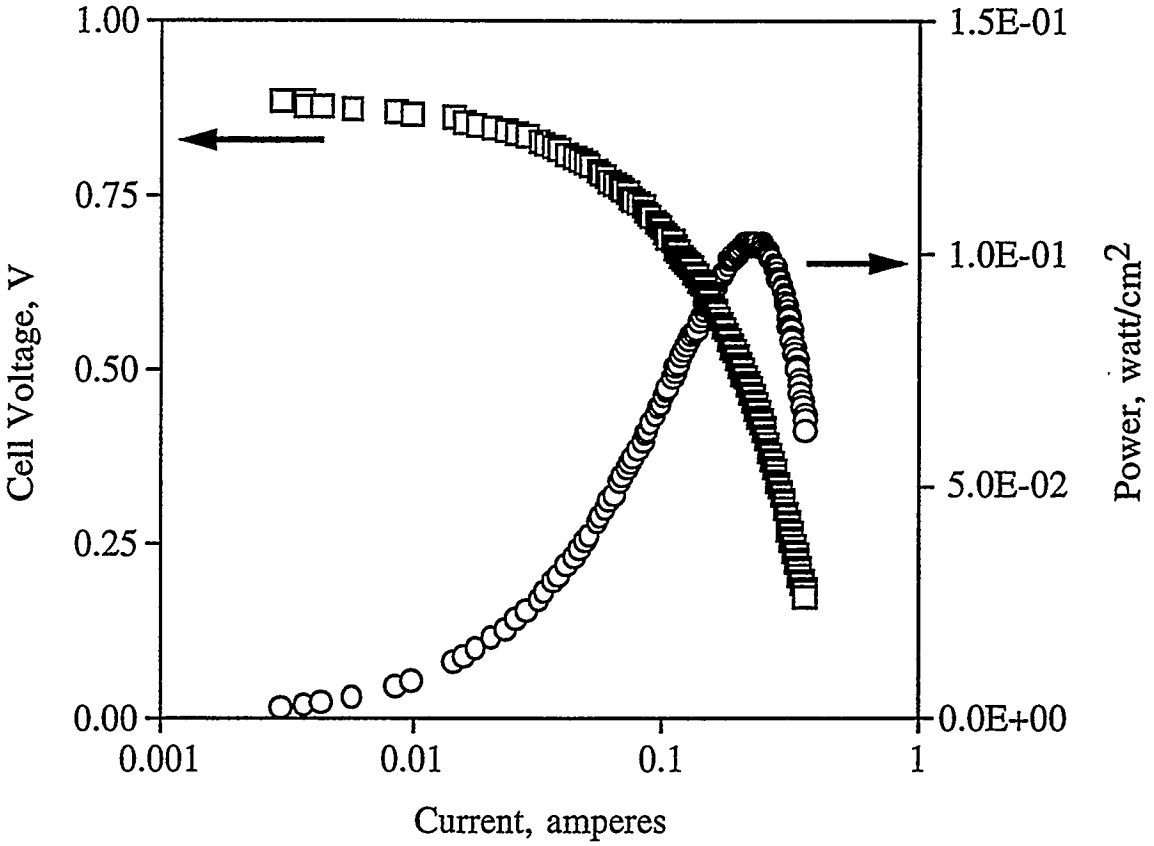

Figure 2. Performance of a single-cell SOFC assembly at 910°C using argon/4% hydrogen as the fuel and air as the oxidant. The open-cell voltage at 910°C was ≈0.9 V.

In all of the compositions tested, the electrical conductivity was found to decrease with increased cerium substitution for zirconium until an equimolar concentration of each was reached (Ce=Zr=0.4). Conductivities increased with increased cerium concentration above that point, with highest conductivities observed for full zirconium replacement by cerium. Conductivities obtained at 1000°C are given in Figure 3. There was no clear trend in conductivity with changes in the ionic radius of the dopant. Lattice parameters increased linearly with the ceria content and with the ionic radius of the dopant, however.

Activation energies for ionic conduction were maximized for equimolar ceria and zirconia contents, as shown in Figure 4. Compositions high in zirconia gave activation energies for ionic conduction higher than analogous compositions high in ceria. While improved chemical durability may well result from the addition of zirconia to cerate ceramics, there appears to be no advantage to such compositions when considering the resultant ionic conductivities.

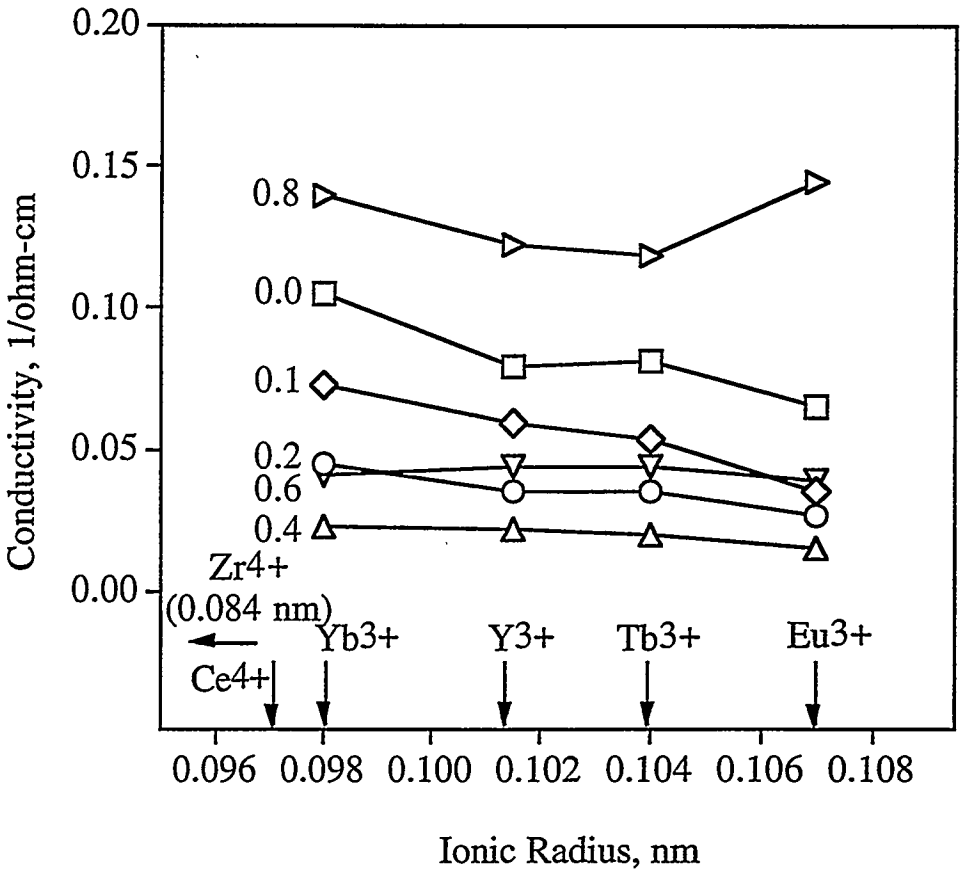

Figure 3. Conductivity of rare earth/zirconia/ceria compositions at 1000°C. Values given are the cerium content in $(MO_{1.5})O_2(ZrO_2)_{0.8-x}(CeO_2)_x$, with M = Yb, Y, Tb, and Eu. A minimum in the conductivity was apparent for an equimolar mixture of ceria and zirconia.

SYNTHESIS OF CERIUM OXYSULFIDE

Cerium oxysulfide is of interest in fossil energy applications because of its expected high stability when exposed to coal slags. The material is typically prepared from the sulfate in flowing hydrogen sulfide at temperatures above 1000°C or by the solid state reaction of cerium oxide and cerium sulfide.[7,8] As traditional synthesis methods are time-consuming and slow, alternate synthesis routes were developed.

Cerium sulfide was precipitated from an aqueous solution of cerium nitrate plus thiourea and triethanolamine. Sulfur is displaced from thiourea to yield urea under these conditions. Thioacetamide was also used with success as the source of sulfur. The cerium sulfide was collected by filtration, washed, and dried in flowing, dry nitrogen. This material was

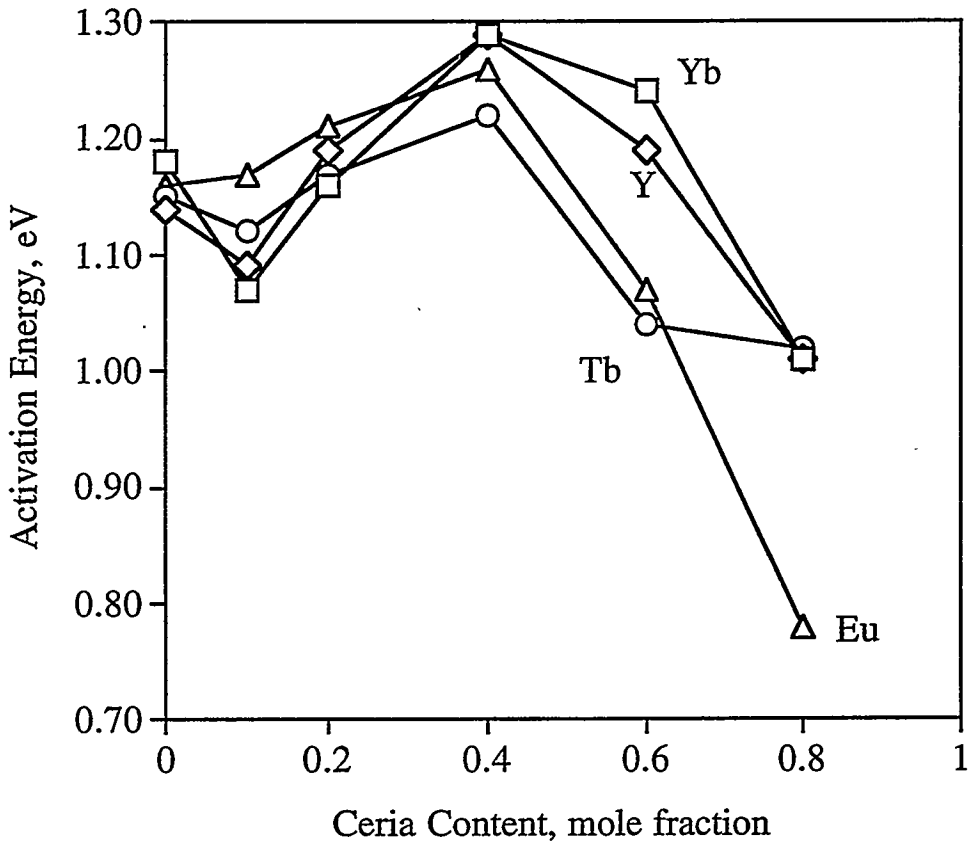

Figure 4. Activation energies for ionic conduction in $(MO_{1.5})O_2(ZrO_2)_{0.8-x}(CeO_2)_x$ compositions as a function of ceria replacement of zirconia. Equimolar zirconia/ceria mixtures resulted in the highest activation energies for each of the dopants.

partially oxidized at 600°C and then converted to the oxysulfide in flowing argon/4 percent hydrogen at 1000°C.

Because of the ease by which the cerium sulfide could be formed in an aqueous solution using thiourea, a combustion synthesis route based on the glycine-nitrate method[6] was utilized, where part of the glycine fuel was replaced with thiourea. Ceric ammonium nitrate, glycine, and thiourea were combined in an aqueous precursor, heated with evaporation to the point of autoignition, and the ash collected. Sulfur was displaced from thiourea prior to combustion, resulting in the formation of fine elemental sulfur particles that partially oxidized during combustion. Precursor mixtures contained a stoichiometric mixture of fuel and oxidant , though the ratio of glycine to thiourea was varied. The combustion reaction yielded finely divided cerium oxysulfide plus cerium sulfate powders.

The cerium oxysulfide plus cerium sulfate powders were pressed into pellets approximately 2 cm. in diameter and 0.2 cm. in thickness uniaxially (50 MPa) and isostatically (140 Mpa). Samples were sintered for 1 hour in the temperature range 1000 to 1650°C in flowing 4% hydrogen/argon or in argon. X-ray diffraction analysis showed only the presence of cerium oxysulfide for sintering temperatures below1400°C, but sintered densities were smaller than 70% of theoretical. Approximately 80% of theoretical density was achieved at a sintering temperature of 1650°C. A sintered density of at least 90% of theoretical is desired for specimens intended for corrosion testing. Samples sintered in argon yielded cerium oxide as a minor component.

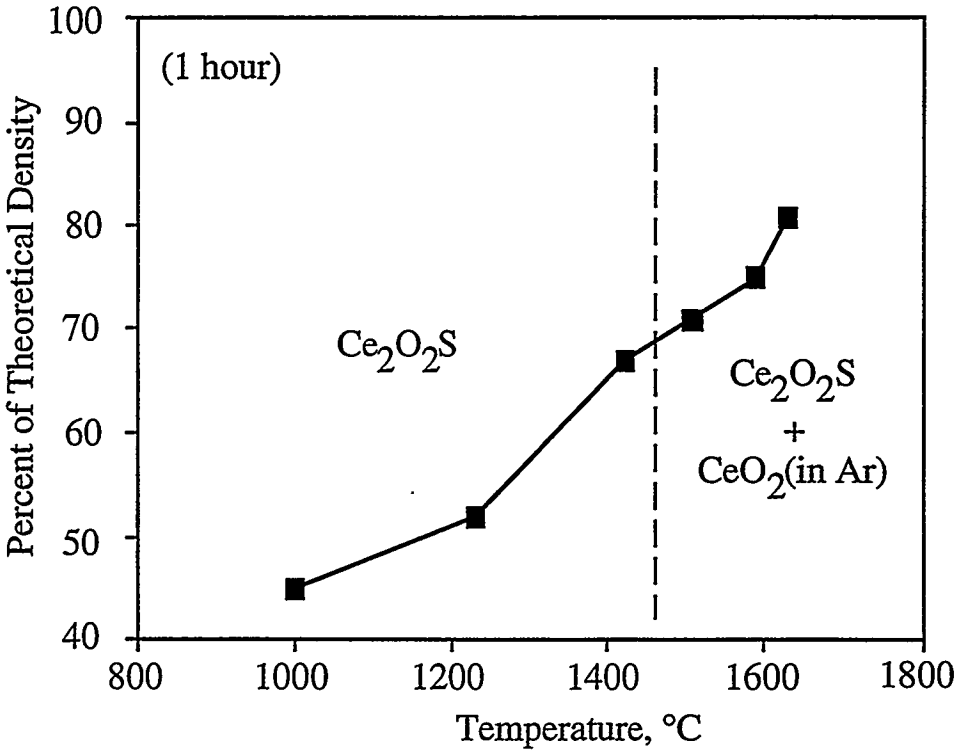

Figure 5. Sintered density versus temperature for cerium oxysulfide, for a sintering time of one hour.

SUMMARY

Single-cell solid oxide fuel cells were constructed using ytterbium-doped strontium cerate as the electrolyte and their performance tested. Using 4% hydrogen as the fuel and air as the oxidant. maximum power output of ≈100 mW per cm^2 electrolyte surface area was obtained at 900°C. Both oxygen ions and protons are potential-determining ions in this electrolyte. Water was produced at both the cathode and at the anode.

A series of rare earth/ceria/zirconia were prepared and their electrical properties characterized. Rare earth dopants included ytterbia, yttria, terbia, and europia. Ionic conductivities were highest for rare earth/ceria and rare earth zirconia compositions; a minimum in ionic conductivity for all series were found for equimolar mixtures of ceria and zirconia.

An alternative synthesis route to preparing cerium oxysulfide powders have been developed using combustion techniques. The powders consisted of a single crystalline phase. Once sintered to full density, these materials are expected to show good chemical durability in the presence of coal slags.

REFERENCES

1. T. Norby, *Solid State Ionics* 40/41, 857 (1990).

2. H. Iwahara, T. Yajima, T. Hibino, and H. Ushida, *J. Electrochem. Soc.* 140, 1687 (1993).

3. N. Bonanos, *Solid State Ionics* 53-56, 967 (1992).

4. I. Kosacki and H. L. Tuller, *Solid State Ionics* 80, 223 (1995).

5. G. W. Coffey, L. R. Pederson, and W. J. Weber, Proc. Mater. Res. Soc. Vol. 369, 395 (1995).

6. L.A. Chick, L.R. Pederson, G.D. Maupin, J.L. Bates, L.E. Thomas, and G.J. Exarhos, *Materials Letters* 10, 6 (1990).

7. W. Krahl and T. Reetz, Materials by Powder Technology PTM-93, ed. F. Aldinger, DGM Informationsges, Oberursel, Germany, p. 563 (1993).

8. R. K. Dwivedi and D. A. R. Kay, *J. Less Common Metals* 102, 1 (1984).

Ceramic Catalyst Materials

A. G. Sault

Fuel Science Department
Sandia National Laboratories
Albuquerque, NM 87185-0710

and

J. Reardon and A. K. Datye

Department of Chemical and Nuclear Engineering
University of New Mexico
Albuquerque, NM 87131

ABSTRACT

This project focuses on the modification of silica and alumina surfaces by titania and hydrous titanium oxide ion-exchange films, and the use of these modified materials as supports for MoS_2 catalysts. Fourier transform infrared spectroscopy (FTIR) studies of molybdena interaction with γ-Al_2O_3 demonstrate that at low loadings molybdenum interacts with the most basic hydroxyl groups, and that these hydroxyls are associated with tetrahedrally coordinated aluminum. Furthermore, hydrodesulfurization (HDS) activity as a function of Mo loading shows a maximum in specific activity with loading. The Mo species bound to tetrahedrally coordinated Al sites are therefore believed to be inactive for the HDS reaction. Only after the tetrahedral Al sites have completely consumed does molybdena adsorb on the alumina in a manner that leads to an active catalyst. According to this scheme, the activity of alumina supported MoS_2 catalysts could be greatly improved by either titrating the tetrahedral Al sites with a modifier, or by using α-Al_2O_3 which contains no tetrahedrally coordinated Al. HDS tests over MoS_2 supported on both α-Al_2O_3 and γ-Al_2O_3 modified by a titania film confirm this hypothesis. Neither support material gives rise to a maximum in activity with Mo loading, but rather exhibits a smooth decrease in activity with loading. Furthermore, for equivalent Mo loadings the activity of both of these support materials exceeds that of unmodified γ-Al_2O_3 due to the fact that no Mo is tied up in the inactive form. FTIR, X-ray photoelectron spectroscopy, and transmission electron microscopy are currently being used to determine whether our model can indeed account for the observed activity trends. Although the surface area of α-Al_2O_3 is too low (~10 m^2/g) for use as a commercial catalyst, the titania coated γ-

Al_2O_3 represents an important, practical improvement in support materials for hydrotreating catalysts.

INTRODUCTION

In previous years, this project has focused on the deposition and characterization of titania films on high surface area substrates, such as silica and alumina. In order to determine the effects that these films have on catalyst activity, we have focused efforts in the current fiscal year on depositing MoS_2 onto modified and unmodified alumina substrates, and measuring the resulting activity for hydrodesulfurization (HDS) of dibenzothiophene (DBT). On unmodified γ-alumina or silica supports it is known that the specific activity of MoS_2 goes through a maximum with molybdenum loading, while on titania or zirconia the activity appears to decrease monotonically with coverage[1]. Unfortunately, due to the low surface area of the titania and zirconia supports, and to the fact that a flow reactor was employed for the activity measurements, the data reported on these two supports did not extend to low enough Mo loadings to confirm the absence of a maximum in activity. Assuming, however, that no maximum occurs for titania and zirconia, the different behavior of γ-alumina and silica relative to titania and zirconia has been attributed to differing morphology of the MoS_2 active phase. For supports that exhibit no maximum with loading, MoS_2 is proposed to lie flat with the basal plane parallel to the support surface, while for supports that exhibit a maximum the MoS_2 is proposed to bond perpendicular to the surface in a so-called "bookend" morphology. The evidence for the bookend morphology is indirect, relying on transmission electron microscopy (TEM) images that show MoS_2 platelets lying parallel to the direction of viewing and perpendicular to the γ-alumina crystallites which preferentially align with the TEM grid. These MoS_2 platelets could easily be located on the sides of γ-alumina particles, however, and therefore appear to be bound in a bookend morphology even though bonding is primarily through interaction of the basal plane with the sides of the particles. Recent TEM images of MoS_2 bound to low surface area silica and γ-alumina particles, where the uncertainty introduced by the possibility of bonding at crystallite edges is eliminated, show no evidence

for a bookend morphology, but show ample evidence for basal plane bonding of MoS_2 (ref. 2).

Given the difficulties arising from a morphological explanation of the activity trends, it seems prudent to explore possible chemical differences between the supports that could explain the data. It is known that at very low loadings molybdena binds to the γ-alumina surface as isolated monomeric species that are very difficult to reduce and convert to the sulfide[3,4]. As coverage increases, polymeric molybdena species begin to form ultimately resulting in bulk MoO_3 particles. Since at low loadings (<1 Mo/nm^2) most of the molybdenum is tightly bound in the inactive form, specific activity for HDS is expected to be very low. As more easily reduced polymeric species form at higher loadings, the specific activity rises, ultimately reaching a maximum at the point at which MoS_2 platelet growth begins to compensate for the increase in the fraction of the molybdenum that is reducible to MoS_2. In order to explain why a similar phenomenon does not operate on titania and zirconia, one must explore the specific interactions that give rise to the inactive Mo species on γ-alumina.

Fourier transform infrared (FTIR) studies of molybdena adsorption on γ-alumina demonstrate that the initial mode of interaction is through the most basic (highest frequency) hydroxyl groups[5]. These hydroxyl groups are associated with tetrahedrally coordinated aluminum cations in the γ-alumina support[6]. It is therefore postulated that the presence of tetrahedrally coordinated cations in the support material can give rise to strongly bound, inactive molybdena species. Comparing silica and γ-alumina with titania and zirconia in this context reveals that supports that give rise to a maximum in activity with coverage do indeed possess tetrahedrally coordinated cations, while supports that show only a monotonic decrease in activity with coverage contain only octahedrally coordinated cations.

Given this excellent correlation, activity studies and spectroscopic and TEM characterization of supported molybdena as a function of loading were performed to verify this explanation of activity trends. Accordingly, we report here the results of activity studies that confirm the published activity trends over a wider range of Mo coverages, and also

explore the potential of titania films to modify γ-alumina substrates such that the unfavorable, highly basic OH groups are consumed prior to molybdena loading.

RESULTS AND DISCUSSION

Based on the information and suppositions presented above, it is informative to compare the HDS activity of MoS_2 measured on several different supports. Mo was loaded onto various supports by aqueous incipient wetness impregnation of ammonium heptamolybdate followed by calcining at 500°C to disperse the molybdenum. Sulfiding was performed *ex situ* at 400°C in a flowing mixture of 10% H_2S in hydrogen. Kinetic measurements were made using a batch reactor rather than the flow reactor employed in earlier studies. This arrangement allows activity measurements to be made with low Mo loadings on very low surface area supports by simply extending the reaction time until measurable conversions are achieved. The advantage of being able to measure activity on such catalysts is offset to a certain degree by the need to account for poisoning of the reaction by competitive adsorption of product H_2S, and for a finite heat up time at the start of the reaction. A method for accounting for these factors is presented elsewhere[7]. The result of the analysis is a psuedo-first order rate constant that provides a measure of the specific activity (per g Mo) for a wide range of Mo loadings.

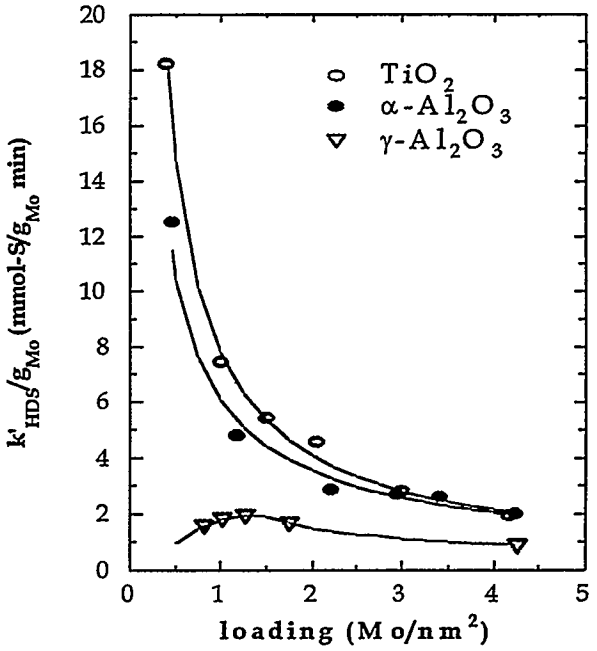

Fig. 1. Activity of MoS_2 on different supports as a function of Mo loading.

Results of this analysis are presented in figure 1, which shows the first order rate

constant as a function of Mo coverage. First, note the maximum in activity for MoS_2/γ-alumina at ~1.0 Mo/nm^2, in excellent agreement with previous measurements of thiophene HDS[1]. Second, when the data for titania supports is extended below 1.0 Mo/nm^2 the monotonic trend of decreasing activity with loading is maintained, unambiguously confirming a fundamental difference between the activity trends on γ-alumina and titania. Finally, and most significantly, α-alumina exhibits an activity trend closely resembling that of titania, with no apparent maximum. This result is entirely consistent the hypothesis that isolated molybdate species, formed by reaction with basic hydroxyl groups bound to tetrahedrally coordinated aluminum cations, give rise to the low activity of MoS_2/γ-alumina at coverages below 1.0 Mo/nm^2. Since no tetrahedrally coordinated aluminum cations are present in α-alumina[8], the possibility of forming the inactive species is precluded and a normal activity trend is observed. While this result alone does not confirm the validity of the proposed explanation for the maximum observed with γ-alumina, it does demonstrate that the effect is related to the structure of the support and not to the specific chemical identity of the support cations.

In order to verify the nature of the chemical interactions leading to the different activity trends for α- and γ-alumina, spectroscopic evidence for the presence or absence of certain molybdena species on each support is required. This evidence is presented in figures 2 and 3. Figure 2 shows FITR spectra of both α- and γ-alumina in the hydroxyl stretching regions. The spectrum of γ-alumina agrees well with literature spectra[5,9], showing multiple bands corresponding to various binding sites and coordinations[6]. The spectrum of

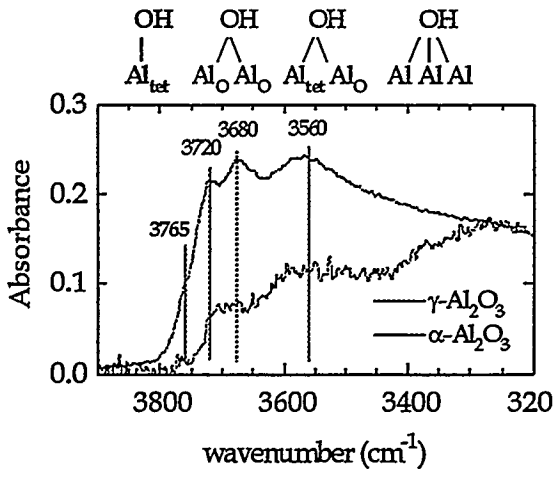

Fig. 2. comparison of FTIR spectra of hydroxyl stretching region on α-alumina and γ- alumina.

α-alumina is of much poorer quality due to the very low surface area, but it is nevertheless apparent that little intensity is present at the high frequencies characteristic of the most basic hydroxyl groups on γ-alumina. Further evidence for a difference in chemical behavior of Mo loaded on the two supports comes from X-ray photoelectron spectroscopy (XPS) measurements of the percent reduction of Mo on α- and γ-alumina after treatment in pure H_2 at 500°C for 12h (figure 3). γ-alumina shows an increase in reducibility with loading as reported elsewhere[4a], consistent with formation of an unreducible, and therefore inactive Mo species at low loadings. α-alumina, on the other hand, shows no variation of reducibility with loading, consistent with the absence of any changes in the bonding mode of molybdena with loading. The constant reducibility therefore gives rise to a monotonic decrease in activity with loading due to the growth of MoS_2 islands and consequent loss of edge sites.

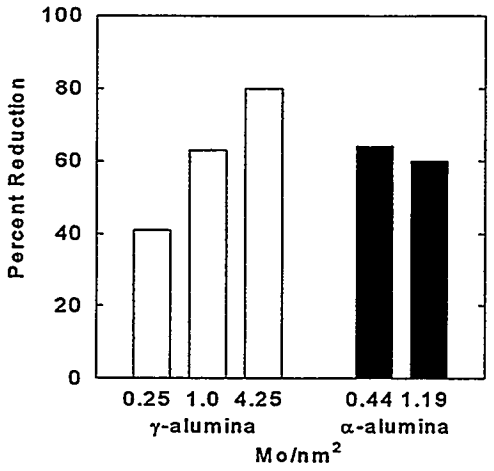

Fig. 3. Extent of Mo reduction at 500°C in hydrogen for 12h, measured by XPS.

While the results for α-alumina are encouraging, and demonstrate the potential of supports without tetrahedrally coordinated cations for improving supported MoS_2 catalysts, the low surface area of α-alumina renders it unsuitable for practical use. In other words, although the activity per gram of Mo is quite high on α-alumina, the activity *per gram or unit volume of catalyst* is very low. In order to apply the knowledge gained so far to the development of an improved practical catalyst, a method must be found to block the adsorption of Mo species at the most basic hydroxyls on γ-alumina. As alluded to earlier, one possible method for accomplishing this result is preadsorption of an additive to consume these basic hydroxyls prior to Mo adsorption. Since a major focus of this program has been the formation of titania films on various supports,

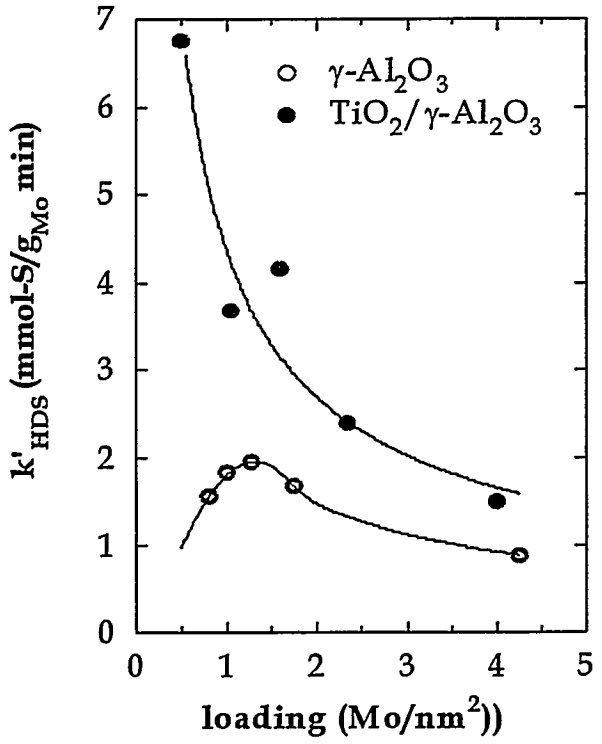

Fig. 4. Comparison of activity trends on γ-alumina *vs.* titania coated γ-alumina.

titania was chosen as the additive. Measurements were made of the activity of MoS_2 supported on titania coated γ-alumina, and figure 4 shows the results for a support coated with 16 wt% titania, an amount sufficient to cover approximately two thirds of the γ-alumina surface. Clearly, the presence of the titania alters the specific activity trends associated with γ-alumina and results in behavior closely resembling that of bulk titania or α-alumina. FTIR spectra show that the titania film indeed preferentially consumes the most basic, high frequency hydroxyls, thereby preventing the formation of inactive Mo species.

A final important result arises from analysis of TEM images of MoS_2 supported on coated and uncoated γ-alumina samples. Figure 5 shows that the two samples are indistinguishable based on MoS_2 morphology alone. Even the presence of titania cannot be detected indicating excellent dispersion of this additive. Thus, even if one concedes that the presence of MoS_2 platelets perpendicular to the viewing direction, as observed in figure 5, is evidence for a bookend morphology, one cannot use this morphology as an explanation for the different activity trends observed on uncoated and titania coated γ-alumina. Instead, a chemical explanation must be sought. Based on the evidence presented here, the formation of an inactive Mo species on γ-alumina associated with tetrahedrally coordinated aluminum cations, and the absence of this species on supports that do not contain tetrahedrally

coordinated cations, must be considered a strong candidate for explaining the observed activity trends.

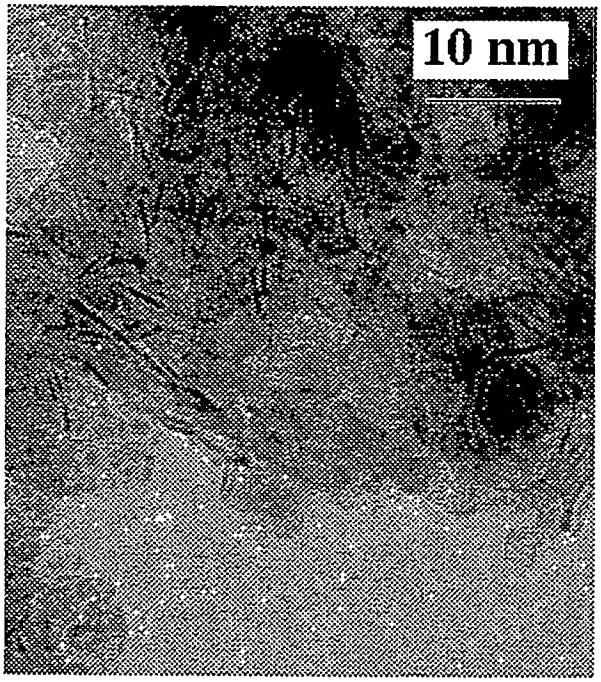

Fig. 5a. TEM image of MoS_2/γ-alumina.

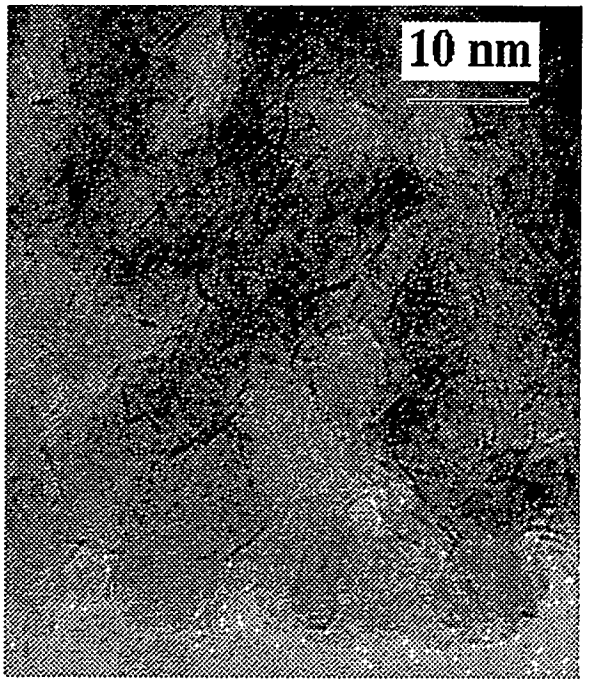

Fig. 5b. TEM image of MoS_2/titania/γ-alumina

CONCLUSIONS

The widely diverging activity trends observed for MoS_2/γ-alumina *vs.* $MoS_2/TiO_2/\gamma$-alumina, coupled with the extreme similarity in MoS_2 morphologies, clearly rules out a morphological explanation for the behavior of different supports. Furthermore, the differences observed between α- and γ-alumina indicate that the activity trends are related to the specific structure of the support surface and not to the chemical identity of the oxide support cations. These conclusions, coupled with spectroscopic data on the nature of hydroxyl groups and Mo reducibility lend strong support to an explanation of activity trends involving the formation of inactive Mo species at low loadings on γ-alumina. These species

result from interaction of molybdena with highly basic hydroxyls associated with tetrahedrally coordinated aluminum cations. As coverage increases, a greater fraction of the molybdenum atoms becomes associated with other sites and the extent of Mo reducibility increases, causing a concomitant increase in activity. Ultimately, growth of MoS_2 platelets with coverage decreases the fraction of Mo atoms located at the active edges of the platelets and activity begins to fall. For supports which lack tetrahedrally coordinated cations, formation of unreducible Mo species does not occur and activity trends are dominated by MoS_2 platelet growth over the entire range of coverages studied. A monotonic decrease of activity with coverage results. By using a titania overlayer to consume the basic hydroxyls that lead to unreducible molybdate species, the activity of γ-alumina can be increased significantly at all Mo loadings, and the activity trends can be made similar to those of α-alumina and titania. This result provides a simple, practical method for increasing the overall activity of supported MoS_2 catalysts.

REFERENCES

1. K. C. Pratt, J. V. Sanders, and V. Christov, *J. Catal.*, **124** (1990) 416.

2. S. Srinivasan, A. K. Datye, and C. H. F. Peden, *J. Catal.*, **137** (1992) 513.

3. H. Hu and I. E. Wachs, *J. Phys. Chem.*, **99** (1995) 10911.

4. a) D. S. Zingg, L. E. Makovsky, R. E. Tischer, F. R. Brown, and D. M. Hercules, *J. Phys. Chem.*, **84** (1980) 2898; b) C. P. Li and D. M. Hercules, *J. Phys. Chem.*, **88** (1984) 456.

5. a) N.-Y. Topsøe and H. Topsøe, *J. Catal.*, **139** (1993) 631; b) Y. Okamoto and T. Imanaka, *J. Phys. Chem.*, **92** (1988) 7102.

6. H. Knözinger and P. Ratnasamy, *Catal Rev. Sci. Eng.*, **17** (1978) 31.

7. J. R. Reardon, A. K. Datye, and A. G Sault., in preparation.

8. Cotton, F. A. and Wilkinson, G., "Advanced Inorganic Chemistry," 4th ed., John Wiley and Sons, New York, 1980, p. 329.

9. T. H. Ballinger and J. T. Yates, Jr., *Langmuir*, 7 (1991) 3041.

NANOPARTICLE SYNTHESIS IN PULSED LOW TEMPERATURE DISCHARGES

R. J. Buss

Sandia National Laboratories
Albuquerque, NM 87185-0367

ABSTRACT

Silicon nitride powders with an average size as low as 7 nm are synthesized in a pulsed radio frequency glow discharge. The as-synthesized silicon nitride powder from a silane/ammonia plasma has a high hydrogen content and is sensitive to oxidation in air. Post-plasma heating of the powder in a vacuum results in nitrogen loss, giving silicon-rich powder. In contrast, heat treatment at 800°C for 20 minutes in an ammonia atmosphere (200 Torr pressure) yields a hydrogen-free powder which is stable with respect to atmospheric oxidation.

Several approaches to synthesizing silicon carbide nano-size powders are presented. Experiments using silane/hydrocarbon plasmas produce particles with a high hydrogen content as demonstrated by Fourier transform infrared analysis. The hydrogen is present as both CH and SiH functionality. These powders are extremely air-sensitive. A second approach uses a gas mixture of methyltrichlorosilane and hydrogen. The particles have a low hydrogen content and resist oxidation. Particle morphology of the silicon carbide is more spherical and there is less agglomeration than is observed in the silicon nitride powder.

INTRODUCTION

There has been much effort in recent years to develop methods for producing materials with nanometer scale substructure. The desire is to control the macroscopic material properties such as toughness, elasticity and porosity by tailoring the microstucture. For ceramic materials, one approach is to synthesize nano-scale particles and develop methods for compressing and sintering these powders. A wide variety of approaches to manufacturing nano-particles of ceramics have been explored with various degrees of success. Thermal plasma techniques[1] in which precursors are atomized and allowed to condense in the afterglow have been highly successful for many materials including

metals and oxides. For thermal plasmas, however, the chemistry of the powder is typically controlled by thermodynamics and some compounds have been especially difficult to make including silicon nitride. Other approaches to synthesizing nano-particulate materials include direct nitridation of silicon, carbothermic reduction of silica, gas phase reaction of $SiCl_4$ and NH_3, laser pyrolysis of gaseous reagents, and thermal pyrolysis.

Almost a decade ago, Buss and Ho patented a process[2] for synthesizing ultrafine particles of ceramic, metal and polymer materials in a low-temperature, non-thermal, radio frequency (rf) plasma. The method involves flowing gaseous precursors at low pressure through a glow discharge. Electron-molecule collisions in the plasma result in fragmentation of the starting gases into reactive free radicals which undergo complex gas-phase chemistry leading to particle nucleation. Properties of the powder were thoroughly characterized by a variety of techniques[3]. In particular, the average particle size and size-dispersion were found to be large, and only weakly controllable. The average particle size was typically 100-200 nm.

During the past decade, particle formation and transport in plasmas has become an area of intense interest and activity[4]. It has developed that these particles, occurring in the plasmas used to manufacture microelectronic devices, can result in serious loss of wafer yield. Stimulated by this economic urgency, many laboratories worldwide have begun investigating the mechanisms governing particle nucleation, growth, trapping and agglomeration. One important discovery by Boufendi and Bouchoule[5] in France was that by pulsing the rf plasma, very tight control of the particle size and dispersion was achieved in the case of silicon particles from silane.

We applied the pulsed plasma technique to the synthesis of silicon nitride powder and achieved reasonable control of particle size as low as 7 nm[6]. The particles made in this way are rich in hydrogen-containing functionalities and the resulting powder is air-sensitive making subsequent handling difficult.

We report here the successful post-plasma heat treatment of the powders to render them air-insensitive. Also discussed are the results of applying the pulsed plasma technique to the synthesis of silicon carbide particles. Several chemical approaches including silane/hydrocarbon plasmas and methyltrichlorosilane(MTS)/hydrogen plasmas are compared.

EXPERIMENTAL

The plasma apparatus used to synthesize the nano-particles has been described previously[6]. Briefly, a vacuum chamber (base pressure 1 mTorr), is equipped with an electrode assembly consisting of a 15 cm diameter powered electrode, perforated with holes to allow gas flow in a showerhead configuration. The plasma region is enclosed by a grounded copper sheet with a grounded high transparency screen across the bottom. The pumping port is located 15 cm beneath the electrode assembly, and is fitted with a single sheet of filter paper.

In a typical experiment, eg. gas flow 2 sccm SiH_4, 12 sccm NH_3, at 200 mTorr pressure, the plasma is pulsed with a square wave on/off cycle (0.1 second on/1.0 second off) for 100 periods. Particle morphology is determined from a transmission electron microscope (TEM) grid placed on the collection filter. By running the plasma for an hour, sufficient powder is accumulated to obtain Fourier transform infrared (FTIR) transmission spectra. In order to obtain large quantities of powder for bulk analysis, the plasma is pulsed for several hours and the filter with accumulated powder is removed.

The post-plasma heat treatment of powders is tested by venting the plasma apparatus with dry nitrogen. The powder is transferred with minimal air exposure to a second vacuum chamber and immediately evacuated. Powders are exposed to air for a maximum of 15 seconds. The powder is then heated in vacuum or in an ammonia atmosphere in a resistively heated tantalum crucible. FTIR spectroscopy is used to study the susceptibility of the powder to oxidation in air. A sample is placed in the spectrometer and spectra are periodically acquired. The

growth of silicon oxide is readily measurable at 1100 wavenumbers (cm^{-1}). The decomposition of the powder heated in vacuum is studied using thermogravimetric analysis with mass spectral analysis of the desorbing gas. Samples of powder weighing 100-200 mg are placed in an alumina crucible and the temperature is ramped at a rate of 10 °C/min with flowing argon as the carrier gas.

Experiments to study the synthesis of silicon carbide use several chemical approaches. Mixtures of silane and methane or ethylene produce powder over a wide range of plasma power (5-50 Watts). Particles are also generated from gas mixtures of argon and hydrogen containing MTS vapor.

RESULTS AND DISCUSSION

The silicon nitride powder synthesized in the pulsed rf glow discharge (0.1 second on-time, 10 sccm SiH_4, 60 sccm NH_3) is rich in hydrogen[3]. The FTIR spectrum (Fig. 1a) shows strong absorptions at the SiH stretch (2100 cm^{-1}), and the NH stretch (3400 cm^{-1}) as well as the NH bending mode (1550 cm^{-1}). When exposed to ambient water vapor in the air, the SiH absorption decreases while the strong SiO absorption (1100 cm^{-1}) grows in as seen in the difference spectrum Fig 1b. Although the rate of oxidation can be slowed by storing the powder in a dry atmosphere, handling of the powder during preparation for sintering is difficult.

Thermogravimetric analysis (Fig 2) of the plasma synthesized powder shows that between 100 °C and 250 °C, weakly bound ammonia desorbs. From 250 °C to 500 °C, a second ammonia desorption occurs which may be associative recombination of NH_2 and H from different silicon sites. From about 250 °C to 900 °C, H_2 gas desorbs (but note that there is some contribution to the mass 2 signal from cracking of ammonia which has not been corrected). Above about 900 °C, the powder ceases to evolve gas. The total weight loss is 8-10%.

Figure 1

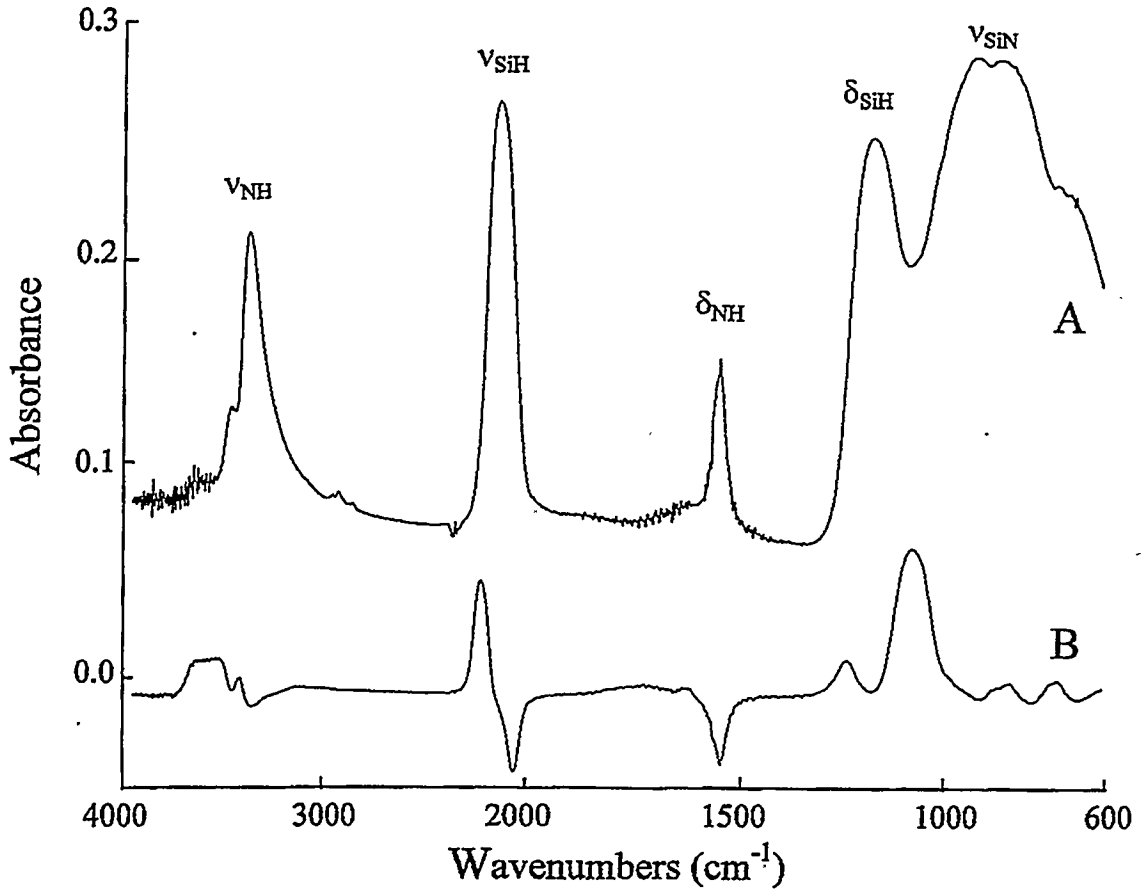

Fig. 1. FTIR spectra of silicon nitride powder a) as synthesized, b) the difference spectrum after 48 minutes exposure to air.

When gram quantities of pulsed plasma synthesized silicon nitride are heated to 800 °C for 20 minutes, the powder changes from pure white to a deep brown. This color is characteristic of silicon-enriched powder. Although the powder is synthesized stoichiometrically rich in nitrogen[3], it is apparent that excessive nitrogen is evolved during heating in vacuo and silicon-rich powder results. This color change was only observed for the powder from pulsed plasmas, with 15 nm or less average diameter. The larger particles, averaging 150 nm, from a continuous discharge remained white on heating in vacuo. This suggests

Figure 2

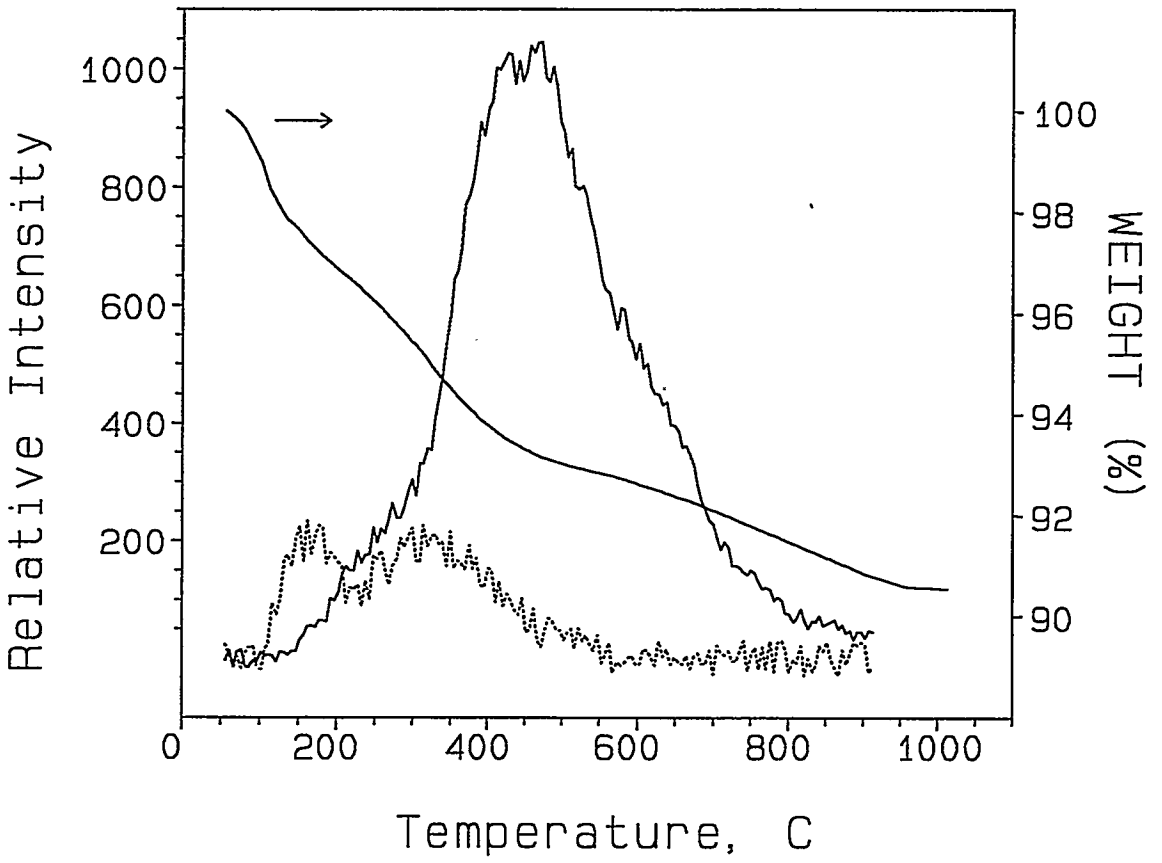

Fig. 2. TGA of plasma-generated silicon nitride powder. The weight loss curve is referred to the right. The mass spectal data for H_2 (solid curve) and NH_3 (dashed curve) are referred to the left.

that the extra loss of nitrogen may occur predominately from the near surface regions of the particles.

The freshly synthesized nano-powder is heated at 800 °C in various pressures of ammonia. At an ammonia pressure of 200 Torr or above, the powder retains its white color. FTIR spectra of these heat-treated samples (Fig. 3a) show the complete elimination of SiH functionality. This powder is resistant to oxidation (or hydrolysis) in atmosphere

Figure 3

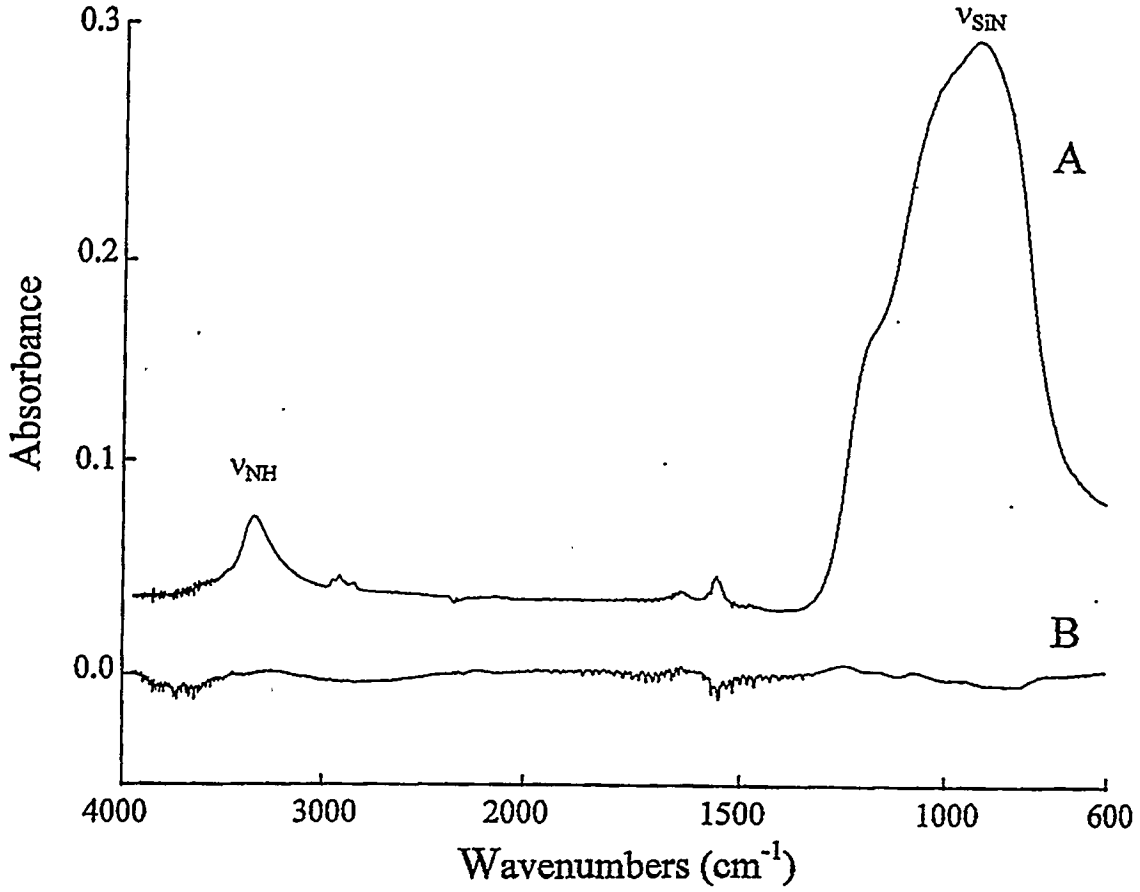

Fig. 3. FTIR spectrum of silicon nitride powder after heating at 800 °C for 20 minutes. A)Fresh from oven, B)Difference spectrum after 24 hour air exposure.

(Fig. 3b); no detectable appearance of SiO functionality is observed after 3 days of atmosphere exposure.

We apply the rf plasma technique to the synthesis of silicon carbide using gas mixtures of silane and methane in analogy with the successful silicon nitride technique. Powder is readily generated from such mixture over a wide range of gas mixtures (10-90% silane) and rf powers (5-50 Watts). The powders formed are extremely sensitive to air-oxidation, making it difficult to obtain FTIR spectra without

significant oxide formation. In fact, on venting the plasma apparatus to air, the powder spontaneously combusted in some instances. The FTIR spectrum (Fig. 4a) shows very significant content of SiH (2100 cm^{-1}), and CH_n (2900 cm^{-1}), functionality. Powder generated from silane/ethylene gas mixtures is indistinguishable from silane/methane mixtures.

Powder is also produced from plasmas containing gas mixtures of MTS and hydrogen, with or without added argon. The FTIR spectrum (Fig. 4b) shows significantly reduced CH and SiH features compared to Fig. 4a. A large feature at 3200 cm^{-1} is probably the result of adsorbed HCl.

Particle morphology of the MTS/H_2 powders is studied with TEM of samples produced from the pulsed plasmas. The morphology is similar to that of silicon nitride, roughly spherical particles with a significant fraction of the mass occurring in large agglomerates. A larger fraction of individual particles exhibit spherical shape, and the degree of hard agglomeration of SiC particles appears to be reduced relative to silicon nitride, but experiments are underway to investigate potential sampling bias. The fluid flow in the plasma apparatus is laminar through the showerhead and through the collection filter. Calculations suggest that the small particles, <100 nm diameter, will be significantly depleted by diffusion to the walls compared to the larger particles and agglomerates. TEM grids placed on the plasma walls appear to confirm this, collecting relatively more of the smaller particles. Large agglomerates are, however, also observed on these wall-mounted TEM grids. Since the fluid flow should prevent the more massive agglomerates from reaching the walls, it is probable that the agglomerates on the sidewalls grow in place by charge dipole induced attraction of incoming small particles at the surface.

Figure 4

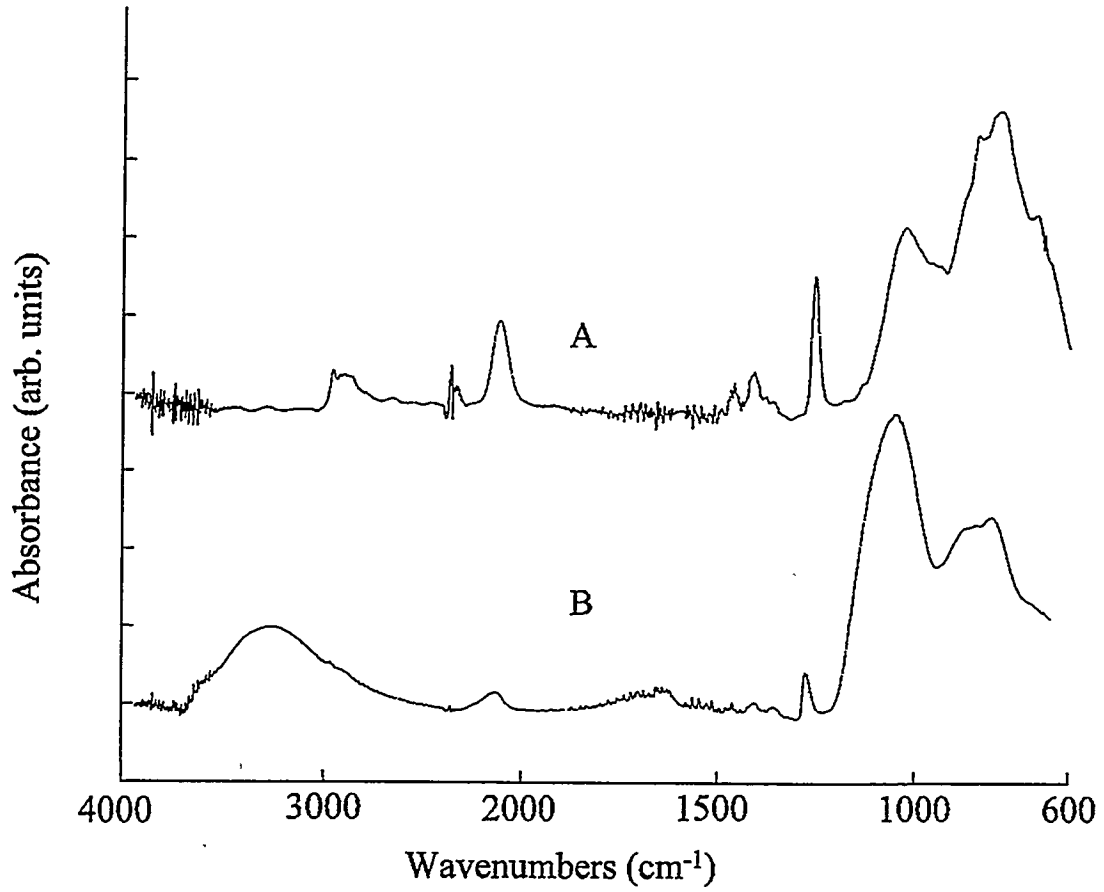

Fig. 4. FTIR of powder from a continuous silane/methane plasma, 50/50 gas mixture, 30 Watts power.

CONCLUSIONS

The silicon nitride powders synthesized by pulsed rf plasma discharge can be stabilized with respect to air-oxidation by post-plasma heat treatment in an ammonia atmosphere at 800 °C. Heating the powder drives off the labile hydrogen, and the ammonia atmosphere prevents excessive loss of nitrogen. Particles can be generated from silane/hydrocarbon mixtures, but they are extremely sensitive to air oxidation. Particles from an MTS/H_2 plasma look promising as a precursor to silicon carbide.

ACKNOWLEDGEMENTS

The author gratefully acknowledges the valuable assistance of Dr. Celeste Drewien for performing the TEMs and Michael Smith for excellent technical support. Also this work was supported by the United States Department of Energy under Contract DE-AC04-94AL85000.

REFERENCES

1. G. J. Vogt and L. R. Newkirk, in *Proc. of the Symp. on High Temperature Materials-III,* edited by Z. A. Munir and D. Cubicciotti (The Electrochemical Society, Pennington, NJ, 1985), p. 164.

2. R. J. Buss and P. Ho, US Patent No. 4,769,064.

3. P. Ho, R. J. Buss, and R. E. Loehman, J. Mater. Res., 4, 873 (1989).

4. see for example, Plasma Sources. Sci. Technol., 3, (1994). Entire volume devoted to the topic.

5. L. Boufendi, A. Plain, J. Ph. Blondeau, A. Bouchoule, C. Laure, and M. Toogood, Appl. Phys. Lett. 60, 169 (1992).

6. R. J. Buss and S. V. Babu, J. Vac. Sci. and Technol., 14(2), 582 (1996).

SESSION III

WORKSHOP ON MATERIALS RESEARCH AND DEVELOPMENT NEEDS FOR THE SUCCESSFUL DEPLOYMENT OF ADVANCED POWER GENERATION TECHNOLOGIES

WORKSHOP ON MATERIALS RESEARCH AND DEVELOPMENT NEEDS FOR THE SUCCESSFUL DEPLOYMENT OF ADVANCED POWER GENERATION TECHNOLOGIES

The 1995 workshop identified several material needs for pressurized fluidized bed combustion (PFBC), integrated coal gasification combined cycle (IGCC), and indirectly fired cycles. The 1996 workshop focused on resolution of some of those issues through the definition or redefinition of projects under way.

KEYNOTE ADDRESS: **John Stringer, Executive Scientist,**
Electric Power Research Institute,
Palo Alto, California.

SESSION A. WORKSHOP ON CERAMIC COMPOSITE INTERFACE COATINGS.

Rapporteurs: R. G. Smith, 3M Company
R. E. Tressler, Pennsylvania State University
Moderator: D. P. Stinton, ORNL

Ceramic composites are critical to high-temperature components for fossil energy systems both as hot-gas filters for IGCC and PFBC systems and as structural components, such as heat exchangers, for the indirectly fired cycles, externally fired combined cycle (EFCC), and Combustion 2000 systems. The development of ceramic composites with oxidation resistant interface coatings is extremely important to NASA, the Air Force, and DOE programs. Applications of these composites were summarized during the workshop and different approaches for oxidation resistant interface coatings will be discussed.

SESSION B. WORKSHOP ON HIGH-TEMPERATURE MATERIALS BASED ON LAVES PHASES.

Rapporteurs: K. S. Kumar, Brown University
J. H. Perepezko, University of Wisconsin
D. J. Thoma, Los Alamos National Laboratory
Moderator: C. T. Liu, ORNL

The Offices of Fossil Energy and Basic Energy Sciences of the Department of Energy jointly sponsored this review of critical issues related to alloy development of new high-temperature structural materials based on Laves phases. Laves phase materials, such as the high-temperature Cr-Nb alloys, are of interest because, characteristically, they are high-melting intermetallics that are extremely hard and strong, although brittle. These metallic, rather than ceramic, materials could provide high strengths up to 2300°F for systems such as the IGCC, PFBC, EFCC, and Combustion 2000.

SESSION C. WORKSHOP ON ALLOYS FOR VERY HIGH-TEMPERATURE APPLICATIONS.

Rapporteurs: N. Birks, University of Pittsburgh
T. B. Gibbons, ABB Combustion Engineering
Q. J. Mabbutt, British Gas
Moderator: I. G. Wright, ORNL

Systems capable of operating at higher efficiencies, such as the low-emission boiler system (LEBS), require materials with higher temperature capabilities, in particular, higher creep strength and environmental resistance. A range of alloys developed from the best of the currently used wrought ferritic and austenitic alloys have improved high-temperature capabilities, and oxide dispersion-strengthened alloys are targeted for extremely high-temperature applications. This workshop examined the temperature capabilities of these alloys compared to current alloys and to the needs of advanced systems to identify their appropriate applications, information and actions required or under way to qualify them for such use, and their limitations.

SESSION D. WORKSHOP ON MATERIALS ISSUES ASSOCIATED WITH LOW NO_x COMBUSTION CONDITIONS IN FOSSIL FUEL-FIRED BOILERS.

Rapporteurs: J. L. Blough, Foster Wheeler
J. N. DuPont, LeHigh University
S. Kung, Babcock & Wilcox
J. Nava, ABB-Combustion Engineering
Moderator: I. G. Wright, ORNL

Some cases of severe corrosion of the furnace wall tubes are being experienced in utility boilers fitted with modern, low-NO_x burners. It has been anticipated for some time that reducing conditions created as part of the low-NO_x combustion process might result in sulfidation attack, but initial experience with such burners did not reveal such problems. The intent of this workshop was twofold: first, to better define the situation in terms of the form and rate of attack and to examine what is known about its root causes, and second, to review the potential for using corrosion-resistant materials as part of the solution. In particular, if the corrosion is due to sulfidizing conditions, the application of an iron aluminide as an overlay coating may prove a viable option.

WRAP-UP SESSION

Workshop attendees gathered for summaries of deliberations from Sessions A through D.

SUMMARY OF WORKSHOP ON CERAMIC COMPOSITE INTERFACE COATINGS

Wednesday, May 15, 1996
Radisson Hotel
Knoxville, Tennessee

Commercialization of fiber-reinforced composites has been limited because of the stability of the interface coatings that control the mechanical properties of the composites. Typical materials are currently manufactured with pyrolytic carbon interface coatings that perform well in inert atmospheres or when stresses are kept very low (<70 MPa). Unfortunately, carbon coatings are not stable at high temperatures in air or oxidizing conditions which results in degradation of the mechanical properties of the composites. The problem of oxidation resistant interface coatings is not unique to the Fossil Program. Such coatings are also a concern to the United States Air Force, the Continuous Fiber-reinforced Ceramic Composites Program, the Fusion Energy Materials Program, and to the European Community. This workshop was organized to compare and discuss the need for and development of oxidation-resistant interface coatings in each of these programs.

STATUS OF COMPOSITE FILTERS: A CURRENT APPLICATION

(Robert Smith, 3M Company)

A novel type of hot-gas filter based on a ceramic fiber-reinforced ceramic matrix composite was developed and extended to full-size, 60-mm OD by 1.5-meter-long, candle filters. A commercially viable process for producing the filters was developed and the filters are undergoing testing and demonstration throughout the world for applications in pressurized fluidized-bed combustion (PFBC) and integrated gasification combined cycle (IGCC) plants. 3M Company ceramic composite filters performed well for 200 hrs in PFBC simulation tests at Westinghouse STC and for 1600 hrs in the Tidd demonstration plant. They have also functioned for thousands of hours in IGCC plants around the world. Both the simulatioon tests and the plant tests are providing data for the use of these filters. Each step in the development process has resulted in insights into the development of superior filters. One area of particular interest in the interface coatings. These materials must be stable in PFBC and IGCC conditions to sustain the mechanical properties of the filters. It is quite possible that different interface coatings will be required for the different combustion conditions.

INTERFACE CONCEPTS FOR AIR FORCE APPLICATIONS
(Sankar Sambasivan, BIRL-Northwestern University)

Easy cleaving oxides are perhaps the only interface concept that draws a direct analogy to C and BN which has proven to be functional in SiC-based composites. The idea is to design a highly anisotropic oxide coating that has inherent low toughness planes which are preferentially aligned along the fiber axis such that interfacial debonding can occur through cleavage along these planes. The first candidate in the oxide family that was tested was mica-based phologopites. These materials reacted extensively with the fiber and matrix such that their use was limited to low temperatures. Since then, several layered oxides have emerged that show promise for high temperature use. Among them, the family of beta aluminas and magnetoplumbites of several compositions are currently being examined. The alkali stabilized beta aluminas are attractive but are plagued with alkali loss problems at elevated temperatures (above 1000°C). The most recent and perhaps the most encouraging result was reported recently by Cinibulk where oriented coatings of hibonite ($CaAl_{12}O_{19}$) were deposited on sapphire fibers. A TEM section of the coated fiber in alumina matrix showed cracks forming parallel to the basal planes of the hibonite. While this was encouraging, no push out for the fiber was observed in these composites presumably due to residual clamping stresses at the interface. A new family of layered perovskites have been proposed by Sambasivan and Petuskey that show highly anisotropic fracture behavior and seem to be well suited for CMC interfaces. Bulk samples of potassium calcium niobate have been prepared and tested for their anisotropic properties. Vickers indents placed on single grains of this material show extensive cracking in the basal direction with no apparent crack initiated in the normal direction. Development of coatings of potassium calcium niobate on to sapphire fibers for subsequent crack deflection tests and identification of other suitable compositions in the family of layered perovskites are in progress.

INTERFACE CONCEPTS AT THE UNIVERSITY OF BORDEAUX
(Dick Tressler, Pennsylvania State University)

Researchers at the Laboratoire Composite Thermostructureaux (LCTS) at the University of Bordeau in France are developing multi-layer SiC/C interface coatings where equivalent total thicknesses of carbon and SiC are deposited as alternating layers. Results indicate that the multilayer interfaces provide for similar behavior to that of equivalent monolayer total carbon thicknesses. A surface treatment has been developed at LCTS that removes the native silica layer from Nicalon fibers so that a carbon rich layer mates with the deposited carbon interface. These materials exhibit greater fiber-interface bonding, resulting in shorter pullout lengths and higher strengths. The tensile curves, however, reveal equivalent strain-to-failure to untreated Nicalon and therefore the material prepared with treated fibers is considered superior. Other work at LCTS focuses on layer-lattice

oxide interface materials. These include the phyllosiloxides developed by them based on phlogopites and fluorophlogopites. Great difficulty was encountered in depositing these phases on fibers.

INTERFACE CONCEPTS FOR THE CFCC PROGRAM
(Rick Lowden, Oak Ridge National Laboratory)

The selection of the appropriate fiber coating composition and deposition technique is one of the most important tasks required for the development of reliable fiber reinforced ceramic composites for elevated temperature applications. The development of improved interface layers is being explored in the Continuous Fiber Ceramic Composite Program's Supporting Technologies Task. The thermochemical and thermomechanical aspects of potential fiber coatings for composite systems of interest have been examined. Vapor deposition, sol-gel, polymer precursors, and other deposition techniques are being evaluated to apply thin layers to fiber tows, cloth, or fibrous preforms for composite fabrication. Techniques developed and refined earlier in the program are being utilized for the characterization of the microstructure and composition of the coatings. Mechanical properties of as-fabricated composites, and specimens exposed to corrosive environments have been evaluated to assess the stability and reliability of new interlayer compositions. Instruments such as the Interfacial Test System have been used to examine the effects of processing, composition, microstructures, and environmental exposure on the properties of the fiber-matrix interface.

Much of the success in the development of improved fiber coatings has paralleled efforts to protect carbonaceous materials. Boron-containing materials such as boron-doped carbon and boron nitride provide improved oxidation resistance as compared to carbon through the formation of a glass layer that forms upon oxidation and seals the surfaces of the exposed interface. There are many questions concerning the performance and reliability of boron-containing layers. For example, there is little information about the relationships between the properties, microstructure, composition, and performance of boron nitride. The effects of processing conditions and contaminants on the microstructure, properties, and oxidation behavior of BN are being examined. The results of the effort will be used to provide input into the successful processing and utilization of BN as an interface coating for CFCCs.

It has been hypothesized that the ideal interface layer for a SiC/SiC composite would be a modified form of SiC. The fiber, interlayer, and matrix would be thermochemically and thermomechanically stable with respect to each other, and the constituents would exhibit similar stability at any operating temperature. An "all SiC" composite would be protected by a silica surface layer, adding to the life of the material in corrosive environments. The interlayer of choice would be a soft or low modulus SiC that would ensure debonding at the fiber-matrix interface and controlled fiber sliding to produce toughness and gradual failure. Silicon carbide interface coatings with controlled composition, microstructure, and

properties are being deposited employing chemical vapor deposition and liquid infiltration techniques. The goal is to develop a "porous" or low modulus SiC material to be used as a fiber coating. Composites fabricated from coated fabric are being characterized and tested.

The performance of multilayer coatings for controlling mechanical interactions at the fiber-matrix interface have been of growing interest in recent years. At least two multilayer systems for use in SiC/SiC composites are being explored in the CFCC Program. Systems consisting of alternating layers of carbon and SiC, and alumina and BN are being deposited by chemical vapor infiltration by Hypertherm and Amercom, Inc., respectively. Composition, microstructure, and properties are being characterized, and the results being used as feedback to the suppliers for future improvements.

INTERFACE CONCEPTS FOR FUSION APPLICATIONS

(Lance Sneed, Oak Ridge National Laboratory)

Fiber-reinforced SiC-matrix composites are being evaluated as a potential first wall material for fusion reactors. Interface coatings are also a significant concern to the Fusion Energy Program but for a very different reason. The Nicalon fibers and the SiC matrix are ideal materials for this application because they do not interact with neutrons during irradiation and become highly radioactive. Therefore, the materials can be much more easily handled, stored, or disposed of after irradiation. Unfortunately, carbon interface coatings swell during irradiation causing the matrix to crack and spall. The Fusion Energy Program is therefore exploring interface concepts that utilize materials that don't interact with neutrons and do not contain carbon. The most promising material at this time is the porous SiC coatings being developed jointly by the Fossil Energy Materials and CFCC Programs. Composites consisting of High-Nicalon fibers (ultra low oxygen), a porous SiC interface, and a SiC matrix have been fabricated for irradiation testing. Mechanical property characterization of the composites revealed high quality materials with flexure strengths of nearly 400 MPa. These materials will be thoroughly characterized after irradiation.

SUMMARY OF WORKSHOP ON HIGH TEMPERATURE MATERIALS BASED ON LAVES PHASES

Wednesday, May 15, 1996
Radisson Hotel
Knoxville, Tennessee

The Offices of Fossil Energy and Basic Energy Sciences of the Department of Energy jointly sponsored the Workshop on High Temperature Materials Based on Laves Phases in conjunction with the Tenth Annual Conference on Fossil Energy Materials held at the Radisson Summit Hill Hotel in Knoxville, Tennessee on May 14-16, 1996. The objective of this workshop was to review the current status and to address critical issues in the development of new-generation high-temperature structural materials based on Laves phases. The one-day workshop included two sessions of overview presentations and a session of discussion on critical scientific and technological issues.

The Laves phases represent an abundant class of intermetallic alloys with possible high-temperature structural applications. Laves phases form at or near the AB_2 composition, and there are over 360 binary Laves phases. The ability of these alloys to dissolve considerable amounts of ternary alloying additions provides over 900 combined binary and ternary Laves phases. Many Laves phases have unique properties which make them attractive for high-temperature structural use. At half their homologous temperature, they retain >0. 85 of their ambient yield strength, which is higher than all other intermetallics. Many of the Laves phases also have high melting temperatures, excellent creep properties, reasonably low densities, and for alloys containing Cr, Al, Si or Be, good oxidation resistance. Despite these useful properties, the tendency for low-temperature brittleness has limited the potential application of this large class of alloys.

The possible mechanisms governing the plastic deformation of Laves phases are discussed extensively at the Workshop. Because of complex crystal structures, Laves phases have limited active slip systems. Theoretically, Laves phases can deform by syncro-shear at ambient temperatures; however, the operation of this mechanism needs to be confirmed experimentally. It is important to point out that monolithic Laves phases such as HfV_2 are deformable at room temperature. HfV_2 can be cold worked extensively without fracture. Effort should be placed on comparison of the different deformation behaviors of HfV_2 and other Laves phases. Twinning is possibly operative in Laves phases. Both theoretical and experimental work is needed in order to define the conditions required for such microtwinning in Laves phases.

Although experience indicates that monolithic Laves phases are generally brittle, dual-phase alloys containing bcc phases demonstrate encouraging deformability. Multilayers

of HfV_2+Nb have been cold-rolled up to 30% without fracture. In addition, dual-phase $NbCr_2$/Nb and NbCr/Cr alloys indicate promising ambient-temperature fracture toughness, with values ranging from 7 to 15 $MPam^{1/2}$.

To fully develop the potential of Laves phases, three main issues need to be addressed: (1) alloy design, (2) structural stability, and (3) property evaluations. Alloy design is required to fully recognize the enormous base of alloying potential in Laves phases, and the role of defects, stacking faults, and bond strengths needs to be better understood. Structural stability is governed by both the atomic size and electronic structure of the Laves phases, and a structural instability may give rise to the tendency for twinning at ambient temperatures. Different sample quality may have resulted in the spread of the literature values for the physical and mechanical properties of Laves phases, and there is a need for full characterization. Moreover, the deformation modes and mechanisms require better definition to couple with the mechanical behavior of the material. In dual-phase bcc/Laves alloys, the deformability of these alloys has been observed, and the role of the bcc phase on the Laves phase deformation needs more attention.

SUMMARY OF WORKSHOP ON ALLOYS FOR VERY HIGH-TEMPERATURE APPLICATIONS

Wednesday, May 15, 1996
Radisson Hotel
Knoxville, Tennessee

In current fossil energy systems, the maximum operating temperatures experienced by critical metal structures do not exceed approximately 732°C (1350°F), and the major limitation on the use of the alloys typically is corrosion resistance. In systems intended for higher performance and higher efficiency, increasingly higher working fluid temperatures will be employed, which will require materials with higher-temperature capabilities, in particular, higher creep strength and greater environmental resistance. There have been significant developments in alloys in recent years, from modifications of currently-used wrought ferritic and austenitic alloys with the intent of improving their high-temperature capabilities, to oxide dispersion-strengthened alloys targeted at extremely high-temperature applications.

The aim of this workshop was to examine the temperature capability these alloys compared to current alloys, and compared to the needs of advanced fossil fuel combustion or conversion systems, with the goals of identifying where modified/new alloys would be expected to find application, their limitations, and the information/actions required or that are being taken to qualify them for such use. The questions that were addressed, and a synopsis of the answers, were as follows:

(1) *What are the temperature capabilities and limitations of current high-temperature alloys, and of advanced alloys?*

Several of the new or improved alloys are capable of meeting the needs of applications such as the Low-Emissions Boiler System (LEBS); the requirements of the High-Performance Power System (HIPPS) cycle are more difficult to meet with conventional alloys, although oxide dispersion-strengthened (ODS) alloys have properties that match some of the needs. Although the property data produced for these alloys are very interesting, they usually are available for relatively short times. The real need, especially for creep, is for long-term data such as are required for ASME Boiler and Pressure Vessel Code qualification; however, such data generation is expensive. A further limitation is that there usually are no data available on the effects of corrosion on strain, and vice-versa; these considerations assume increased importance as metals are applied at higher fractions of their melting temperatures. There is a need for a better method for extrapolating short-term data to speed up the ability to use new alloys; an associated problem is that the ASME Code is overly conservative.

(2) *How do these capabilities match the apparent needs of current and planned power generation cycles, and what are the likely applications of current and new high-temperature alloys?*

Neil Birks of the University of Pittsburgh presented a methodology for matching the stress and strain criteria for a given component in a given cycle to the capabilities of available alloys. This approach appears to have great merit since it provides in diagrammatic form the first step in selecting alloys that could be considered for specific applications. This approach is based on the mechanical property requirements, and must be supplemented by considerations of environmental compatibility, fabricability, and repairability. Of concern in higher-temperature applications is the problem resulting from the differences in coefficient of thermal expansion when joining ferritic and austenitic alloys. A case can be made for eliminating austenitic alloys in some applications by using improved ferritic steels to their maximum temperature (which is approaching that of some austenitic alloys), and then changing to superalloys, or ceramics.

(3) *What are the pacing alloy properties required for the various advanced cycle scenarios? Can we prioritize the needed property-temperature-environment combinations?*

The desired mechanical properties are highly dependent on the particular component and cycle being considered. In addition, using improved alloys to upgrade the temperature capabilities of a given component necessitates consideration of the impact on the materials used for components downstream. In the case of advanced steam boilers, for instance, higher-temperature steam capability from the use of improved superheater/reheater alloys results in a need for improved alloys for the main steam lines and the steam turbine. If such alloys are not available for fabrication of those components, the improved superheater/reheater alloys will not be used. Considerations of weldability and repairability also are important, especially with complex systems. Overall, materials selection is governed by the ASME Boiler Code which, unfortunately, is in need of updating since the maximum temperature considered is approximately 900°C (1650°F), and 816°C (1500°F) for some materials, and many of the newer alloys have not been Code-qualified.

(4) *Where do ODS alloys fit into the overall need for high-temperature materials in advanced power generation cycles?*

As indicated by the ranking of alloy properties by system/component requirements in (2), ODS alloys have useful creep strength at temperatures significantly higher than for advanced, conventional structural alloys. For instance, the stress to cause rupture in 10,000 hr. at 1300°C (2372°F) is approximately 20 MPa (2.9 ksi; in the axial direction). This strength, combined with the excellent environmental resistance up to at

least 1300°C, suggests that ODS alloys are alternative candidates for a number of applications for which ceramics are targeted. If ODS alloys were used in advanced cycles to handle working fluid temperatures up to, for instance, 1200°C (2200°F) or so, the very high-temperature duty ceramic heat exchanger part of the circuit could be relatively small, and possible more readily designed and fabricated. Such alloys are also candidates for handling high-temperature steam in advanced steam cycles.

(5) *At what stage of development is commercial ODS-alloy heat exchanger tubing? And, given the specialized nature of ODS alloy processing, what is its near-term availability? What practical experience is available for processing, forming, and joining ODS alloys?*

Processing of ODS alloys has progressed so that reproducible properties are achieved. The strength in the transverse direction (hoop strength in tubes) is lower than in the axial direction, but improvements are being made continually. ODS-FeCrAl alloys are available in rod, sheet, foil and tubular forms. The maximum size currently available of seamless tubes is 3 in OD (0.2 in wall) x 11 ft long. There are two major suppliers. Since the alloys have highly-directional properties, fabrication and joining require special considerations. The alloys can be bent (after preheating to 300°C), and can be joined. However, fusion welding creates weak zones since it redistributes the oxide dispersion. Joining of ODS-to-ODS and ODS-to-conventional alloys by diffusion bonding, explosive bonding, and friction bonding has been demonstrated. The friction bonding techniques also are applicable to joining ODS alloys to ceramics. There is experience in fabricating ODS tube-to-header joints; British Gas has produced and tested a harp-design heat exchanger that consists of 36 ODS tubes each 3.7 m (12 ft) long. Although these alloys have excellent resistance to corrosive gases, information is needed on their resistance to ash and slag deposits, such as are found in coal-combustion and conversion environments.

SUMMARY OF WORKSHOP ON MATERIALS ISSUES ASSOCIATED WITH LOW-NO_x COMBUSTION CONDITIONS IN FOSSIL-FIRED BOILERS

Wednesday, May 15, 1996
Radisson Hotel
Knoxville, Tennessee

It was anticipated by some members of the high-temperature corrosion community that the fitting of low-NO_x burners to coal-fired power plants would lead to an increase in furnace wall corrosion, as a result of the relatively substoichiometric conditions created by the staged combustion process. These expectations were not borne out by initial experience. Recently, however, cases of severe furnace wall corrosion have been reported by some U.S. utility boilers retrofitted with modern low-NO_x burners.

There is extensive experience of furnace wall corrosion in utility boilers in the U.K., which indicates that excessive fireside corrosion rates (>100 nm/hr; 34 mil/yr.) are experienced when tubes are exposed simultaneously to substoichiometric gaseous environments (CO>3.0 percent) and high radiant heat fluxes. Such conditions may be generated when flame impingement occurs. Where such conditions persist, increases in fuel chlorine content will exacerbate the rate of metal loss. In the absence of either circumstances, corrosion rates are much reduced and little influence of coal chlorine content is anticipated. Although the corrosion is essentially sulfidation caused by H_2S in the flue gas, the contribution of fuel sulfur in the corrosion experience by U.K. boilers is unresolved, partly because of the relatively small range in sulfur content of coals burned in U. K. utility boilers.

The intent of this workshop was three-fold:

- to better define the problem in terms of the form and rate of attack,
- to examine what is known about its root causes, and
- to review the potential for using corrosion-resistant materials as part of the solution.

The questions that were addressed, and the responses were:

(1) *Is the fireside corrosion being experienced in boilers retrofitted with low-NO_x burners a significant problem?*

The overwhelming opinion of the workshop was that boilers retrofitted with low-NO_x burners are experiencing significant corrosion of the furnace walls. The rates of metal loss are in the range 96 to 226 nm/hr (33 to 78 mil/yr.), compared to the 49 to 87 nm/hr (17 to 30 mil/yr.) experienced before retrofitting low-NO_x burners.

(2) *Is the problem actually associated with low-NO_x operation? Or is the cause a combination of changes made in boiler operation that coincided with the installation of low-NO_x burners?*

The observation of all of the boiler manufacturers represented at the workshop (ABB-Combustion Engineering; Babcock & Wilcox, and Foster Wheeler) was that the problem was directly linked to the operation of low-NO_x burners. Boilers with historically high furnace wall corrosion rates have exhibited increased corrosion with low-NO_x burners. Further, this form of attack has occurred in eight tangentially-fired boilers that are burning coal with a sulfur content in excess of 1.5 percent, and that have a history of furnace wall corrosion. The corrosion occurs in locations on the back walls where the flame pattern apparently is distorted as the gas flows toward the furnace 'nose.' Higher than usual heat fluxes are measured in those areas.

(3) *Can we define the rate of material wastage and the type of attack in such a way that direct comparisons can be made with existing understanding of possible corrosion mechanisms?*

Where detailed measurements have been made, the flue gas in contact with the walls in areas where the accelerated corrosion is observed has levels of CO>5 percent, and H_2S up to 500 ppm, which indicates highly-sulfidizing conditions. In addition, carbon-rich deposits (up to 8 percent loss on ignition) containing FeS (pyrites), ZnS, and FeC are found. The corrosion scales consist of an outer layer of iron sulfides, with an inner layer consisting mostly of iron oxides but containing some sulfides adjacent to the metal surface. The corrosion morphologies appear consistent with gas-phase sulfidation attack.

(4) *What is needed to allow the root cause of the corrosion to be assessed: are available failure analysis data suitable for more extensive study? Do we know enough to simulate the attack in the laboratory? Are field probe tests needed?*

Laboratory simulation (EPRI project at Babcock & Wilcox) reproduced the corrosion morphologies found in actual boilers but, for the same metal temperature and gas CO and H_2S levels, the rate of corrosion was significantly lower than found in the boiler. Comparing the corrosion rates and conditions measured in the U.S. boilers with the U.K. criteria for excessive furnace wall corrosion suggests that a high heat flux, i.e. flame impingement, also is experienced in the boilers, but was not simulated in the laboratory tests. The same laboratory tests suggested that 300-series stainless steels are extremely resistant to the simulated conditions. It was considered that there is a need for field testing of alloys and coating compositions known to exhibit resistance to sulfidation attack, applied by coating methods with the potential for depositing non-porous, crack-free layers.

(5) *What remedial measures are being used? How effective are they?*

The main approach to overcome this corrosion problem appears to have been to use high-alloy coatings. In some cases, affected areas have been coated, in others, test panels of different coatings have been installed in boilers. Commercial plasma sprayed coatings appear to be less effective than, for instance, high-velocity oxy-fuel and weld overlay coatings because of coating porosity. Cracking of coatings of austenitic alloys also has led to loss of protection. The best approach was thought to be to use a high-chromium ferritic alloy together with an application method that produces a dense coating. The best reported performance from coatings monitored by LeHigh University was an increase in life to 18 months, from 6 months for bare tubes. Other suggested remedial measures were to avoid high-sulfur coal, and to employ air blanketing of the affected areas.

(6) *Is there a role for materials/coatings to mitigate this problem?*

Although it was expected that the problem could be mitigated by proper tuning of the low-NO_x burners for a given boiler operating at a given output on a given coal, it was considered unlikely that this would be achieved in all cases. Therefore, there is a continuing need for the application of more resistant alloys or coatings locally in the affected regions. The desired coating appears to consist of an alloy capable of reliably forming a protective scale of chromium or aluminum oxide, that could be deposited in a non-porous, crack-free condition, at a low cost. In addition to the high-Cr austenitic alloys usually associated with good sulfidation resistance, high-Cr and high-Al ferritic alloys (for instance, Fe_3Al) should be considered as candidates.

SESSION IV

NEW ALLOYS

ODS IRON ALUMINIDES

I. G. Wright, B. A. Pint, E. K. Ohriner, and P. F. Tortorelli

Oak Ridge National Laboratory
P. O. Box 2008
Oak Ridge, Tennessee, 37831-6156.

ABSTRACT

The overall goal of this program is to develop an oxide dispersion-strengthened (ODS) version of Fe_3Al that has sufficient creep strength and resistance to oxidation at temperatures in the range 1000 to 1200°C to be suitable for application as heat exchanger tubing in advanced power generation cycles. The program has two main thrusts: (a) alloy processing, which involves mechanical alloying and thermomechanical processing to achieve the desired size and distribution of the oxide dispersoid, as well as the desired alloy grain size and shape, and (b) optimization of the oxidation behavior to provide increased service life compared to ODS-FeCrAl alloys intended for the same applications. Control of the grain size and shape in the final alloy is very dependent on the homogeneity of the alloy powder, in terms of the size and distribution of the dispersed oxide particles, and on the level of strain and temperature applied in the recrystallization step. Studies of the effects of these variables are being made using mechanically-alloyed powder from two sources: a commercial powder metallurgy alloy vendor and an in-house, controlled environment high-energy mill. The effects of milling parameters on the microstructure and composition of the powder and consolidated alloy are described. Comparison of the oxidation kinetics of ODS-Fe_3Al alloys with commercial ODS-FeCrAl alloys in air at 1000-1300°C indicated that the best Fe_3Al-based alloys oxidized isothermally at the same rate as the ODS-FeCrAl alloys but, under thermal cycling conditions, the oxidation rate of ODS-Fe_3Al was faster. The main difference was that the ODS-Fe_3Al experienced significantly more scale spallation above 1000°C. The differences in oxidation behavior were translated into expected lifetimes which indicated that, for an alloy section thickness of 2.5 mm, the scale spallation of ODS-Fe_3Al leads to an expected service lifetime similar to that for the INCO alloy MA956 at 1100 to 1300°C.

INTRODUCTION

Interest in advanced cycles that involve indirectly-fired gas turbines, in which coal- or gas-fired high-temperature heat exchangers are used to heat a working fluid in a closed system, has led to investigation of materials for heat exchangers capable of operation at temperatures on the order of 1200 to 1300°C. The candidate materials are ceramics and, possibly, oxide dispersion-strengthened (ODS) alloys. An ODS

FeCrAl alloy was found to meet the strength requirements for such an application in which the working fluid at 0.9 MPa was to be heated from 800 to 1100°C over a tube length of 4 m [1].

The oxidation life of ODS FeCrAl alloys is determined by their ability to form or reform a protective alumina scale, and can be related to the time for the aluminum content of the alloy to be depleted to some minimum level [2]. As a result, the service life is a function of the available aluminum content of the alloys and the minimum aluminum level at which breakaway oxidation occurs. Hence there is a limit on the minimum cross section which can be safely employed at temperatures above 1200°C. Because of their significantly higher aluminum content (≥28 atom %/≥16 wt. percent compared to ≈9 atom %/5 wt. percent), alloys based on Fe_3Al afford a potentially larger reservoir of aluminum to sustain oxidation resistance at higher temperatures and, therefore, offer a possible improvement over the currently-available ODS FeCrAl alloys, providing they can be strengthened in a similar manner.

The main thrusts of this program are to develop the alloy processing parameters that are required to achieve the typical ODS alloy structure that confers creep strength at extreme temperatures, and to optimize the alloy oxidation behavior to provide increased service life compared to ODS-FeCrAl alloys intended for the same applications. Development of the desired alloy microstructure involves control of the size and distribution of the oxide dispersoid, as well as the desired alloy grain size and shape. The ability to control the recrystallization of ODS alloys is very dependent on the homogeneity of the initial alloy powder, in terms of the size and distribution of the dispersed oxide particles, and on the level of strain and temperature applied in the recrystallization step.

DEVELOPMENT OF MECHANICAL ALLOYING PARAMETERS FOR ODS Fe_3Al

Experimental Procedures

A two-liter size horizontal attritor mill (Zoz GmbH, Kreustal, Germany) was installed at ORNL in order to perform mechanical alloying of iron aluminide powder while maintaining oxygen contents comparable to those in commercial mechanically alloyed materials. The grinding media consisted of high-carbon alloy steel balls of 5 mm diam. The rotational speed of the mill was maintained at 900 rpm, and the milling atmosphere was a static vacuum. The mill was operated by placing the media and powder in the mill, evacuating with a mechanical pump to a pressure of about 5×10^{-2} torr over several hours, and sealing the mill by use of a vacuum valve.

The starting powder was (in weight percent) Fe-15.9Al-2.2Cr-0.02B (FAS), which was screened to -100 /+400 mesh. An addition of 0.47% Y_2O_3 powder was made to each run. Two sources of Y_2O_3 were used: one was a powder of nominal size of 5 μm, and the second was a colloidal suspension of Y_2O_3 in water with a reported particle size of 0.1 μm. This material was dried and heated at 500 ° C for 1 hour to produce a powder which had a typical particle size of 0.5 to 1 μm. After conditioning the mill and grinding media by running the mill with FAS powder for 4 hr, an initial milling run was made using the 5 μm size Y_2O_3 addition. The mill contained 2 kg of grinding media and 200 g of powder. Samples were taken of the powder after total milling times of 1, 2, 4, 8, and 16 hr. Samples were taken through a sampling tube which allowed the milling chamber to remain under vacuum until the end of the total 32 hr run time. The samples were analyzed for oxygen and nitrogen content, and the powder characterized by scanning electron microscopy (SEM). Samples were also polished metallographically and viewed by SEM.

Three additional mill runs were made, each for 24 hr, using colloidal Y_2O_3 with 2 kg of grinding media. The powder weights were 200, 300, and 400 g, corresponding to 10, 15 and 20% of media weight. Two runs were also made using 3 kg of media and powder weights of 450 and 600 g, corresponding to 15 and 20% of media weight, respectively. About 60 g of powder was typically found compacted against the corner of the chamber wall, and this material was segregated from the loose powder recovered from the mill.

The powders were placed in mild steel cans (5 cm OD and about 3 cm ID), evacuated and sealed. Prior to extrusion at a ratio of 10:1, the cans were preheated to 1100°C for 1 hr. An additional extrusion of the 600 g lot of milled powder was made at an extrusion ratio of 16:1. The extruded material from the 200 g powder lot (10:1 extrusion ratio) and the materials from the 600 g powder lot (10:1 and 16:1 ratios) were examined by optical metallography and chemically analyzed for oxygen, nitrogen and carbon. Metallographic analyses were performed on as-extruded material and also on samples heated at 1275°C for 8 hr in an evacuated quartz tube. Transmission electron microscopy (TEM) was performed on the alloy extruded at the 16:1 ratio.

Results and Discussion

The average particle size of the initial milled powder samples was found to increase for up to 4 hr of milling, then decrease to 16 hr , after which time it remained constant. Also, the particle size of the milled powder and SEM showed no obvious changes after 24 hr milling at loadings of 2 or 3 kg of media and 200

to 600 g of powder. The polished powder samples when viewed by SEM contained a distribution of light-colored streaks, which were shown by energy dispersive X-ray analysis to be essentially pure iron. These regions apparently were associated with wear particles from the steel balls which became distributed in the milled powder. The oxygen content of the milled powder as a function of milling time is shown in Fig. 1. The calculated starting oxygen content consists of 1,000 ppm from the addition of 0.47% of Y_2O_3 and 60 ppm in the FAS powder. The increase in oxygen content up to 1,700 ppm after 32 hr was attributed to leakage of air into the mill. The attritor mill when running empty had a leak-up rate of about 0.03 torr/min, as compared to a leak-up rate of about 0.005 torr/min when idle. The increase in oxygen content with time was consistent with the measured leak-up rate. An effort was made to determine the source of the increased leak rate while the mill was operating. Helium leak detection was not successful in measuring any transport of helium into the mill.

A weight gain was measured as a result of the milling process, apparently due to wear of the media; its dependence on the milling parameters (after 24 hr of milling) is shown in Fig. 2. The trend was to a significant decrease in weight gain at higher ratios of powder:media weight. The weight gains ranged from 3% at a 10% ratio to about 1% at a 20% ratio. The effect of changing the media weight from 2 to 3 kg appeared to have a minimal effect on the relative weight gain in milling.

The microstructures of the extrusions examined to date are shown in the optical micrographs in Figs. 3 (a) and (b). All the materials showed oxide stringers elongated in the extrusion direction. The extrusion produced from material milled with 200 g of powder and 2 kg of media had a uniform microstucture, whereas the extrusions produced with higher mill loading exhibited regions of large grains, which were

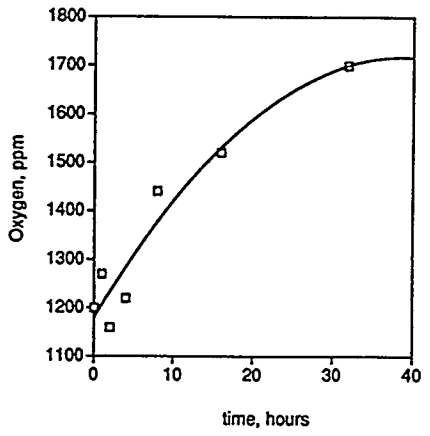

Fig. 1. Oxygen pickup during vacuum attritor milling.

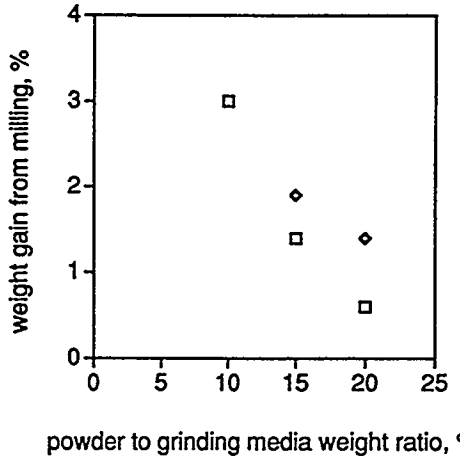

Fig. 2. Effect of milling parameters on weight gain from milling media wear.

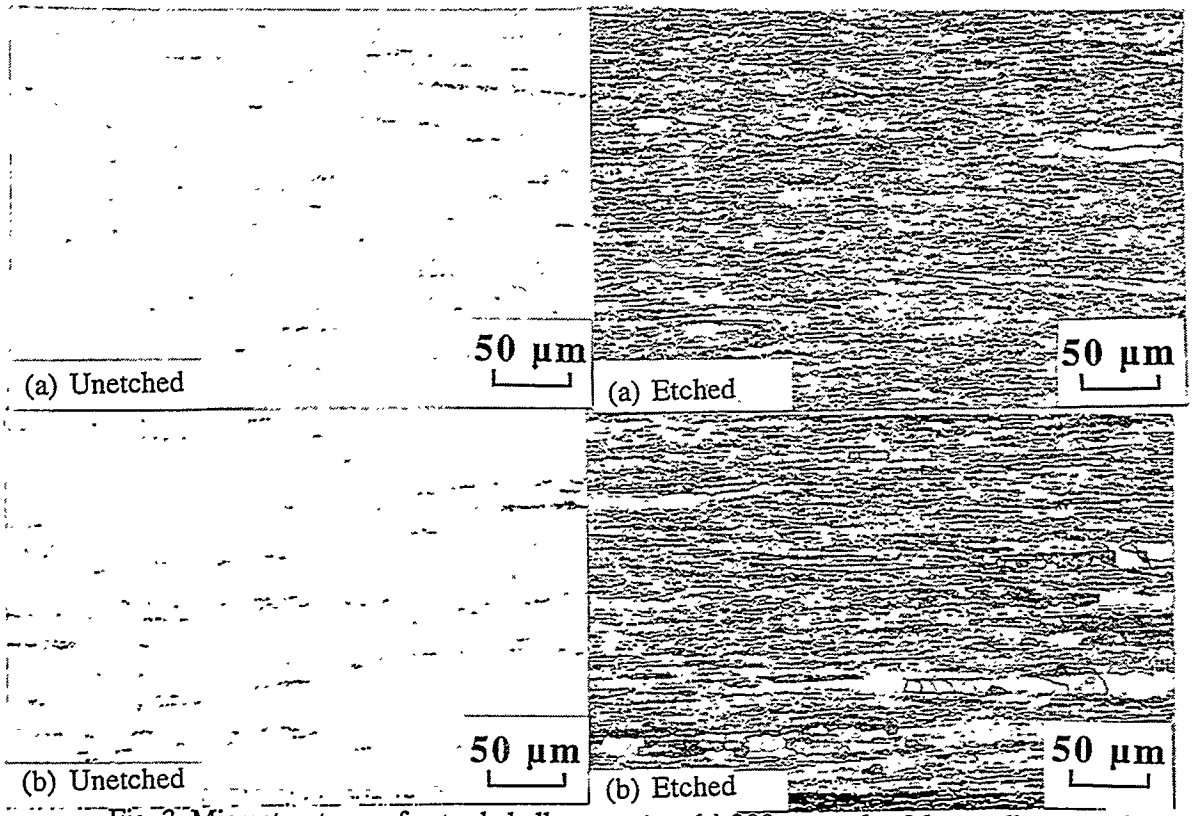

Fig. 3. Microstructures of extruded alloy powders (a) 200 g powder:2 kg media; extrusion ratio 10:1 and (b) 600 g powder:3 kg media; 16 :1.

attributed to inadequate mixing of Y_2O_3 particles during the milling. Transmission electron microscopy of the material milled with a powder load of 600g and extruded at a ratio of 16:1 indicated a bimodal distribution of oxide particles with the larger particles in the range of 0.2 to 1 µm. The smaller particles were mostly in the range of 0.01 to 0.03 µm. Preliminary analysis showed that all of the particles were complex oxides containing both yttrium and aluminum. The matrix was the ordered B2 phase.

Table 1. Chemical Analysis of Extruded Bars

Sample Powder		Extrusion Ratio	Concentration, ppm			
Lot No.	Size, g		Oxygen	Nitrogen	Carbon	Sulfur
220	200	10:1	1,620	160	740	20
360B	600	10:1	1,640	180	370	20
360A	600	16:1	1,760	100	400	20

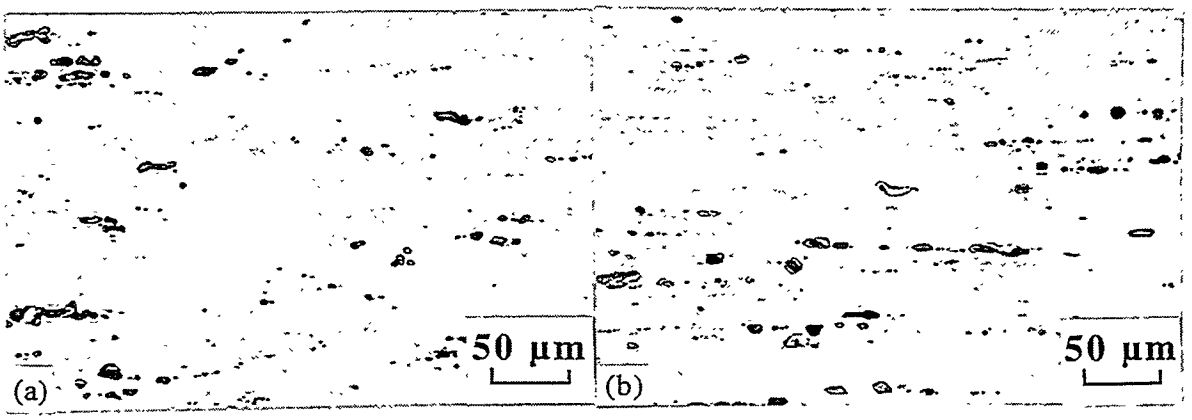

Fig. 4. Stringers of a second phase (possibly an oxide) in extruded alloys (600 g mill load) after recrystallization heat treatment (a) extruded at 10:1, as polished and (b) extruded at 16:1, as polished.

Chemical analysis results of three extruded bars are shown in Table 1. Oxygen content, in the range of 1,620 to 1,760 ppm, and nitrogen contents in the range of 100 to 180 ppm, are consistent with those obtained in an earlier 32 hr milling run; the oxygen contents are significantly lower than those obtained in a smaller attritor mill used in this program (of the order of 1% by weight) and are very similar to those reported for commercial mechanically-alloyed materials. For the 600 g powder lot,carbon contents of 370 and 400 ppm are within, but on the high end of the range of carbon contents measured in previous work and found in commercial ODS materials. The 740 ppm carbon value for the 200 g lot is considered high for this type of material. The carbon content of the steel balls is about 1%; the observed wear of the media would result in a calculated increase in carbon content in the milled powder of 100 to 300 ppm. These values are somewhat lower than the measured carbon contents shown in Table 1, but are within a factor of 2 of the measured values; there may be another source of comparable magnitude.

The microstructure following heating at 1275°C in vacuum was characterized by large quantities of a second phase in all three materials. The phase appeared to be an oxide,and was often strung out in the direction of extrusion. Figure 4 shows these features in as-polished sections; the features appeared to coincide with the location of the much smaller oxide stringers present in the as-extruded materials. The amount of second phase appeared to be higher in regions near the edges of the specimens, near the boundary with the can material. Detailed analysis is in progress to determine the source the second phase.

The material from the 600 g milling lot heat treated at 1275°C showed localized regions of visible grains among large regions with no visible grain boundaries. The material from the 200 g milling lot could

not be etched to show any grain boundaries, which may indicate that very large grains had been achieved by this treatment, although additional characterization is needed to confirm this.

HIGH-TEMPERATURE OXIDATION BEHAVIOR OF ODS-Fe_3Al ALLOYS

Experimental Procedures

The alloys studied included two FeCrAl-based commercially-available oxide dispersion-containing alloys—Kanthal APM and INCO MA956—and an ODS-Fe_3Al alloy (FAS3Y) made in an earlier phase of the program at ORNL. The compositions of the alloys are shown in Table 2. Kanthal APM is not optimized for high-temperature creep strength, but forms a protective alumina scale that exhibits excellent resistance to spallation [3]; this alloy, therefore, was considered a standard for high-temperature oxidation resistance. INCO MA956 represents the class of ODS alloys available as high-strength, high-temperature tubing. The Kanthal APM was obtained in the form of 1 mm-thick strips [3], whereas the MA956 was a nominally 3 mm-thick plate. The ODS-Fe_3Al alloy was an as-extruded rod, nominally 1.6 mm (0.0625 in) diameter.

Table 2. Compositions of Alloys (weight percent)

Constituent	FAS3Y	Kanthal APM	INCO MA956*
Dispersoid	Y_2O_3-Al_2O_3	ZrO_2-Al_2O_3	Y_2O_3-Al_2O_3
Cr	2.25	20.42	19.22
Al	16.3	5.54	4.32
Y	0.37	<0.01	0.5
Zr		0.10	
Ti	0.07	0.03	0.36
Si	0.10	0.23	
Mn	0.15	0.08	
C	0.03	0.03	0.01
O	0.0533**	0.0526	0.20
S	0.0061	0.001	0.011

*Analysis for sample of rod stock
**Before mechanical alloying

Specimens of dimensions 1.5 x 1.0 x 0.2 cm thick, or 1.25 cm diameter discs of thickness 1-2 mm from the ODS-Fe_3Al, were polished to a 0.3 μm alumina surface finish, and ultrasonically cleaned in acetone and methanol before exposure. Each specimen was placed in individual lidded, cylindrical alumina crucibles, which were then exposed in air for 500 hr intervals to 5,000 hr at 1000°C, and at 1100, 1200 and 1300°C at 100 hr intervals up to 1,500 hr. The alumina crucibles were baked at 1400°C for 8 hr prior to

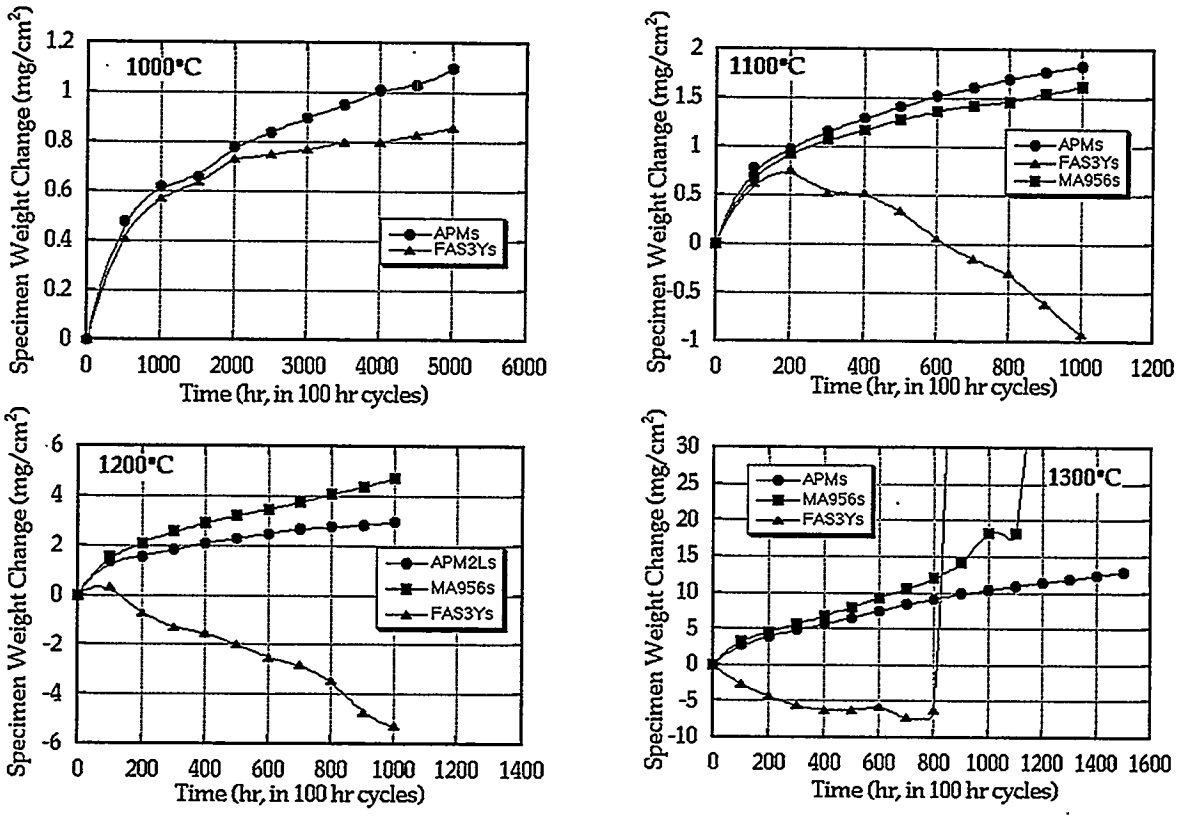

Fig. 5. Specimen weight change data after exposure to thermal cycling conditions.

use. Separate weighing of the specimens and crucibles allowed the total weight gain and the extent of scale spallation to be measured. The specimens and the crucibles (containing any spalled oxide) were weighed after cooling to room temperature on a Mettler model AE 240 balance.

Results and Discussion

The trends in specimen weight change are shown in Fig. 5. The ODS-FeCrAl alloys exhibited net weight gains at all four temperatures, whereas the ODS-Fe_3Al showed a net weight loss, following an initial gain, at 1100°C and higher. The overall oxidation rates (rate of oxygen uptake), from the sum of the specimen weight change and the spalled scale, as well as the weight of spalled scale, showed that, at 1000°C, the oxidation rate of the ODS-Fe_3Al alloy was essentially the same as that of APM, with slightly more spallation from the ODS-Fe_3Al. With increasing temperature, the overall rate of oxygen uptake of the ODS-Fe_3Al increased faster than that for APM as a result of the increasing rate of scale spallation. The oxidation behavior of MA956 was intermediate between these two alloys. Log-log plots

of these data were made to determine the values of the parameters k and n in the oxidation rate equation, expressed as:

$$\Delta m = k \,.\, t^n \qquad (1)$$

where Δm is the weight change per unit area due to oxygen uptake, t is time, and k and n are constants. The values of the oxidation rate exponents, n, are listed in Fig. 6. The excellent oxidation behavior of APM was reflected in values of n that were consistently less than expected for parabolic scale growth ($n = 0.5$). The n values for the other two alloys, which suffered increasing degrees of scale spallation with increasing temperature, increased from slower to faster than parabolic as the extent of scale spallation increased.

For ODS-FeCrAl alloys, the lifetime under high-temperature oxidation conditions may be limited by the ability of the alloy to maintain or reform its protective alumina scale [2]. Hence, a major point of comparison between ODS-Fe_3Al and competing ODS-FeCrAl alloys is the oxidation-governed lifetime for a given thickness of alloy. Using the same considerations as Quadakkers and Bongartz [2,4], the kinetic data reported above were used to construct 'oxidation life diagrams' for the three alloys. As long as oxidation of the alloy involves the formation (and reformation following scale spallation) of an alumina scale, the effective life of the alloy can be calculated from the rate of consumption of aluminum (proportional to Δm, mg/cm^2), and the total amount of aluminum available. Measurements on specimens oxidized to the point of breakaway oxidation, where an alumina scale no longer forms, have shown that the aluminum concentration profile in the alloy remains essentially flat [4,5], so that the aluminum reservoir available for use in protective scale formation can be calculated from:

- the initial aluminum content of the alloy (C_o, weight percent),
- the aluminum level at which a protective alumina scale can no longer be formed (C_b), and
- the thickness of the section being oxidized (d, cm).

Hence:

$$k \,.\, t^n \,.\, M = (C_o - C_b)/100 \,.\, d/2 \,.\, \rho \qquad (2)$$

where M is the weight fraction of aluminum reacted as Al_2O_3 corresponding to the oxygen uptake, ρ is the density (mg/cm^3) of the alloy, the units of k are mg/cm^2.hr, and t is in hours. Rearranging, the time at which a protective alumina scale can no longer be formed, or the time to breakaway oxidation (t_b), becomes:

$$t_b = [4.44 \times 10^{-3} \,.\, (C_o - C_b) \,.\, r \,.\, d/k]^{1/n} \qquad (3)$$

Values of C_b have been determined to be of the order of 1.15 wt. percent for APM [4] (the same value was assumed here for MA956), and 1.8 to 2.4 wt. percent for Fe_3Al [5]. The resulting diagrams relating lifetime (t_b) to wall thickness (d) are shown in Fig 6. Figure 7 summarizes the effect of temperature on the oxidation-governed lifetime of the three alloys for a section thickness of 2.5 mm (0.1 in.). Overall, at 1000°C when the extent of scale loss from FAS3Y by spallation is small, its larger usable aluminum reservoir (16.3 vs 4.65 wt. percent) results in a longer life than for APM. As the proportion of the aluminum

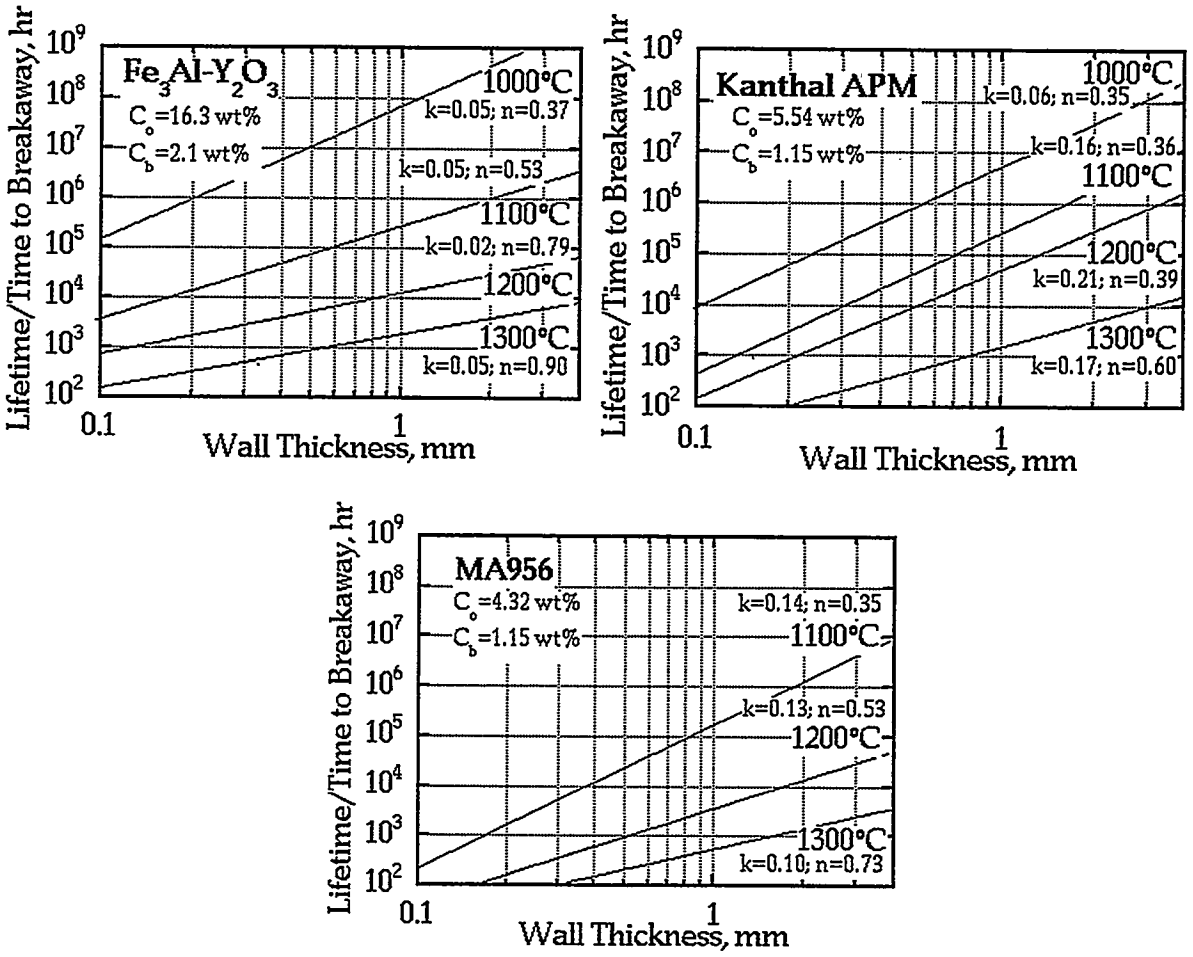

Fig. 6. Calculated oxidation-governed lifetimes as a function of wall thickness

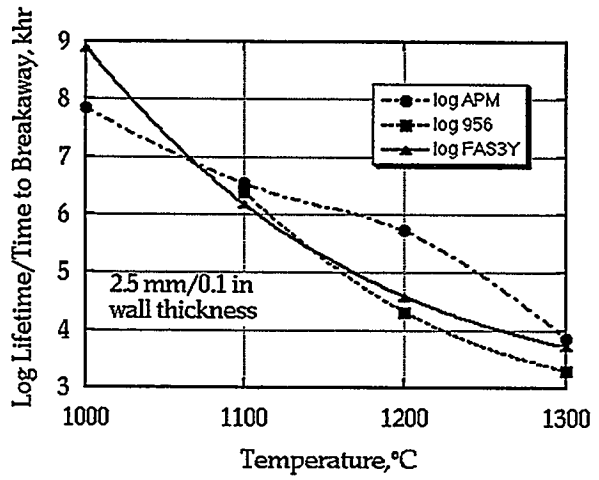

Fig. 7. Comparison of calculated lifetimes for a 2.5 mm thick alloy section.

reservoir consumed to replace scale lost by spallation increases with increasing temperature, the advantage of the large initial reservoir of FAS3Y compared to APM is lost as the temperature is increased to 1300°C, whereas at 1300°C all three alloys exhibited essentially the same calculated lifetimes. The effect of increasing scale spallation on the oxidation-governed life of APM becomes apparent only above 1200°C. In contrast, the moderate scale spallation of MA956 results in calculated lifetimes similar to those of FAS3Y. These oxidation exposures are continuing to determine if scale spallation eventually plays a role in limiting the oxidation lifetime of APM, and to generate data that can be used to test and refine the approach outlined here.

CONCLUSIONS

Milling in a static vacuum produced low levels of oxygen contamination in the alloy similar to those found in commercial-scale ball-milled powder. There remains a possibility of achieving even lower levels of oxygen pick-up, below the range of 500 to 700 ppm now obtained, by better understanding of sealing issues associated with the mill.

Wear of the steel grinding media gives rise to several issues associated with the milled powder:

- an increase in the average iron content of the powder, which can readily be compensated for by adjusting the initial powder composition,
- inhomogeneity as evidenced by local iron-rich regions in the milled powder associated with wear particles detached from the grinding media toward the end of the milling run, and
- an increase in carbon content in the milled powder. Use of ceramic media is a possibility, but experience in its use in milling of ductile metal powder has not been good.

The heat treatment of the extruded materials at 1275°C for 8 hr resulted in very large grains in the fully-milled alloy, and etching was unable to reveal any grain boundaries. The Y_2O_3 powder currently available appears to be too coarse to achieve a uniform distribution of very fine particles. An experimental batch of Y_2O_3 having a nominal 30 nm particle size has been ordered from a commercial vendor. Currently the most important issue is the presence in all the materials of large stringers of a second phase following heat treatment at 1275°C. The second phase has the appearance of an oxide; if this is the case, a possible source may be air entrapped or adsorbed on the starting powder particles.

The overall rate of oxidation of an ODS-Fe_3Al at 1000°C in air under thermal cycling conditions was found to be similar to that of the ODS-FeCrAl alloys Kanthal APM and INCO MA956 whereas, from 1100 to 1300°C, its oxidation rate was faster than those alloys due to a greater tendency to scale spallation. Nevertheless, the larger reservoir of aluminum in the ODS-Fe_3Al resulted in a longer calculated oxidation-governed lifetime for the ODS-Fe_3Al at 1000°C, for a given alloy thickness. At 1100 and 1300°C, all three alloys exhibited essentially the same calculated lifetimes but, in the intervening temperature range, APM clearly gave the longest lifetimes, with FAS3Y slightly better than MA956. Exposures are continuing to generate oxidation kinetics for a larger fraction of the alloy lifetimes, to allow the calculations to fully reflect the actual oxidation behavior. Work is in progress with the aim of decreasing the tendency for scale spallation by the ODS-Fe_3Al alloy, which could result in an obvious lifetime advantage commensurate with its larger aluminum reservoir compared to the ODS-FeCrAl alloys.

ACKNOWLEDGMENTS

The authors acknowledge the support of the Fossil Energy Advanced Research and Technology Development (AR&TD) Materials Program, U. S. Department of Energy, under contract DE-AC05-84OR21400 with Lockheed Martin Energy Research, Inc. BAP was supported by the U. S. Department of Energy Distinguished Postdoctoral Research Program administered by the Oak Ridge Institute for Science and Education. The authors thank colleagues at ORNL: A. Duncan, who was responsible for the TEM work, V. K. Sikka, K. S. Blakely, M. Howell, L. D. Chitwood, and J. R. DiStefano for their contributions and invaluable discussions.

REFERENCES

1. F. Starr., A. R. White., and B. Kazimierzak., *in* Materials for Advanced Power Engineering 1994, D. Coutsouradis, et al., Eds., (Kluwer Academic Publishers, 1994) pp. 1393-1412

2. W. J. Quadakkers, K. Bongartz, F. Schubert, and H. Schuster *in* Materials for Advanced Power Engineering 1994, D. Coutsouradis, et al., Eds., (Kluwer Academic Publishers,1994) pp. 1533-1542

3. B. A. Pint, A. J. Garratt-Reed, and L. W. Hobbs, Materials at High Temperatures, **1** (1995) 3

4. W. J. Quadakkers, and K. Bongartz, Werkstoffe u. Korrosion, **45** (1994) 232

5. J. H. DeVan, P. F. Tortorelli, and M. J. Bennett, Proc. Eighth Annual Conference on Fossil Energy Materials, Oak Ridge, TN, (CONF-9405143; ORNL/FMP-94/1, 1994) pp. 309-320

THE INFLUENCE OF PROCESSING ON MICROSTRUCTURE AND PROPERTIES OF IRON ALUMINIDES

R. N. Wright and J. K. Wright

Idaho National Engineering Laboratory
Lockheed Idaho Technologies Company
Idaho Falls, ID 83415-2218

ABSTRACT

An Fe-28%Al alloy containing 5% Cr has been synthesized by reaction of elemental powders, followed by consolidation using hot extrusion. The resulting material is fully dense, homogeneous, and has a grain size of less than 5μm. Reaction synthesis results in an Al_2O_3 dispersion that is uniformly dispersed during hot extrusion. Under some circumstances the hot extruded material undergoes secondary recrystallization, resulting in grain sizes greater than 25 millimeters. The fine grained material exhibits improved yield strength compared to the coarse grained material up to test temperatures of 800°C. Creep testing has shown that the coarse grained material has significantly improved time to rupture compared to fine grained material. The oxide dispersion strengthened material has significantly improved creep resistance compared to conventional powder metallurgy material. With proper heat treatment, the coarse grained material exhibits time to rupture of 425 hours at 650°C and a stress of 75 MPa, compared to 40 hours for conventional material of similar composition.

INTRODUCTION

Recent work indicates the problem of limited ductility exhibited by Fe_3Al may be overcome by small additions (2-5 wt%) of chromium.[1] Tensile elongation of Fe_3Al+ 5% Cr is found to approach 20% with little sacrifice in resistance to oxidation and sulfidation.[2] Unfortunately, the yield strength of Fe_3Al rapidly decreases above 500°C, thereby reducing the suitability of this material for high temperature applications.[2] Nickel-based materials, suffering from a similar decrease in high temperature strength, are strengthened through the incorporation of oxide particles (oxide-dispersion-strengthened or ODS alloys). The oxide particles impede dislocation motion, prevent grain boundary sliding, and inhibit grain growth at elevated temperatures, thus increasing the high temperature strength and creep resistance of these alloys.[3] Since the oxide dispersion affects the mechanisms of deformation, a similar improvement in high temperature strength is expected by incorporating an oxide dispersion into Fe_3Al.

This work examines the high temperature mechanical properties of fully dense Fe_3Al, produced by reaction synthesis from elemental powders followed by hot extrusion, and ascertains the influence of a dispersion of oxide particles on the observed increase in high temperature strength. In

this work, the surface oxide coating the elemental powders prior to reaction synthesis provide the desired dispersion of oxide particles in the processed material. The results are compared to Fe_3Al processed by hot extrusion of pre-alloyed powders, which lacks a dispersion of oxide particles. High temperature characterization of the various materials includes determination of their high temperature mechanical properties as a function of grain size and oxide particle size.

EXPERIMENTAL PROCEDURE

Reaction synthesized material was made using carbonyl iron (8 μm diameter), helium gas atomized aluminum (10 μm diameter) and chromium (1-5 μm diameter) powders, mixed in the proper portions to yield Fe-28%Al-5%Cr. Reaction between the elemental powders occurred during a 2 hour thermal treatment at 1100°C in flowing argon. After canning in mild steel, full density rod was produced by hot extrusion (either 9:1 or 16:1 reduction in area) at extrusion temperatures from 900°C and 1200°C. Consolidated material lacking an oxide dispersion was produced via extrusion of pre-alloyed powder of composition Fe_3Al+ 5%Cr, made by gas atomizing a mixture of Fe_3Al alloyed with 5% chromium. The extrusion process was carried out at 1000°C with a 9:1 reduction in area.

Grain growth experiments were performed during one hour heat treatments in flowing argon at various temperatures. The mean grain size was determined by the linear intercept method on photomicrographs taken of polished and etched samples. Mechanical properties were evaluated during elevated temperature tensile or creep tests. Round cross section tensile bars, machined by centerless grinding from a portion of each of the materials, were tested in tension at various temperatures in laboratory air or in constant load creep tests.

DISCUSSION OF CURRENT ACTIVITIES

Characterization of Reaction Synthesized Material

The distribution and nature of the particles in the reaction synthesized material is of particular interest in this study. Characterization of the individual particles and their distribution is possible using transmission electron microscopy (TEM). The iron oxide on the elemental iron particles is reduced to iron by the aluminum during the reaction;[4] the oxygen available from this reduction reacts to form Al_2O_3. Extrusion

causes extensive deformation to the preform, forming stringers of particles. Electron diffraction from larger particles indicates their crystal structure to be that of α-alumina. EDS and Auger spectroscopy also show the particles to contain small amounts of chromium and possibly iron.

We have demonstrated previously that the extruded oxide dispersion containing Fe_3Al exhibits behavior similar to that of oxide dispersion strengthened nickel.[5,6] Ni-based materials show extreme grain growth at high temperature as a few grains with high mobility boundaries break away from pinning particles and grow rapidly, driven by the reduction in total grain boundary area. The final grain size after secondary recrystallization is determined by the density of nuclei with high boundary mobility.[6] Therefore, the exact nature of the annealing response in the Ni-based materials is a function of the processing history, volume fraction of dispersoid and annealing schedule, and is consistent with the behavior of the material used in this study.[5,6]

In the oxide dispersion containing Fe_3Al when extrusion is carried out in a 9:1 reduction in area, material extruded at 900°C will undergo secondary recrystallization, while that extruded at 1100°C will not. In the current work, extrusion was carried out in a 16:1 reduction in area and material extruded at 900, 1000, and 1100°C underwent secondary recrystallization, while that extruded at 1200° did not. Detailed determination of the mechanisms responsible for the unusual grain growth of extruded, reaction synthesized material remains under investigation. An analysis by Hillert[7] suggests three conditions are necessary:

1. Second phase particles prevent normal grain growth.
2. The average grain size cannot exceed a critical value which is determined by dispersoid size and volume fraction.
3. At least one grain much larger than the average grain size must be present.

The reaction synthesized material has a critical grain size of about 7 μm.[8] Since all of the reaction synthesized materials have approximately the same grain size after primary recrystallization, and all of the grain sizes are below the critical value, it appears differences observed in tendency to undergo secondary recrystallization are a result of differences in grain shape, texture, and/or the distribution of dispersoid.

Changing the extrusion temperature, and heat treatment of the extruded material, leads to significant differences in the average size of the oxide particles. TEM micrographs of the oxide dispersion in material extruded at 900 and 1100°C after heat treatment are shown in Figure 1 a, b and c. The oxides in Figures 1a and 1c represent the extremes observed for the extrusion conditions examined, with average sizes of 120 and 330 nm,

respectively. The effects of altering the oxide particle size on the mechanical properties are shown below.

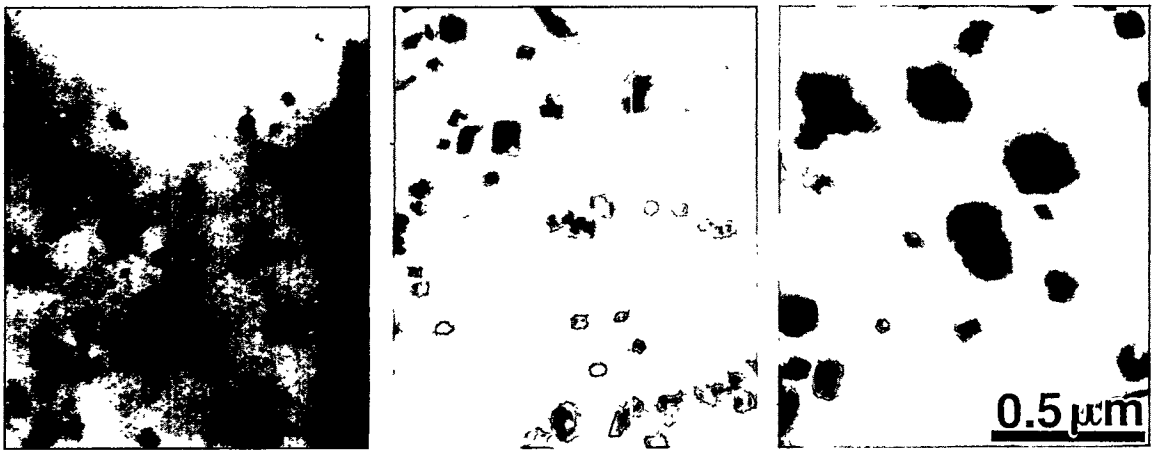

Fig. 1. TEM micrographs of oxide particles resluting from: a) 900°C extrusion, 900°C 1 hour anneal; b) 900°C extrusion, 1300°C 1 hour anneal; and c) 1100°C extrusion, 1300°C 1 hour anneal.

Mechanical Properties

Figure 2 shows the yield strength of ODS Fe_3Al alloys as a function of grain size. The fine grained material has nearly twice the yield strength of the pre-alloyed P/M material, and is also significantly stronger than coarse grained ODS material. The effect appears most dramatic at room temperature; however, the increment of strengthening has been retained at 800°C where the ODS material is still twice as strong despite severely diminished strength for all of the materials. The 2.7 μm grained material is strongest at all test temperatures while retaining room temperature ductility of approximately 2%; however the yield strengths of the 113 and 1000 μm grained materials do not vary significantly from one another. We have demonstrated previously that grain boundary sliding is not a significant deformation mechanism in the fine grained material for temperatures up to 900°C.

Despite the improved tensile properties in the fine grained material, very large grains are typically necessary in ODS alloys to achieved maximum creep properties. Creep curves are shown in Figure 3 for conventional powder metallurgy Fe_3Al, fine grained ODS material (900°C extrusion followed by one hour anneal at 900°C) and coarse grained ODS material

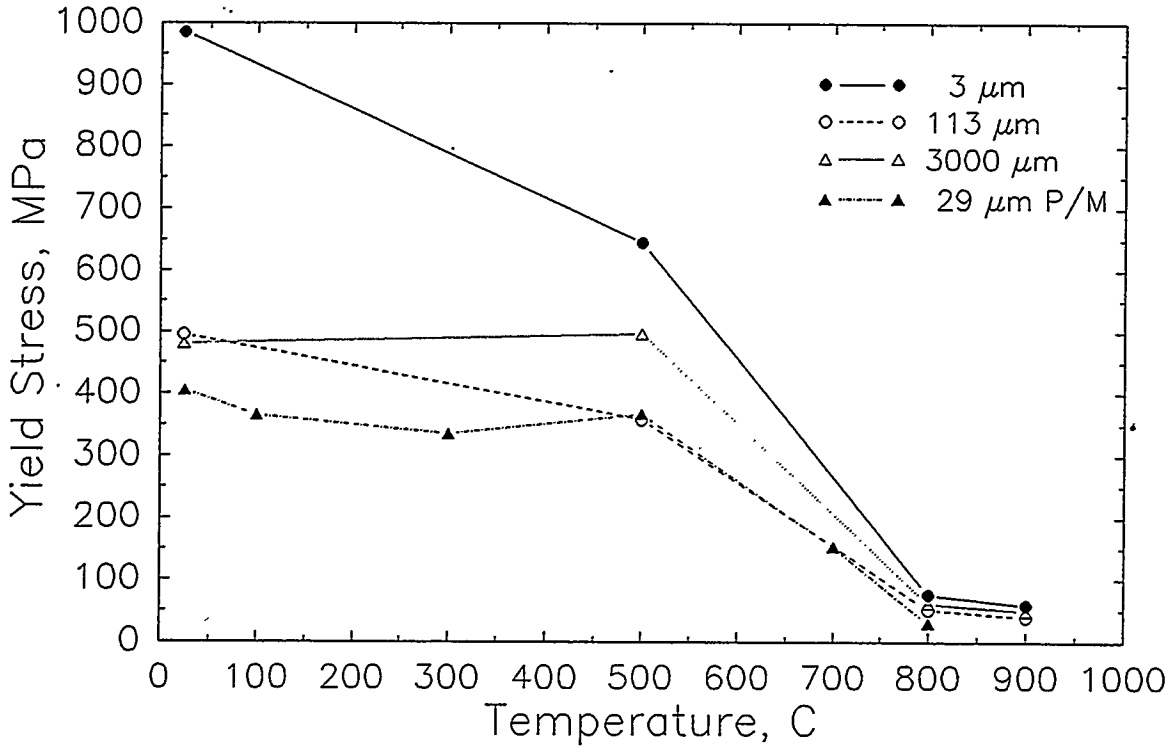

Fig. 2. Tensile properties of ODS alloys as a function of grain size.

(900°C extrusion followed by one hour anneal at 1200°C) tested at 650°C and 75 MPa. It is evident from the figure that both of the ODS materials have significantly reduced minimum creep rates, and greatly increased time to rupture compared to the conventional P/M material. It is also apparent that increasing the grain size increases the time to rupture. The coarse grained ODS alloy shows an order of magnitude increase in time to rupture for the creep conditions examined.

As noted above, heat treatment causes the average oxide size to increase, and because of a fixed volume, this results in increased spacing between particles. While coarsening of the oxide is generally not desirable in application because of expected degradation of properties with time as the oxide spacing increases, it offer the opportunity to quantify changes in creep properties. Several samples with large secondary recrystallized grain size and varying oxide sizes were creep tested at 650°C and 75 MPa and the results are shown in Figure 4. It is apparent that increasing the oxide particle size degrades the creep resistance, such that for the largest oxide particle size (approximately 330 nm) the ODS material essentially has the same properties as the conventional P/M material shown in Figure 3.

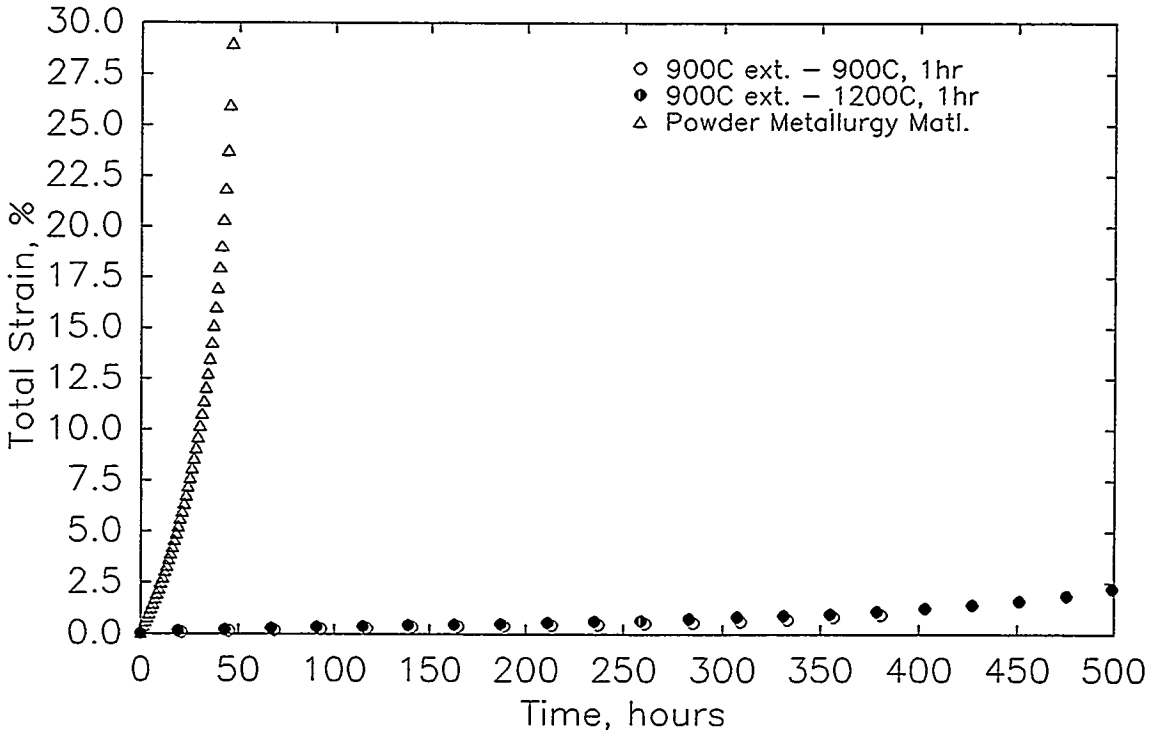

Fig. 3. Creep properties of ODS alloys compared to conventional P/M alloy at 650°C and 75 MPa.

The interaction of the oxide particle dispersion with dislocations during deformation was examined using TEM for both tensile and creep deformation. In tension at temperatures of 25 and 500°C, the particles caused extensive pinning of dislocations, and it appeared that large pile-ups of dislocations occurred around particles. At 800°C, individual dislocations were observed pinned only by the largest particles. In material deformed in creep at 650°C, it appears that individual dislocations and dislocation arrays are pinned by the larger oxide particles. Micrographs of the observed dislocation structures are shown in Figures 5 a and b for tensile deformation at 800°C and creep at 650°C, respectively. In both cases, the interaction between dislocations and particles appears to be attractive, and the dislocation contrast is not evident at the particle-dislocation interface.

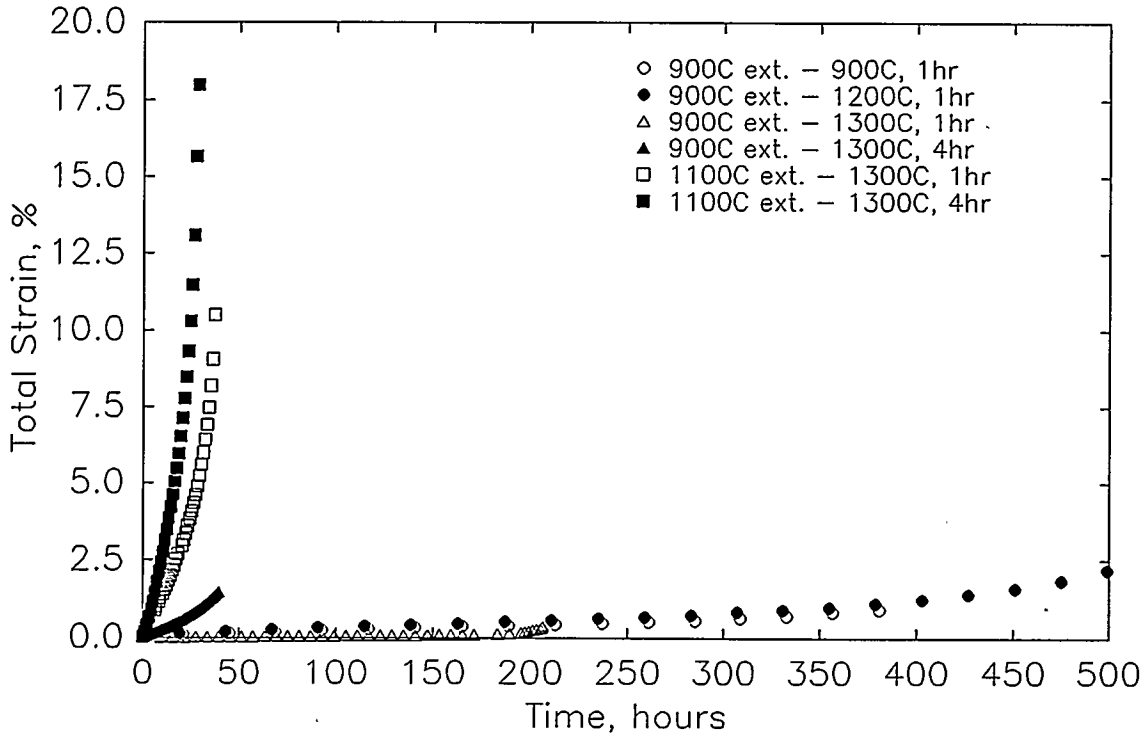

Fig. 4. Creep properties of ODS alloy as a function of heat treatment.

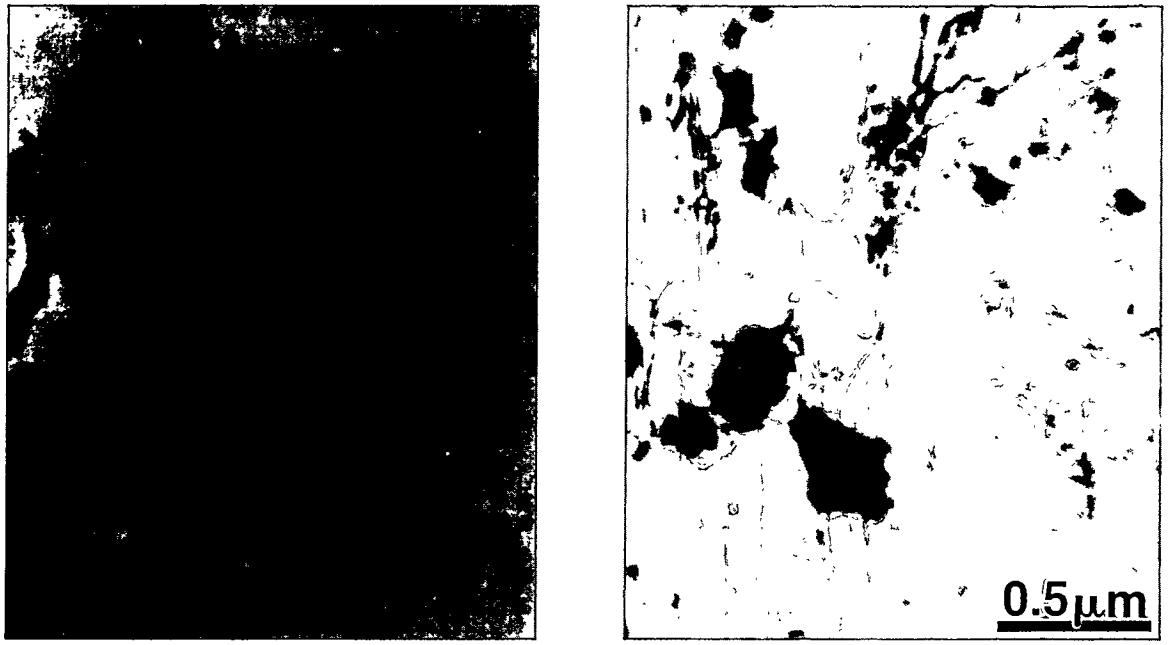

Fig. 5. Dislocation structures in ODS alloy after: a) Tensile test at 800°C; and b) Creep test at 650°C and 75 MPa.

CONCLUSIONS

Fe_3Al containing an oxide dispersion has been formed using reaction synthesis followed by extrusion. If the extrusion temperature, reduction ratio, and post-consolidation annealing treatment, are properly controlled secondary recrystallization can result with a final grain size greater than 25 millimeters.

Fine grain size material resulting from primary recrystallization has significantly increased yield strength compared to conventional powder metallurgy material of the same composition, or coarse grained secondary recrystallized material. However, the coarse grained material exhibits greater creep resistance at 650°C and 75 MPa. With proper extrusion ratio and heat treatment, the coarse grained ODS material has time to rupture at 650°C and 75 MPa that is more than an order of magnitude greater than comparable P/M material. Coarsening the oxide dispersion significantly degrades the creep properties.

ACKNOWLEDGEMENTS

The authors gratefully acknowledge the assistance of T. C. Morris and L. R. Harper in conducting experiments.

REFERENCES

1. C.G. Mckamey, J.H. DeVan, P.F. Tortorelli, and V.K. Sikka, J. Mater. Res., 6, 1779 (1991).

2. C.R. Clark, R.N. Wright, J.K. Wright, and B.H. Rabin, Scripta Met., 32, 1883 (1995).

3. R.L. Cairns, L.R. Curwick, and J.S. Benjamin, Metall. Trans., 6A, 179 (1975).

4. B.H. Rabin and R.N. Wright, Metall. Trans., 22A, 277 (1991).

5. T. M. Lillo, R. N. Wright, J. K. Wright, and B. H. Rabin. Proc. Inter. Conf. Heat Resistant Alloys II, K. Natesan, et al., eds., ASM International, p. 579, 1995.

6. J.J. Petrovic and L.J. Ebert, Metall Trans., 3, 1131 (1972).

7. M. Hillert, Acta Met., 12, 227 (1965).

8. B. H. Rabin, J. K. Wright, R. N. Wright, and C. H. Sellers, J. Mater. Res., 9, 1384 (1984).

WELD OVERLAY CLADDING WITH IRON ALUMINIDES

G.M. GOODWIN

Oak Ridge National Laboratory
P.O. Box 2008
Oak Ridge, Tennessee 37831-6096

ABSTRACT

The hot and cold cracking tendencies of some early iron aluminide alloy compositions limited their use to applications where good weldability was not required. Considerable progress has been made toward improving this situation. Using hot crack testing techniques developed at ORNL and a systematic study of alloy compositional effects, we have established a range of compositions within which hot cracking resistance is very good, essentially equivalent to stainless steel. Cold cracking, however, remains an issue, and extensive efforts are continuing to optimize composition and welding parameters, especially preheat and postweld heat treatment, to minimize its occurrence.

In terms of filler metal and process development, we have progressed from sheared strip through aspiration cast rod and shielded metal arc electrodes to the point where we can now produce composite wire with a steel sheath and aluminum core in coil form, which permits the use of both the gas tungsten arc and gas metal arc processes. This is a significant advancement in that the gas metal arc process lends itself well to automated welding, and is the process of choice for commercial weld overlay applications.

Using the newly developed filler metals, we have prepared clad specimens for testing in a variety of environments both in-house and outside ORNL, including laboratory and commercial organizations.

As a means of assessing the field performance of this new type of material, we have modified several non-pressure boundary boiler components, including fuel nozzles and port shrouds, by introducing areas of weld overlay in strategic locations, and have placed these components in service in operating boilers for a side-by-side comparison with conventional corrosion-resistant materials.

INTRODUCTION

Alloys based on the intermetallic compound Fe_3Al exhibit many attractive properties, particularly excellent resistance to high temperature oxidation. Their use in commercial applications has been limited, however, by the limited workability of wrought material and the susceptibility of weldments to both hot and cold cracking. Prior efforts [1-5] have systematically evaluated the effect of alloy composition on hot cracking.

By the use of the Sigmajig test [6], we have found that hot cracking can essentially be eliminated by the addition of carbon and the control of maximum levels of niobium, zirconium, and other alloying elements. Cold cracking, however, remains an issue, and recent efforts have been aimed at minimizing its occurrence, concurrent with development of welding filler metals, processes, and procedures aimed at commercial applications.

FILLER METAL DEVELOPMENT

Due to the difficulty in fabricating wrought solid wire of these compositions, the welding development efforts have utilized several alternate forms of filler metal. Early work [1-2] used strip sheared from sheet, which, although useful to investigate compositional effects, could not be considered for commercial applications. Subsequently, aspiration casting, where liquid metal is drawn into a quartz tube producing solid rod, was used as a means for evaluating a number of experimental compositions.[3-5] This technique proved successful, but can only produce rods of limited length (about 12-in. maximum) and diameter (about 1/8-in. minimum), thus restricting its use to the manual gas tungsten arc (GTA) process with relatively high heat input. It was realized from the onset that what was needed was a filler metal of small diameter, (approximately 1/16-in.) available in coil form, which could be used with both the GTA and gas metal arc (GMA) processes, permitting better control of dilution and semi-automatic welding. A novel technique for meeting these needs was found in the form of a composite filler wire, shown in cross-section in Figure 1.

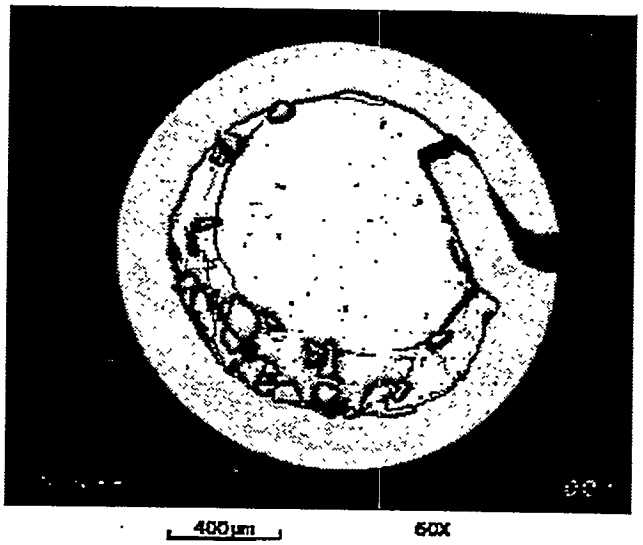

Figure 1. Composite filler wire for producing iron aluminide deposits, consisting of an iron sheath, aluminum core, and other alloying elements in granular form.

The wire consists of an iron sheath of approximately 0.009-in. thickness surrounding a core wire of commercially pure aluminum. Other alloying elements (C, Cr, Mo, Zr, B) are added as granular ferroalloys. After forming and crimping, the composite wire is drawn to eliminate void space and to

arrive at precise final diameter, in this case 0.0625-in. The resulting product is readily produced in coil form and can thus be used with automatic wire feeders for a number of welding processes.

Figure 2 shows a cross-section of a multi-pass weld pad produced using the automatic GMA process on 1-in. thick 2-1/4Cr-1 Mo steel plate.

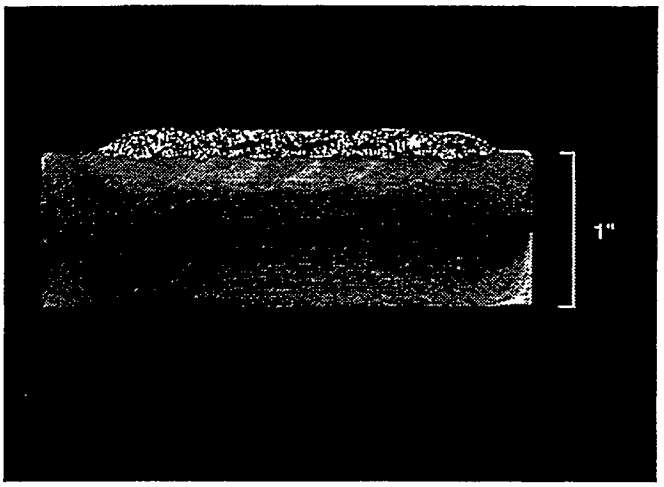

Figure 2. Multipass weld pad produced with composite filler metal using the automatic gas metal arc process on 2 1/4 Cr-1 Mo base plate.

The welding parameters used are summarized in Table 1.

Table I. Welding Parameters for Gas Metal Arc Weld Overlay Using 1/16-in. Diameter Composite Iron Aluminide Wire

Current:	245 Amperes, Reverse Polarity (DCEN)
Voltage:	27 volts
Wire Feed:	190 inches/minute
Travel:	13.1 inches/minute
Shield Gas:	Argon, 45 cubic feet/hour
Bead offset:	3/8-in.
Electrode Stickout:	3/4-in.
Preheat:	350° C
Postweld Heat Treatment:	750° C, 1 hour

The weld deposit had approximately 30% dilution and was free of cracks, voids, and porosity. Usability of the wire was found to be excellent and arc spatter was minimal. It was concluded that this form of wire could readily be used in commercial applications with the automatic GMA or GTA processes.

COMPOSITIONAL EFFECTS

As noted earlier, control of composition of the weld deposit was accomplished to essentially eliminate hot cracking in these alloys.[4] Control of cold cracking, however, has proven to be more elusive, showing a rough correlation with aluminum content[5], and a clear dependence on geometry, weld preheat, and postweld heat treatment conditions. The dependence on aluminum level is known to be complex, based on the observations of cracking in high and very low aluminum level alloys[7]. In order to clarify this relationship, we are preparing wire compositions which will bracket the range of aluminum levels which can be produced using the composite wire technique with dilution levels consistent with commercial practice. The desired chromium level in the alloy is also debatable, depending on the service conditions to be encountered, so heats of the composite wire have been produced with and without chromium. Table II summarizes the alloy compositions currently under study, and notes two additional heats which have been ordered. The latter heats represent the highest and lowest aluminum levels which can be produced with the composite wire approach, based on the thickness of the iron sheath and the diameter of the aluminum core wire.

As is noted in the table, the weld process, substrate, and dilution substantially affect the composition of the overlay clad deposit, particularly the aluminum level. Note that with an aim of 20 weight % Al for an all weld metal (undiluted) deposit, we actually achieved 21.8 weight % using the GTA process; when this same wire was used on dissimilar substrates (2 1/4 Cr-1 Mo steel and 310 stainless steel) with two weld processes, GMA and GTA, the aluminum levels were 12.6 and 15.3 weight % respectively. The higher aluminum loss with the GMA process is undoubtedly due to higher dilution and vaporization in the arc.

HEAT TREATMENT EFFECTS

It was established earlier [4,5] that weld preheat and postweld heat treatment were often effective at avoiding cold cracking during welding or upon subsequent cooling from completion of the weld. Optimization of these heat treatment conditions is important for economic and environmental considerations, as heat treatments are expensive, time consuming, and can cause hardship to the operator.

TABLE II: COMPOSITION OF EXPERIMENTAL HEATS OF IRON ALUMINIDE ALLOYS

HEAT	WEIGHT %	Al	Cr	C	Zr	Mo
Stoody I	Aim, All weld metal	20	7	0.1	0.25	0.25
	Actual, All weld metal	21.8	7.3	0.06	0.40	NA[c]
	Actual, Clad Deposit [a]	12.6	6.0	0.08	0.20	0.44
	Actual, Clad Deposit [b]	15.3	12.7	0.05	0.22	0.04
Stoody II	Aim, All weld metal	20	--	0.1	0.25	0.25
	Actual, All weld metal	21.5	--	0.08	0.25	NA
Stoody III	Aim, All weld metal	12	--	0.1	0.25	0.25
Stoody IV	Aim, All weld metal	26	--	0.1	0.25	0.25

a Single layer automatic gas metal arc on 1-in. thick type 2 1/4 Cr-1Mo steel
b Single layer manual gas tungsten arc on 1/2-in. thick type 310 stainless steel
c NA - Not Analyzed

A series of welds was produced with preheat and postweld heat treatment reduced in 50° C steps starting at 350° C and 750° C respectively. It was found that preheat temperatures as low as 250° C would sometimes yield crack free deposits, but that 350° C was required to completely avoid cracking for a standard test geometry (4x6x1-in. block of 2 1/4 Cr-1 Mo steel). Similarly, reduced postweld heat treatment temperatures would often produce sound deposits which would subsequently crack during liquid penetrant examination. It appears that 350° C and 750° C are minimum temperatures required for the standard geometry with this range of compositions.

ENVIRONMENTAL TESTING

To establish the corrosion resistance of weld overlay clads in a variety of environments, we have prepared specimens of differing geometries and substrates for testing by several organizations.

In house testing at ORNL (Peter Tortorelli) utilizes strips of overlay deposit removed from different substrates, and tested independent of the substrate. This program has evaluated numerous aluminide filler metals. For gas corrosion tests at Babcock & Wilcox (Steven Kung), we clad twenty plate specimens of Type 310 stainless steel with the Stoody I filler metal using the manual GTA process, and for molten salt characterization at Lawrence Livermore National Laboratory (Donald Stevens), we used the same filler metal to overlay rod and plate specimens of Inconel 600. Results from all the tests will help determine the optimized alloy composition.

INDUSTRIAL SERVICE TESTING

In order to demonstrate the performance of the iron aluminide compositions in a commercial environment, we have modified several non-pressure boundary components of a paper mill recovery boiler. These components will be placed in service along with others of conventional materials, and will thus give a side-by-side comparison of performance. Figure 3 shows black liquor nozzles of the splash plate type, used to fire the fuel slurry into the boiler. Each is approximately 6-in. long. Figure 3(a) is a new part made of wrought type 316 stainless steel, and Figure 3(b) shows a similar part which has been removed from service and weld repaired using the Stoody I filler metal.

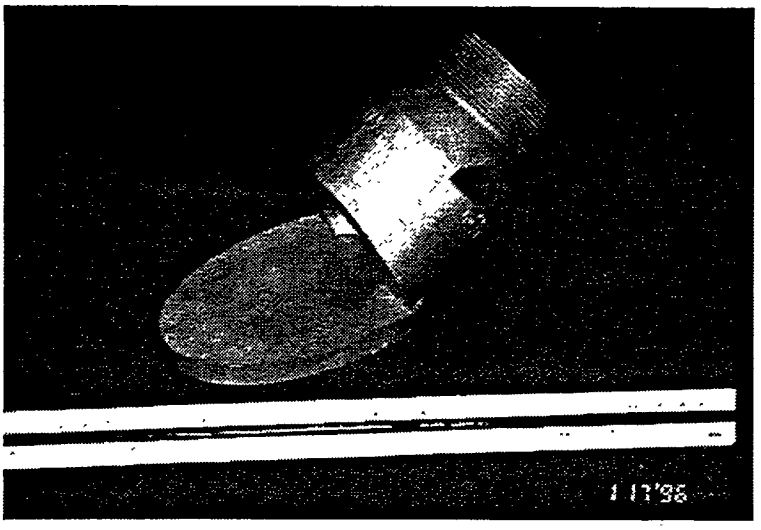

Figure 3. Splash plate type black liquor nozzles:
(a) new

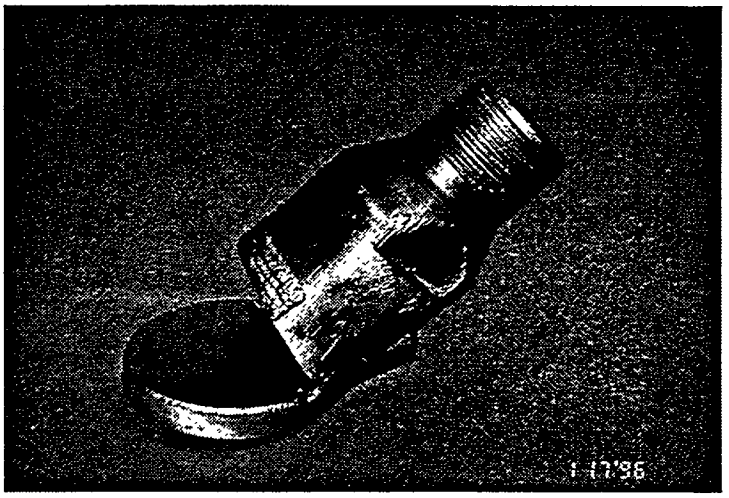

Figure 3. Splash plate type black liquor nozzles:
b) weld repaired after service by overlay cladding of splash plate (circular plate) and top of nozzle barrel. Each is approximately 6-in. long.

The splash plate (circular plate) has two layers of weld overlay which has subsequently been surface ground, and the leading edge of the nozzle barrel has a patch of overlay in a region where erosion commonly occurs.

Figure 4 shows a swirl cone type black liquor nozzle, after service, (a), and after weld overlay repair, (b). Major erosion/corrosion areas which have been clad are the outlet orifice (top), and the leading edge of the swirl cone [(b), left].

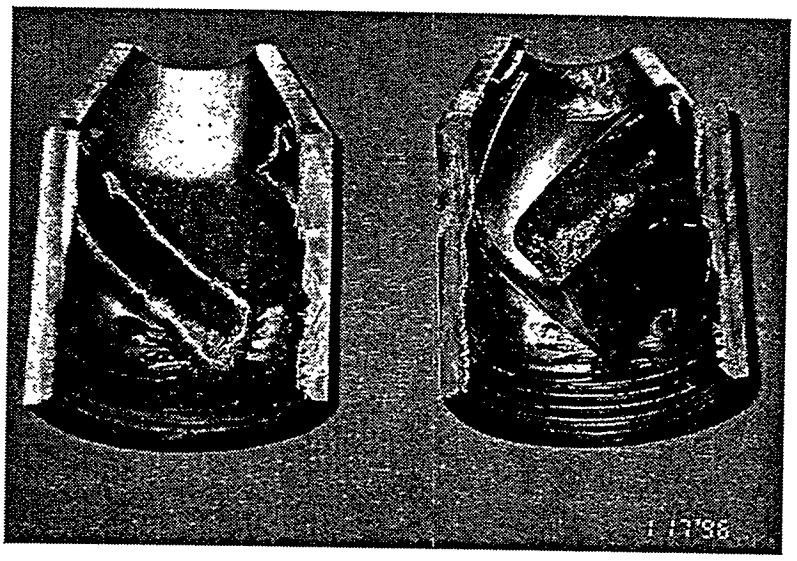

Figure 4. Swirl cone type black liquor nozzles:
(a) After service

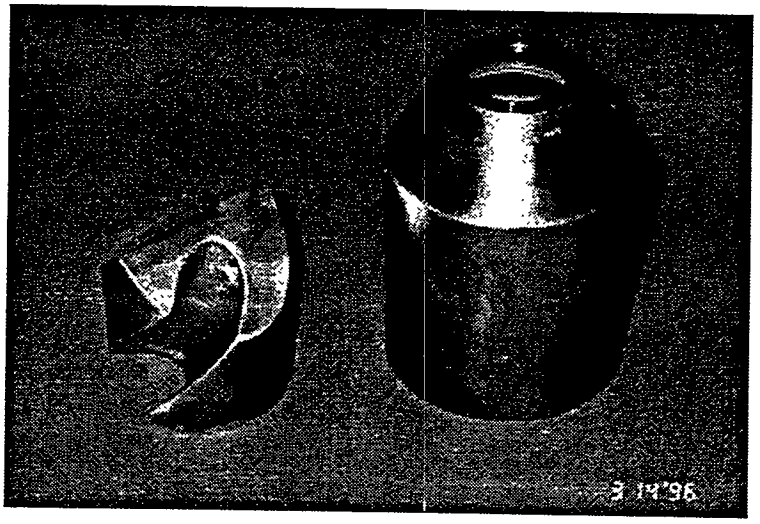

Figure 4. Swirl cone type black liquor nozzles:
(b) Weld overlay repaired at outlet orifice (right, top) and swirl cone leading edge (left, top). Approximately 4-in. long.

Figure 5 shows four sections of a liquor gun port shroud fabricated from 1/2-in. thick type 410 stainless steel plate. These plates are welded into the gun port openings in a hexagonal array (two long plates on the sides, short plates on tops and bottoms) to protect the water wall tubes, and often experience severe erosion/corrosion. The pads of aluminide overlay will give a direct comparison of their performance with that of the standard type 410 plate.

Industrial service testing is seen as an excellent way to rate these new alloys versus conventional alloys, and to guide our development toward additional commercial applications.

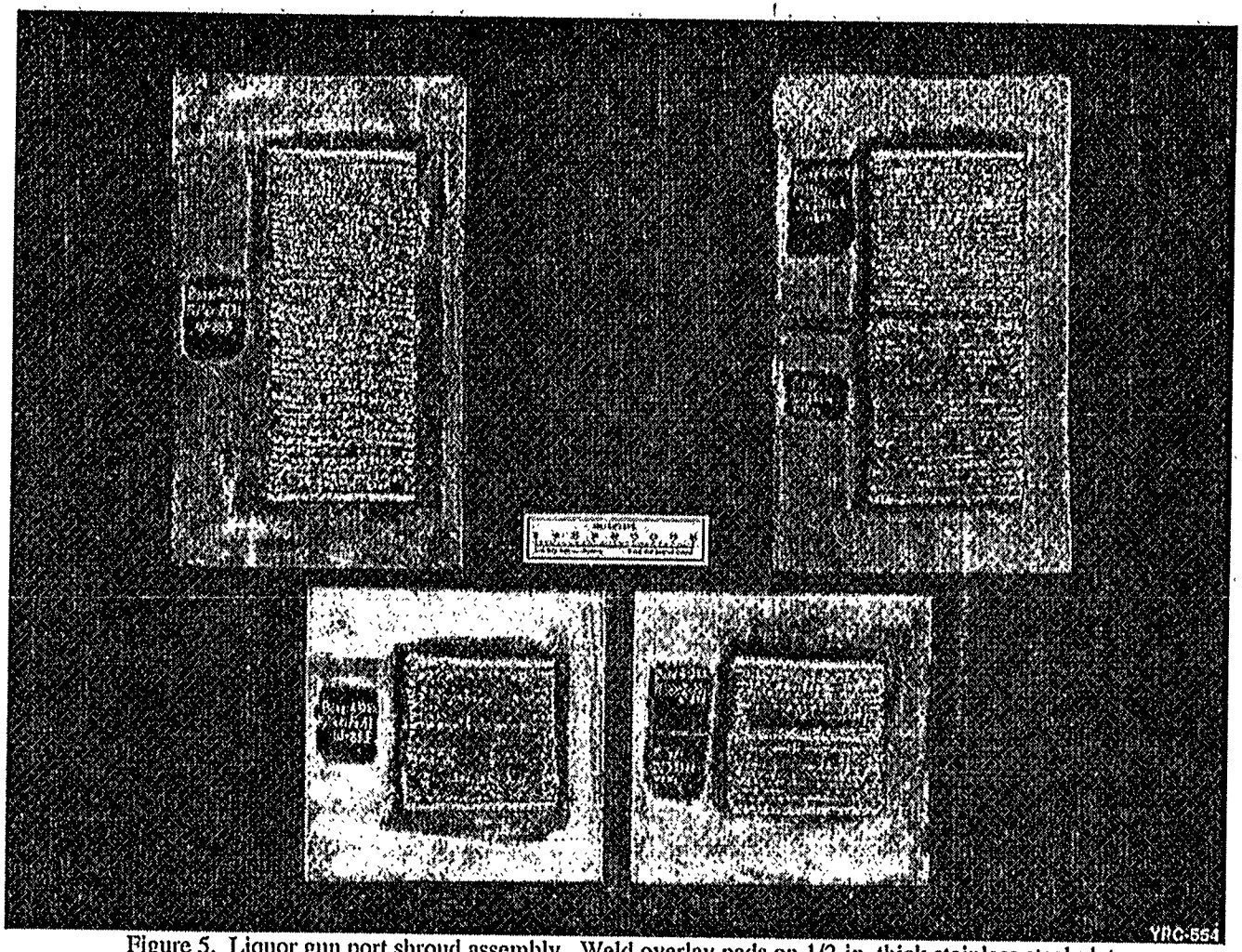

Figure 5. Liquor gun port shroud assembly. Weld overlay pads on 1/2-in. thick stainless steel plate will show comparative erosion/corrosion performance.

SUMMARY

Considerable progress has been made in the development of iron aluminide alloys for weld overlay cladding applications. Filler metals were produced in coil form using a composite approach with an iron sheath and aluminum core wire, permitting the use of automated gas metal arc and gas tungsten arc welding. Compositional modifications were made to essentially eliminate hot cracking, and efforts continue to reduce or eliminate cold cracking by optimizing composition and welding parameters, especially preheat and postweld heat treatment.

Clad specimens were prepared for testing in-house and elsewhere to confirm corrosion performance, and overlay welded components were placed in service in commercial boilers for a side-by-side comparison with currently used materials.

REFERENCES

1. T. Zacharia and S.A. David, *"Weldability of Iron Aluminides"*, proceedings of the Fifth Annual Conference on Fossil Energy Materials, ORNL/FMP-91/1, Oak Ridge National Laboratory, September 1991.

2. T. Zacharia, P.J. Maziasz, S.A. David, and C.G. McKamey, *"Weldability of Fe_3Al Based Iron Aluminide Alloys"*, proceedings of the Sixth Annual Conference on Fossil Energy Materials, ORNL/FMP-92/1, Oak Ridge National Laboratory, July 1992.

3. G.M. Goodwin, C.G. McKamey, P.J. Maziasz, and V.K. Sikka, *"Weldability of Iron Aluminides"*, proceedings of the Seventh Annual Conference on Fossil Energy Materials, ORNL/FMP-93/1, Oak Ridge National Laboratory, July 1993.

4. G.M. Goodwin, P.J. Maziasz, C.G. McKamey, J.H. Devan, and V.K. Sikka, *"Weldability of Iron Aluminides"*, proceedings of the Eighth Annual Conference on Fossil Energy Materials, ORNL/FMP-94/1, Oak Ridge National Laboratory, August 1995.

5. G.M. Goodwin, *"Weld Overlay Cladding With Iron Aluminides"*, proceedings of the Ninth Annual Conference on Fossil Energy Materials, ORNL/FMP-95/1, Oak Ridge National Laboratory, August 1995.

6. G.M. Goodwin, *"Development of a New Hot Cracking Test - The Sigmajig,* Weld J. 66(2) 335-S - 305-S (1987)

7. V.K. Sikka, G.M. Goodwin, D.J. Alexander, and C.R. Howell, *"Welding and Mechanical Properties of Cast FAPY (Fe-16 at % Al-Based) Alloy Slabs"*, ORNL/TM-12944, Oak Ridge National Laboratory, May 1995.